In-situ investigation of pulsed corona discharge

Research Report
ISSN 0167-9708
Coden: TEUEDE

Eindhoven
University of Technology
Netherlands

Faculty of Electrical Engineering

In-situ Investigation of Pulsed Corona Discharge

by
Y.L.M. Creyghton
W.R. Rutgers
E.M. van Veldhuizen

EUT Report 93-E-279
ISBN 90-6144-279-6
November 1993

Eindhoven University of Technology Research Reports

Eindhoven University of Technology

Faculty of Electrical Engineering
Eindhoven, The Netherlands

ISSN 0167-9708 Coden: TEUEDE

IN-SITU INVESTIGATION OF PULSED CORONA DISCHARGE

by

Y.L.M. Creyghton
W.R. Rutgers
E.M. van Veldhuizen

EUT Report 93-E-279
ISBN 90-6144-279-6

Eindhoven
November 1993

CIP-DATA KONINKLIJKE BIBLIOTHEEK, DEN HAAG

Creyghton, Y.L.M.

In-situ investigation of pulsed corona discharge / by Y.L.M. Creyghton, W.R. Rutgers, E.M. van Veldhuizen. - Eindhoven : Eindhoven University of Technology, Faculty of Electrical Engineering. - Fig, photos, tab. - (EUT report, ISSN 0167-9708 ; 93-E-279)
With ref.
ISBN 90-6144-279-6
NUGI 832, 812
Subject headings: flue gas cleaning / corona / pulsed power

In-situ investigation of pulsed corona discharge
Y.L.M. Creyghton, W.R. Rutgers, E.M. van Veldhuizen

This work is the final report on behalf of the EUT of the JOULE project CLEAN (contract no. JOUF 0053-C) which was sponsored by the European Community.

Abstract

High voltage pulses are created with spark gap switched circuits to create positive corona streamer discharges. The pulse voltage rise time is in the order of tens of nanoseconds and its duration is less than one microsecond to avoid breakdown. The corona discharge is investigated with electrical and *in-situ* optical techniques to determine the energy per pulse and the behaviour of the discharge. The highest energy per pulse is 9 J per meter anode length. The discharge stucture is determined with Schlieren photo's and CCD images, the number of streamers is always 4-7 cm^{-1}. The streamer diameter is determined with the CCD camera and is found to be 200 μm. Emission spectroscopy is used to determine the gas temperature, which remains close to room temperature, and the electron energy, which is 10 eV in the streamer head, 1 eV in the secondary streamer and 0.5 eV in the residual streamer channel. The discharge is used to remove NO from gas mixtures and flue gas. The best cleaning efficiency observed is 50% or 125 ppm NO removal at an energy input of 6 Wh/Nm^3, this result is obtained with short electrical pulses (20 ns) and a high gas humidity (10%). Models for the streamer propagation and the chemical reaction kinetics are described and are shown to be in qualitative agreement with the measurements.

Keywords: pulsed corona, streamer discharge, flue SO_2/NO_x removal, discharge structure, streamer propagation, reaction kinetics, spectroscopy

- Creyghton Y.L.M., and W.R. Rutgers, E.M. van Veldhuizen
  In-situ investigation of pulsed corona discharge.
  Eindhoven: Faculty of Electrical Engineering, Eindhoven University of Technology, 1993
  EUT Report 93-E-279

- Adresses of the authors:

  Y.L.M. Creyghton
  E.M. van Veldhuizen
  Section of Electrical Energy Systems
  Faculty of Electrical Engineering
  Eindhoven University of Technology
  PO Box 513, 5600 MB Eindhoven, The Netherlands

  W.R. Rutgers
  KEMA N.V.
  Utrechtseweg 310
  6812 AR Arnhem, The Netherlands

Contents

1. Introduction

This final report summarises the work made under contract JOUF-0053-C for the European Economic Community in the period of July 1990 until June 1993. This contract is being undertaken by a consortium comprised of ENEL from Italy, AEA Technology from the UK and the Eindhoven University of Technology from The Netherlands. This part, section A: "In situ investigation of pulsed corona discharge", is the report from the EUT and is dedicated to the work performed under this contract in the period from July 1993 until June 1993. Since this report is a review and a summary of previous work parts of it can be found in previous publications (refs. [1-14]).

The work at EUT is part of the scientific program of the Division Electrical Energy Systems, within the project "Coal & Electricity". As such, it is for its largest part financed by the University. Nowadays, our research has to be partly financed by external institutions. Besides the European Commision other contributors are NV KEMA, STW (Stichting Technische Wetenschappen) en NWO (Nederlandse organisatie voor Wetenschappelijk Onderzoek), who we all want to thank for their support.

The global aim of the work is the clean use of coal for power generation. The combustion of coal in power plants leads to formation of sulphur and nitrogen oxides in the exhaust gas. This is in many cases a major contribution to acid rain. In Europe regulations for power plants become increasingly severe. The development of better techniques is required, now and in the future when a strong increase in coal consumption for power generation is expected. Good and efficient cleaning techniques are obligatory in most countries.

There are many processes to clean exhaust gas, some are already applied, others are under investigation. Plasma catalysis is one of the new combined processes and there are several methods to initiate this process. It has several advantages: a) it simultaneously removes SO_2 and NO_x, b) the end product is a dry powder, c) the end product can be used as fertilizer, d) the process can be retrofitted in existing power plants and e) the total costs are expected to be lower than for existing chemical cleaning processes. The probably oldest plasma technique is the electron beam (or e-beam) [15], the second is the pulsed streamer corona [16] and the most recent one is the dielectric-barrier discharge [17,18]. The latter discharge is also in use as a source for ultraviolet light [19] and for ozon production [20].

The e-beam method is the most advanced in technical terms, but recently doubts have risen about the reliabilty and the costs for large scale applications [21,22]. At this moment ENEL is constructing the largest facilty in the world to test the corona method with exhaust gas from a coal-fired power plant [23]. The dielectric-barrier discharge is up to now only demonstrated at laboratory scale with artificial gas mixtures [17,18].

The results of the discharge methods are encouraging from a point of view of the cleaning effect. Many uncertainties, however, still exist on the requirements of the power supply, the physical and chemical processes that occur in the gas, the energy efficiency and the extrapolation to large scale systems.

- The power supply still has two major questions. The first is the shape of the applied voltage, i.e. rise time, amplitude and time duration. The second problem is the life time of the switch in the power supply if pulses are used.
- The plasma physics part of the discharges is currently in development at many places, but the non-equilibrium discharge in a gas mixture is extremely complicated and a large effort is still required for a full understanding and also for quantitative predictions.
- The chemistry of the cleaning proces is also very complicated. Results of the models available do not confirm the experiments: they predict lower cleaning efficiencies than observed experimentally [24]. The answer to this shortcoming may be the inclusion of chemical reactions in the liquid phase, as happens in the atmosphere when acid rain is formed [25]. This proces is also mentioned as a possibility to obtain higher cleaning efficiencies (upto a factor 10!) [26].

These problems will be adressed by the partners of this project. Chapter 2 describes how this work is divided in work packages. The packages for the EUT will be treated in more detail. The remaning part of this report presents the work and the results obtained at EUT, where the subdivision in work packages and activities is maintained as far as possible.

2. Objectives (Work packages and activities)

The work is divided among the three partners into nine work packages (WP):

WP1: Generation and propagation of corona streamers (TUE)
WP2: Radical production (TUE)
WP3: Narrow pulse power supply equipment and testing (ENEL)
WP4: Innovative pulsed power supplies (AEA Technology)
WP5: Design and testing of reactor electrode structures (ENEL)
WP6: Basic compound injection (ENEL)
WP7: End products (ENEL)
WP8: Process experimental investigations (ENEL)
WP9: Electromagnetic compatibility (AEA Technology)

The parts of EUT will be discussed in detail here. This concerns work packages 1 and 2, which both aim at experimental in-situ investigation of the pulsed corona discharge, in combination with model calculations, in order to provide a better understanding of the processes involved. Quite roughly it can be stated that WP1 deals mainly with the physical processes and WP2 with the chemical aspects. The results are to be used for the optimisation of the overall cleaning process in technical and economical terms.

Work package 1: Generation and propagation of corona streamers

Objectives:

Investigate pulsed corona discharge with nanosecond rise time as used for flue gas treatment for its fundamental physical aspects. Perform measurements to investigate the structure of the discharge with optical in-situ methods.

Activity 1.0: The small set-up

Create a reactor cell, the so-called small set-up, which uses a variety of discharge configurations and gas mixtures from cylinders. A pulsed power supply is to be constructed which offers a large range of parameter variation for amplitude, rise time, repetition rate and DC bias. Also methods for the determination of the electrical quantaties will be developed.

Activity 1.1: Discharge structure

Schlieren photography will be used to record the heat released in the discharge paths. Therefore it not only reveals the spatial structure of the discharge but it also gives information about the heat dissipation.

Activity 1.2: Spectroscopy

The optical emission of the discharge will be spectrally resolved with a monochromator. This gives an indication of the average electron energy and the gas temperature in the discharge channel.

Activity 1.3: Light emission

The optical emission of the discharge will be recorded with photomultipliers and a CCD camera with or without a gated image intensifier. This gives information about the streamer stucture in space and time. Streamer inception properties and propagation velocities will also be measured using optical emission.

Activity 1.4: Measurements in flue gas

As far as possible the optical measurements performed at the small set-up will be repeated at the large set-up. (Due to the limited optical acces Schlieren and CCD measurements are not possible.)

Activity 1.5: Streamer propagation modelling

A one-dimensional model for streamer propagation will be made, based on the flux-corrected-transport algorithm. Its results are to be compared with data from the experiments, but the model also provides results which are not accessible for direct measurements, such as electric field strenghts and particle densities. (The model work is performed at IVTAN, i.e. the Institute for High Temperatures, in Moscow, (partly) as a subcontract of this project.)

Work package 2: Radical production

Objectives:

To perform measurements on the chemical aspects of the cleaning process. It will be attempted to perform in-situ measurements of active particles in the discharge. Also a model for the chemical kinetics will be developed.

Activity 2.0: The large set-up

A second reactor is to be created, the so-called large set-up, which uses air or flue gas from a methane burner. It will have its own power supply with higher voltage amplitude and power output and it will be equipped with controlled injection of SO_2, NO and NH_3 and a safety system against electrical and chemical hazards.

Activity 2.1: Time resolved UV emission and absorption spectroscopy

A diagnostic systems will be installed in order to detect chemically active

species such as OH and ozone.

Activity 2.2: Determination of cleaning efficiency and end products

A limited effort has been put into a measurement of the cleaning efficiency and the analysis of end products. This is necessary for a comparison of our results with those of other investigators.

Activity 2.3: Model of the chemical kinetics

The time dependence of the density of chemical species will be calculated from a set of first order differential equations. An reaction analyser will be added to find the dominant reaction paths (work also performed at IVTAN). The results will be compared with experimental data.

The combination of WP1 with the small set-up and WP2 with the large set-up cannot be maintained strictly. Electrical measurements are, of course, also performed at the large set-up, and some chemical measurements to determine the cleaning efficiency have been done at the small set-up. Nevertheless this subdivision is maintained throughout the report.

3. Experimental arrangements

3.1 Introduction

The systems that are made for the experiments are described in this chapter. Most of this work belongs to Activities 1.0 and 2.0, the work packages will be mentioned at each item when it is considered appropriate.

3.2 Corona configurations

The general aspect of a corona discharge is a pair of asymetric electrodes with one electrode having a strong curvature. Three geometries are often applied in laboratory experiments: point-plane, wire-plane and wire-cylinder. The last one is the best for gas treatment in practical applications with large flow volumes. The other ones are in some cases easier to access, experimentally and theoretically.

All three configurations are used, but not with every measurement method. Only a description of the geometries will be given here, their use will be indicated in the according experimental sections. A point-plane set-up is given in fig. 3.1 with the typical dimensions as used in the experiments. Fig. 3.2 gives the wire-plane situation, fig. 3.3 the wire-cylinder for experiments in air. These three possibilities are all used in the small set-up for the activities of WP1. For the large set-up only a wire-cylinder configuration is used for measurements in air and flue gas. A segmented inner cylinder is made in the last configuration to perform current measurements on different parts or to do a balanced measurement of the current with a part of the wire insulated.

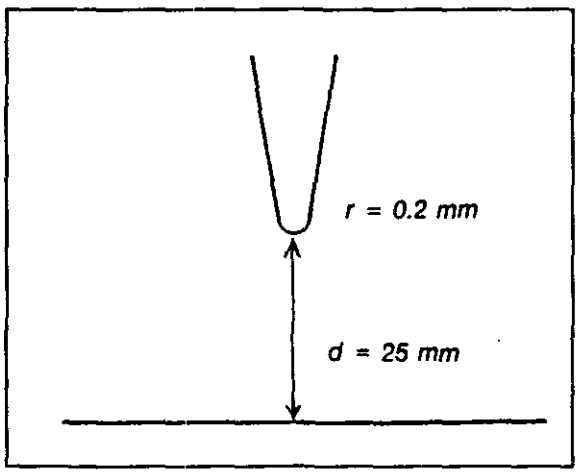

Fig. 3.1: Point-plane configuration

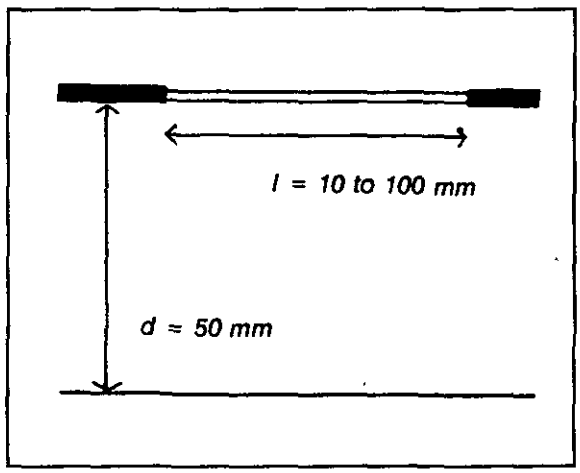

Fig. 3.2: Wire-plane configuration

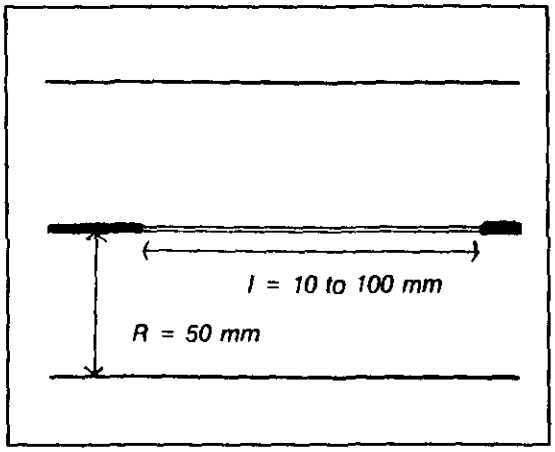

Fig. 3.3: Wire-cylinder configuration

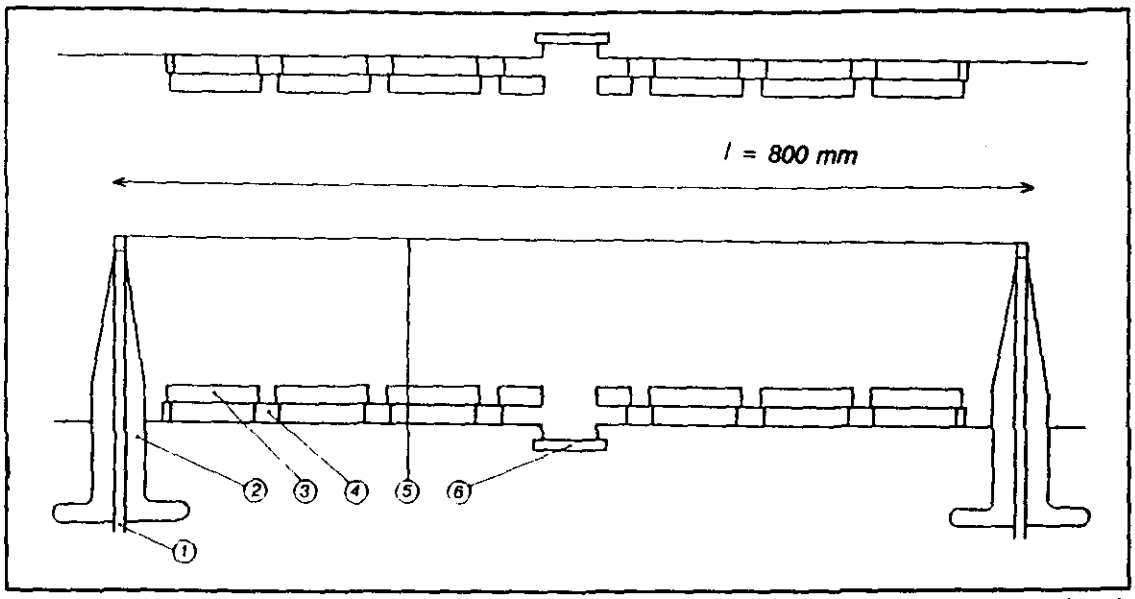

Fig. 3.4: Wire-cylinder system for flue gas experiment. 1: high voltage feed-through, 2: teflon insulator, 3: cathode rings, 4: support rings, 5: corona wire, 6: viewing port

3.3 Gas mixture system (WP1)

The small corona cylinder as shown in fig. 3.3 gives a simple possibility to perform measurements in pure gases. The diagram of the gas flow system used for this purpose is given in fig. 3.5. High purity gases are taken from cylinders through reducing valves and flow controllers. The basic gas used in these experiments is nitrogen. The flow is empirically adjusted to a value where all air influences are avoided (150 ltr/hr). Reproducible results are than obtained provided a settling time of severall minutes is taken into account.

The amount of mixtures is adjusted realative to the nitrogen flow. The gases that have been added are oxygen or carbon dioxide or both, upto a relative amount of 50%. All experiments with the mixtures have been perfor-

med at room temperature. During the NO removal experiments in the small set-up the gas is flowing through water, both have the possibilty of electrical heating in order to change the temperature and the relative humidity of the gas.

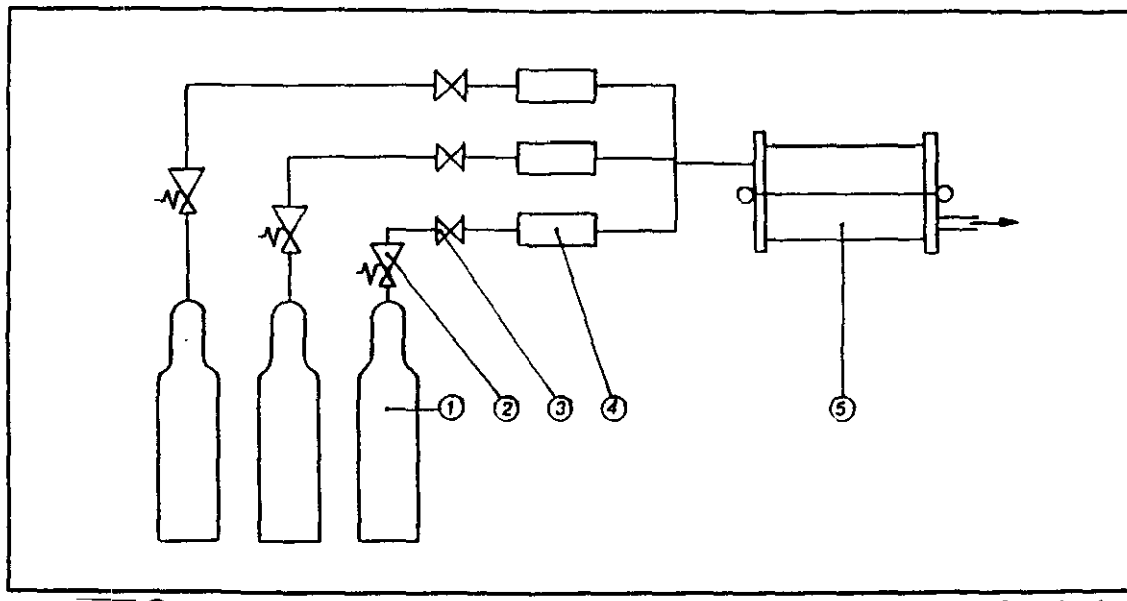

Fig. 3.5: Gas mixing system, 1: gas cylinders, 2: reducing valves, 3: closing valves, 4: flow meters, 5: corona cylinder.

3.4 Natural gas burner (WP2)

A clean gas is a big advantage for optical experiments, specially for absorption techniques. Therefore a natural gas burner is chosen to produce flue gas. Such a system also has the advantage of flexibility of operation and no concerns about the supply. Since the experiments are to be performed at realistic conditions, as far as possible, the corona dimensions should not be too small (see fig. 3.4). The required burner capacity, following from the required flow velocity, is in the order of 100 kW thermal power.

A burner is installed from the firm Klöckner, type KL.30.1.RG. It is a small size industrial system with a low-NO_x burner having a maximum capacity of 185 kW. The inlet gas flow can be adjusted downto 25% of its maximum. A mechanical coupling to the inlet valve for air ensures the proper air-to-fuel ratio across this entire range. The maximum gas consumption is ~20 m^3/hr, giving a flue gas production of ~200 m^3/hr. The burner is connected to a boiler, Fröling FSM-130-NT, with has the same maximum power as the burner. A picture of the two components is given in fig. 3.6.

The temperature of the flue gas at the exit of the boiler depends on the gas flow of the burner and on the temperature of the water in the boiler. The upper and lower limits that can be obtained are 250 and 70 °C. These values are coupled with a certain flow rate, so a heat exchanger is installed in order to reduce the temperature at high flow rates. This exchanger can be by-passed

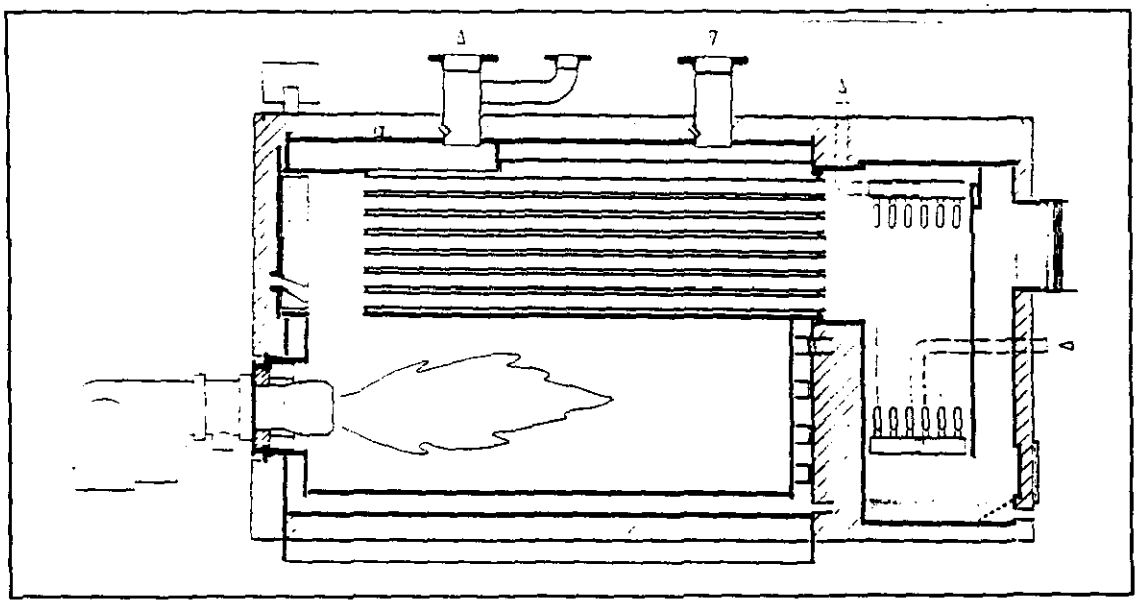

Fig. 3.6: Burner, boiler and heat exchanger

with valves. A three-way valve behind the heat exchanger controls the separation of the gas flow into two parts: one goes to the corona experiment and the other goes directly into the chimney. In this manner both the temperature and the flow rate of the flue gas can be controlled at the experiment. The temperature range is from 160 to 70°C and the flow velocity from ~0.5 to 5 m/s. These ranges are sufficient for experiments under realistic conditions.

The water content of the flue gas from a methane burner is two times higher than from a coal burner due to the different ratio of C and H atoms (gas: C/H = 1/4, coal: C/H ≈ 1/1). The measured concentrations for our burner are 8% CO_2 and 16% H_2O, for coal this will be 12% CO_2 and 6% H_2O. The influence of the water content can be checked with our burner in only one way. The installation can be equipped with an oil burner which gives equal concentrations for CO_2 and H_2O, because here C/H = 1/2. Measurements will have to be carried out at a coal fired plant if further comparison is required.

SO_2 and NO injection is done from cylinders with mass flow controllers, Tylan FC 280-S. These enable amounts of additives from 0 to 2000 ppm. The full scale range of the controllers is adjustable with calibrated orifices. The accuracy is always 1% of the full range.

Figure 3.7 gives an overview of the complete burner system with corona set-up and the chimney.

3.5 Control and safety system (WP2)

The corona discharge experiment in flue gas has several aspects that are

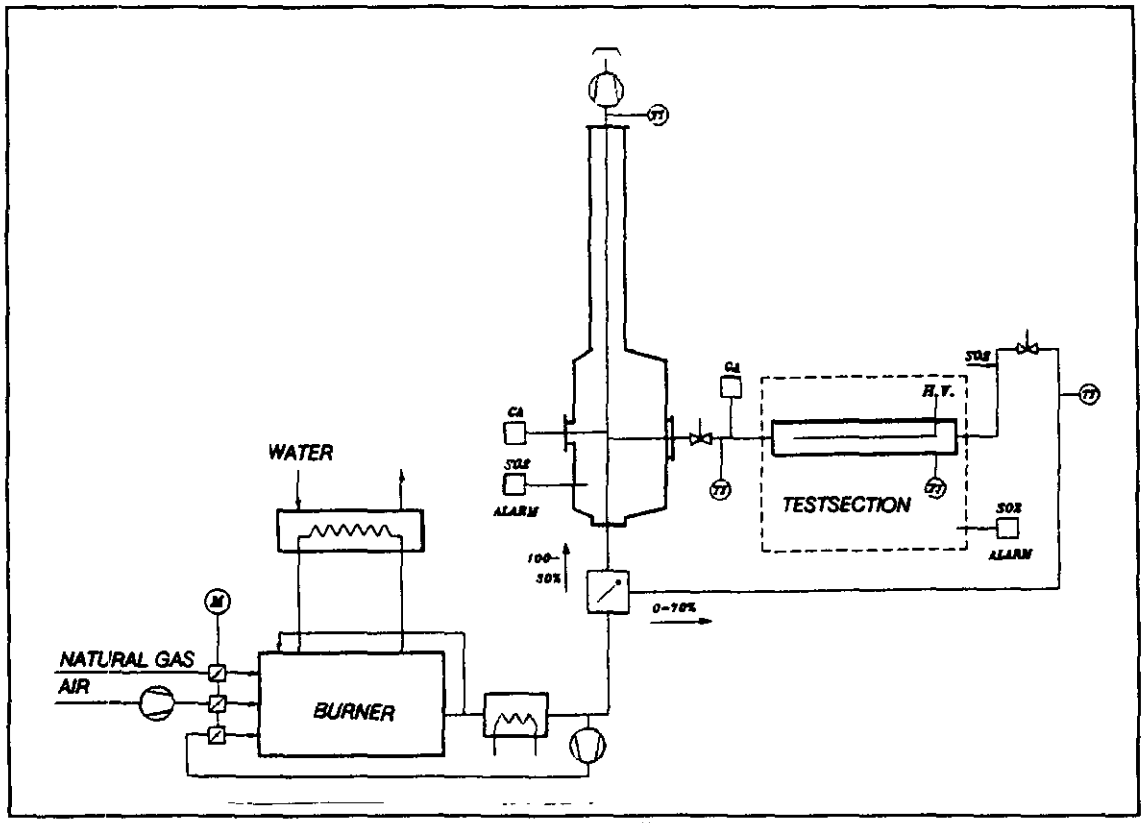

Fig. 3.7: A schematic drawing of the total flue gas set-up

potentially dangerous. These are the natural gas burner, the chemical additives and the high voltage. All these items require specific precautions to ensure the safety of the people in the laboratory.

The gas burner has its own control and safety system, the EDS, i.e. Electronic Diagnostic System, made by Oskamp, Naarden. This system monitors the pressures of the natural gas, the burner and the exhaust gas and the temperatures of the water in the boiler and the exhaust. It controls the gas and air valves and the ignition system. This garantees a safe operation of the burner. There is a possibilty to switch off the burner with a remote control.

The addition of chemical components is performed downstream as far as possible to minimize the risk of leakage. Mixing is not a problem since the flow is very turbulent. A separate SO_2 alarm is installed close to the corona cylinder, which detects SO_2 at a level of 1 ppm.

The experimental section is controlled by a progrogrammable logic controller (PLC), Siemens S5-100U. This is a small size, industrial controller with a modular build-up, consisting, in our case, of a processor unit, two units with 8 digital inputs, two units with 8 digital outputs and one unit with two analog outputs. It is a stand alone system and the processor continuously checks the inputs and sets the outputs according to its internal program. The input for the hand programmer has been adapted to match its current loop

signals to an RS-232 line, so that communication with a personal computer (PC) is possilble. This enables programming with the PC, but also reading and writing of the settings of the ports of the PLC.

The inputs of the PLC are connected to switches that detect the state of the gate valves, the blowers, the burner, the SO_2 alarm, the flow detectors, the water leakage detector and the air supply. The digital outputs can switch on and off the gate valves, the blowers, the valves for the flow controllers, the high voltage interlock and the alarm indication. It can switch of the burner but switching on must be performed manually and can be done only if this switch is in the right position. The analog outputs go to the flow controllers for the chemical additives.

The PLC program consists of a lists of statements mainly of the type IF ... THAN .... For example, if a gate valve is closed, than the burner cannot be switched on. Or, if SO_2 is detected the alarm indication will go on and the burner will be switched off. This program is excecuted in a continuing loop and provides a high degree of safety also because the hardware is specially designed for this purpose. All valves are chosen so that in case of a failure of the mains supply they automatically fall into the safe position by means of a mechanical spring or by pressurized air from a back-up vessel.

The communication with the PC allows the use of a supervision program. The choise is made for the program WIZCON (PC Soft International Ltd., USA). This is a software package for industrial use on the plant-floor level. It supervises PLC's, enabling the operator to interact with the activity in the plant through animated pictures. It can work with many PLC's simultaneously, it can perform background logging and make graphs and reports.

Commucation with PLC's is performed by so-called VPI's (Virtual PLC Interface). The main function of a VPI is translating a general "read" or "write" instruction into a set of detailed commands for a specific piece of hardware. The response must also be translated back to WIZCON.

Two VPI's have been written, one for the Siemens PLC and the other for a CAPRO computer. The CAPRO is a autonomous CAMAC crate controller/processor (obtained from INCAA BV, Apeldoorn). CAMAC is a modular system for (fast) measurements and control in a laboratory environment. It is used in the flue gas set-up to monitore thermocouples and to read out the mass spectrometer and the electrochemical cells. The signals of the Chromel-Alumel thermocouples (Thermocoax) are amplified and than digitized with a 12 bit A/D converter (model 5302, Bi Ra Systems, Inc., USA). The other signals are digitised directly.

Wizcon also continuously reads the data from both systems and acts according to its own program. For example, if the flue gas temperature exceeds a certain value it will switch off the burner. This is a second layer for the safety in the laboratory, but it must never be the first one because it relies on software.

3.6 Pulsed power supplies

The shape of the voltage applied to the corona wire is an essential part of the process. One of the reasons to built small size laboratory set-ups is that parameter variation of the pulse shape is virtually impossible in large scale systems. In a laboratory environment there are two reasons to create pulses with a well defined, adjustable shape. The first is that one wants to investigate the dependence of the process on the pulse parameters. A range of parameter settings (much) wider than anticipated for the practical application is therefore desirable. The second reason is that a clean, oscillation free pulse shape enables a better evaluation of the discharge current and energy input, allowing a more detailed interpretation of the measurements.

The standard method in a laboratory to make high voltage pulses is to discharge a capacitor with a spark gap switch. This is a relatively easy method, a possible circuit is given in fig. 3.8. An uncommon feature of this arrangement is that the spark gap side with the trigger pin is grounded [27]. The spark gap is home-made and is has an adjustable gap distance and an air flow system which allows to operate the spark gap at pressures higher than one atmosphere. Two version are made. The first is shown schematically in fig. 3.9a and is used upto 50 kV, it can handle upto 2.5 bar and the gap distance is from 10 to 40 mm. The second, shown in fig. 3.9b, goes upto 100 kV, 5 bar and 50 mm.

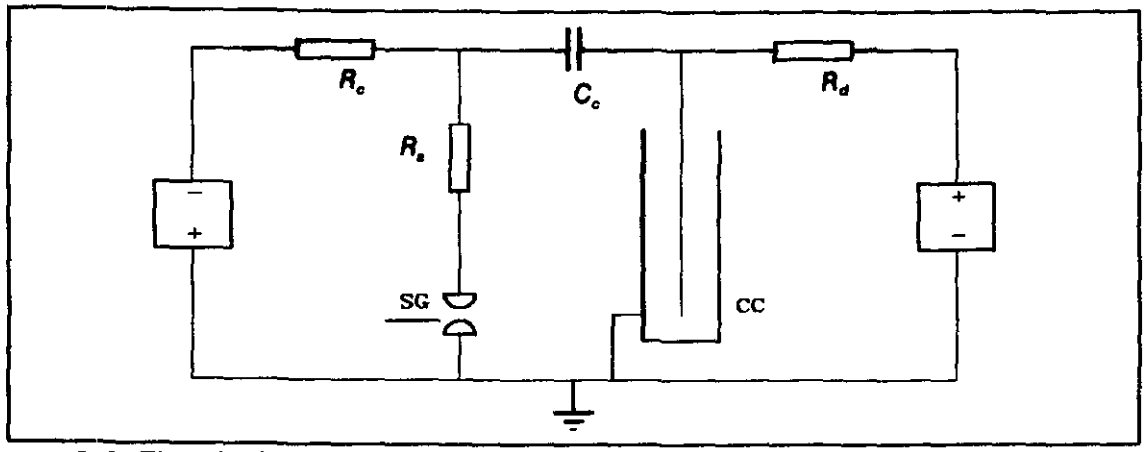

Fig. 3.8: Electrical circuit of the pulsed power supply. SG is the spark gap and CC the corona cylinder.

A 60 kV circuit has been constructed for the experiments with the small set-up. In this case the coupling capacitor, C_c, is 2 nF, the series resistor, R_s, 0-4 kΩ, the charging resistor, R_c, 10 MΩ and the discharging resistor, R_d, 50 MΩ. The series resistor is used to determine the rise time, which simultaneously reduces voltage oscillations. A second way to change the rise time is to put a small capacitor parrallel to the gap. In this case remains more or less a constant voltage source. The DC power supply is an OL603/8N made by Wallis Hivolt Ltd., UK. The capacitors are from LCC, USA, the resistors for R_s are the RCEC type from MCB, France. The resistors for R_c and R_d are home made from 10 kV resistors, type VR68, NV Philips, the Netherlands. A DC voltage can be added

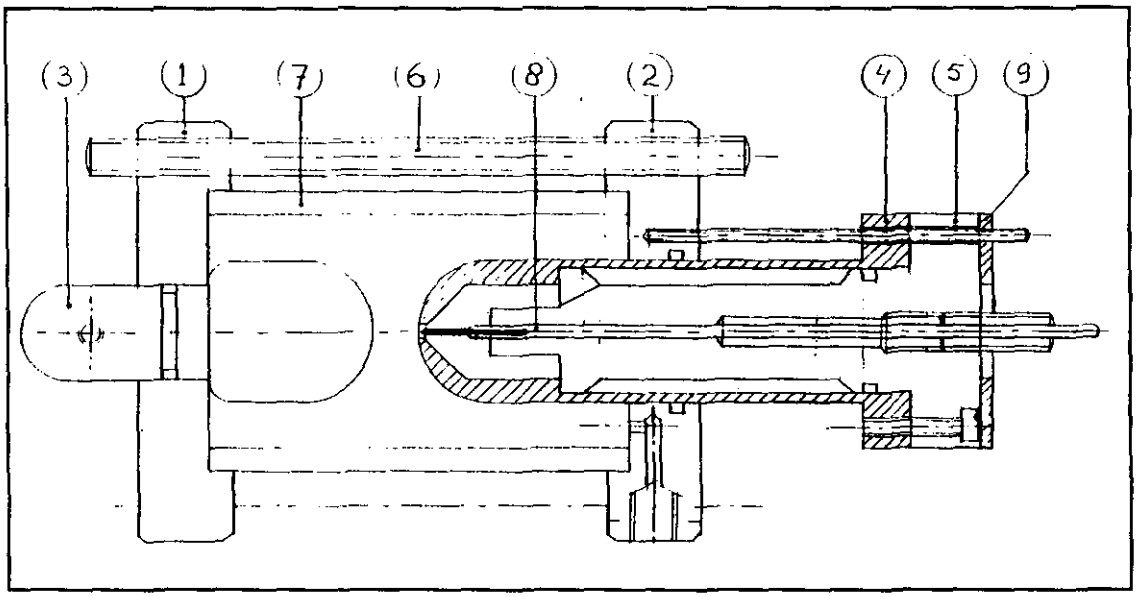

Fig. 3.9a: Spark gap for 10-50 kV and 1-2.5 bar

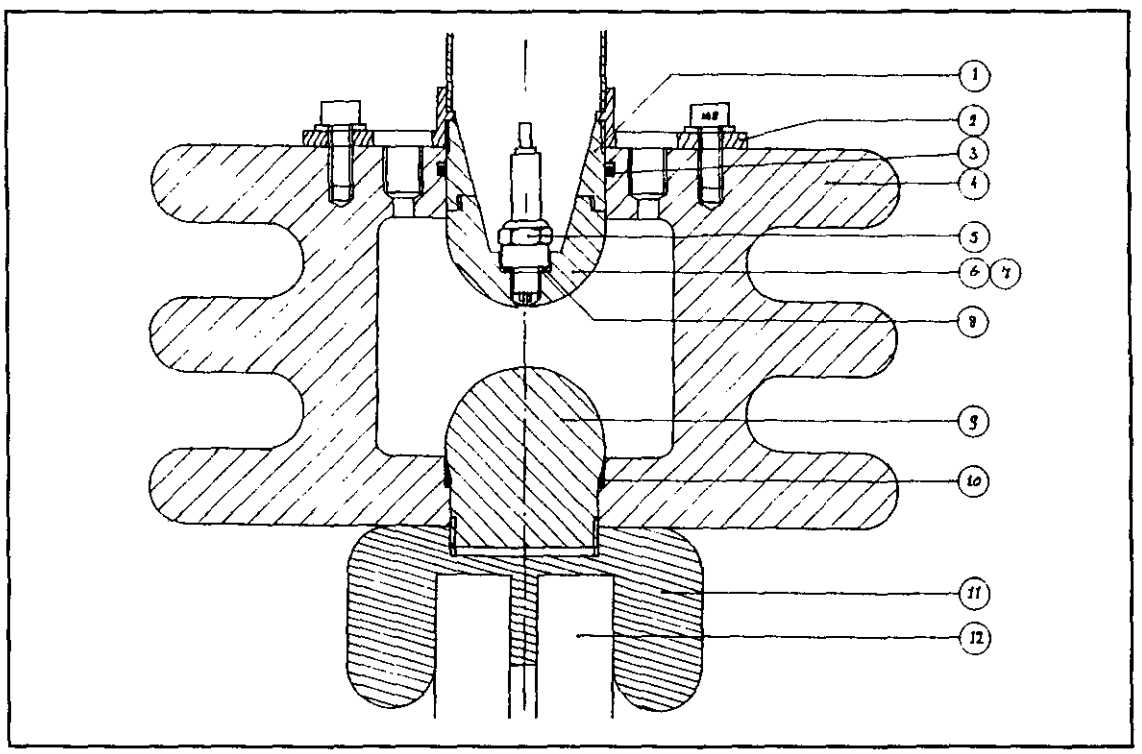

Fig. 3.9b: Spark gap for 20-100 kV and 1-4 bar

from 0 to 30 kV with a KV30-5S supply from Kilovolt Cooperation, USA.

The maximum voltage in the experiment is determined by the breakdown voltage of geometries used (see figs. 3.1-4) and is in the range form 30 to 40 kV. This voltage can be higher when the pulses are made very short. This can be done with a second spark gap which is triggered less than 1 μs after the first, for example using a delay line [28] or a second triggered spark gap.

The second circuit uses the same scheme, however with a maximum amplitude of 100 kV, which is used for the larger wire-cylinder reactor of the large set-up. This requires a more careful HV design of all the components and their connections in order to avoid spraying and damage when there is an occasional breakdown. The rise time of this circuit can be increased with an additional series resistor or a series inductance. The DC power supply here is a RR100-6N/220 made by Gamma High Voltage Research Inc., USA. The capacitors are 40A025 types from CSI capacitors, USA. They are 5 nF and 40 kV each, so for 100 kV three capacitors in series are needed. By putting series in parrallel values of 1.7, 3.4 and 5 nF total capacity can be obtained, mostly 5 nF is used. The connections between the capacitors are constructed in such a way that above 40 kV a breakdown in air will discharge a capacitor so an internal damage will be avoided. The resistor R_s in this case is the AL701 from Allen Bradley, UK, with a value of 1 kΩ. These resistors can be placed in parallel to obtain values of 0.25, 0.33, 0.50 and 1.0 kΩ. The resistors R_c and R_d are made in a similar way as the first, but with more components and air flow for cooling. Another KV30-5S power supply can be used for an additional DC bias.

3.7 Voltage and current measurement

The rate of rise of the corona voltage pulses must be very high in order to have an efficient initiation of the desired processes, i.e. 1 kV/ns or more. Since the amplitudes are also high, from 20 to 100 kV, they cannot be measured directly, it is necessary to use a voltage divider. Two types are possible: resistive and capacitive. The resistive divider has the advantage that it can measure DC, the capacitive is usually better at high frequencies. In practice the two are sometimes combined as is the case with the P6015 made by Tektronix, USA. This probe divides 1000x, has an input resistance of 100 MΩ, an input capacitance of 3 nF, a rise time of 10 ns and a matching network to match its impedance to the measuring apparatus in order to provide a linear frequency characteristic. This need for matching is a minor disadvantage, a major disadvantage is its limitation to 40 kV, although it is sometimes used for 100 kV pulses with modified insulation. This probe is used in all our experiments.

A second probe that is used is the capacitive voltage divider, model VD-305A, made by Pearson Electronics, Inc., USA. In air, this unit can withstand 50 kV and it has a division ratio of 11500:1. When filled with oil the maximum voltage is 300 kV and the division ratio 5000:1. It's capacitance is 18 pF and the shortest usable rise time 100 ns. This is not fast enough to determine pulse rise times, but this can be done at 40 kV with the Tektronix probe since the shape of the voltage pulse does not depend on the maximum voltage with the pulsed power supply used here. The Pearson can than be used to determine the actual maximum voltage on the wire. This is necessary to verify if extra losses occur.

The pulse current is measured with current transformers, often called Rogowski coils. Two types are available, both from Pearson Electronics, Inc.,

USA. The smallest is the model number 2877 with an inner diameter of 0.25 inch, a rise time of 2 ns and a sensitivity of 1 V/A, the second is model number 150 which has a 2 inch diameter, a rise time of 20 ns and a sensitivity of 0.5 V/A. Both types have an internal integrator and an output impedance of 50 Ω, so their outputs will be halved when they are terminated with a 50 Ω load.

The wave form measurements are performed with oscilloscopes. The fastest oscilloscope available for our experiments is the DSA601 form Tektronix Inc. This oscilloscope has two digitizers with a sampling time of 2 ns, so it can provide two channels with 2 ns sampling time or one channel with 1 ns sampling time. The effective resolution of these digitizers at their maximum speed is 6.5 bit, including the effects of the analog cicuitry. The scope has an internal memory to store data and it has many possibilties for triggering and calculations, such as integrating or Fourier transform. The second scope used is the model 9400 by LeCroy, France. It has two channels with a sampling time of ten nanoseconds. Both scopes have the possibility of computer connection by RS-232 or IEEE. IEEE is usually preferred because of its higher data transfer speed. This is essential for several optical measurements.

3.8 Triggering circuits

Two possibilities are often applied for the triggering of the spark gap. The easiest one is to make a rotating spark gap where the triggering is performed mechanically. The rotating spark gap consists of two metal spheres at fixed position and two spheres on the ends of a rotating axis that fits just between the fixid spheres. When the rotating spheres approach the fixed ones there will be a breakdown and the switch is closed because the discharge path has a relatively low resistance. When the spheres move away the discharge stops and the switch opens again. The spheres can be insulated from the motor drive so this switch has no EMC problems. The disadvantage for laboratory experiments is that its switching frequency is not very stable and it is not possible to trigger it in combination with a piece of equipment that should go first, e.g. the flash lamp in the absorption experiment.

The second triggering possibility is the use of an electrical pulse with sufficient voltage and energy. This pulse can be made by a pulse transformer or by a vacuum tube such as a small thyratron. The first option is preferred since the thyratron is expensive and has a limited life time. Transformers are made with a ferrite core using a primary coil of 10 windings and a secondary coil of 200 windings. The input pulse is made with a power MOSFET transistor (BUZ45 from Siemens) that switches a capacitor of 100 μF, charged at 300 V, with a switching time of 50 ns and a maximum current of 10 A. The electrical circuit is given in fig. 3.10.

This creates a secondary pulse of 10 kV or lower when there is a breakdown at the ends of the leads. If these ends are far apart the breakdown

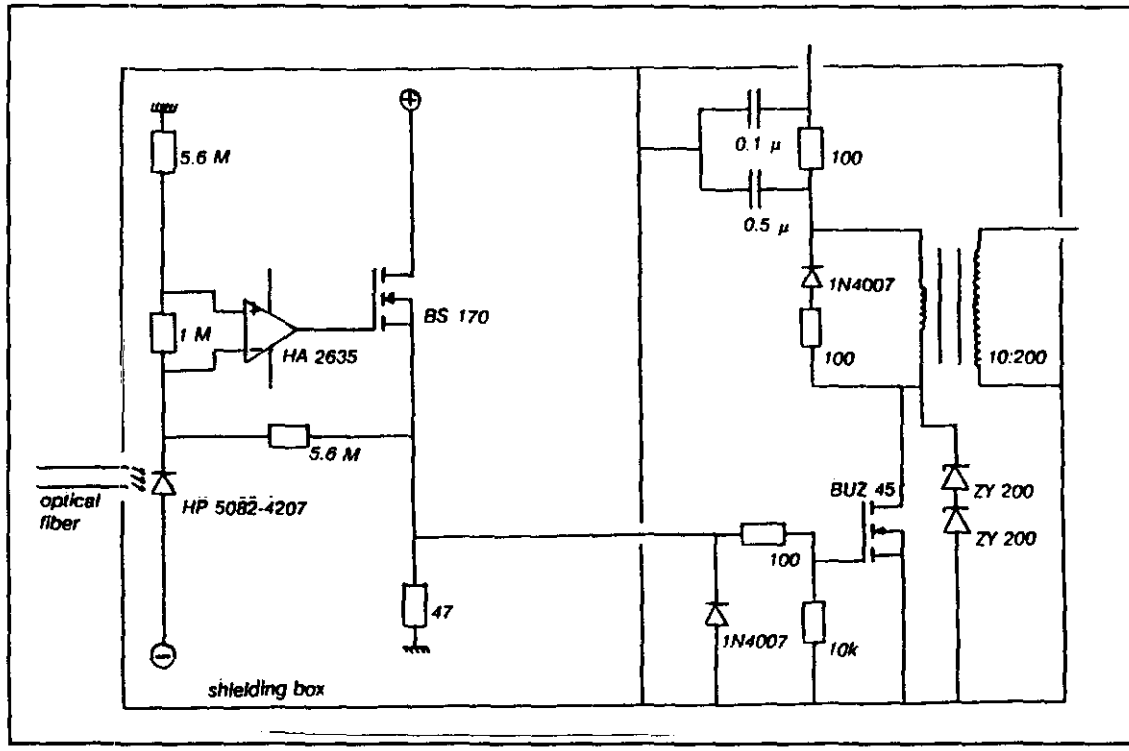

Fig. 3.10: Circuit for 10 kV trigger pulse

may occur inside the transformer. Than the windings have to be replaced. The 10 kV secondary pulse is sufficient for the spark gap shown in fig. 3.9a upto a pressure of 2.5 bar. The breakdown at the trigger pin has been observed with the voltage probe and the oscilloscope and this shows that the jitter in time is less than 200 ns. This is sufficiently accurate to trigger the corona in combination with the other equipment used in our experiments. The diodes in fig. 3.10 are essential to protect the transistor from reversed current pulses that come back from the transformer. Two circuits like this can be used to make a high voltage pulse with a width less than 1 μs.

4. Diagnostics

4.1 Introduction

This chapter gives a description of the measurement methods used and some background information on their previous achievements in similar applications. Besides the work package number also the specific activity is indicated where it is considered appropriate.

4.2 Optical emission (WP1, A1.3 and A1.4)

Optical emission is detected using photomultipliers, quartz fibers and lenses. The photomultiplier measurements have been applied to wire-cylinder configurations only. The light of a cylindrical volume, directed along the corona wire and with a diameter of 3 mm, is focused on a fiber and is registrated by a photomultiplier with a rise time of 2 ns. Streamers are produced at the non-insulated part of the wire, 10 - 40 mm from the lens. The small divergence of the optical volume (solid angle $< 1^\circ$) makes it possible to relate the leading edge of the optical signal to the time at which streamers pass the boundary of this volume. The streamer propagation velocity is calculated from the time delay between signals from two radial positions with a distance of 4 mm, see figure 4.1. The photomultiplier output signals are measured with an oscilloscope (Tektronics DSA 601) with 1 GHz sampling frequency. The optical signal per pulse is due to a number of streamers (ranging from 1 - 10 depending on the radial position). There is a considerable variation in the time delay from pulse to pulse but when several hundreds of pulses are averaged the calculated delay becomes well determined and reproducible.

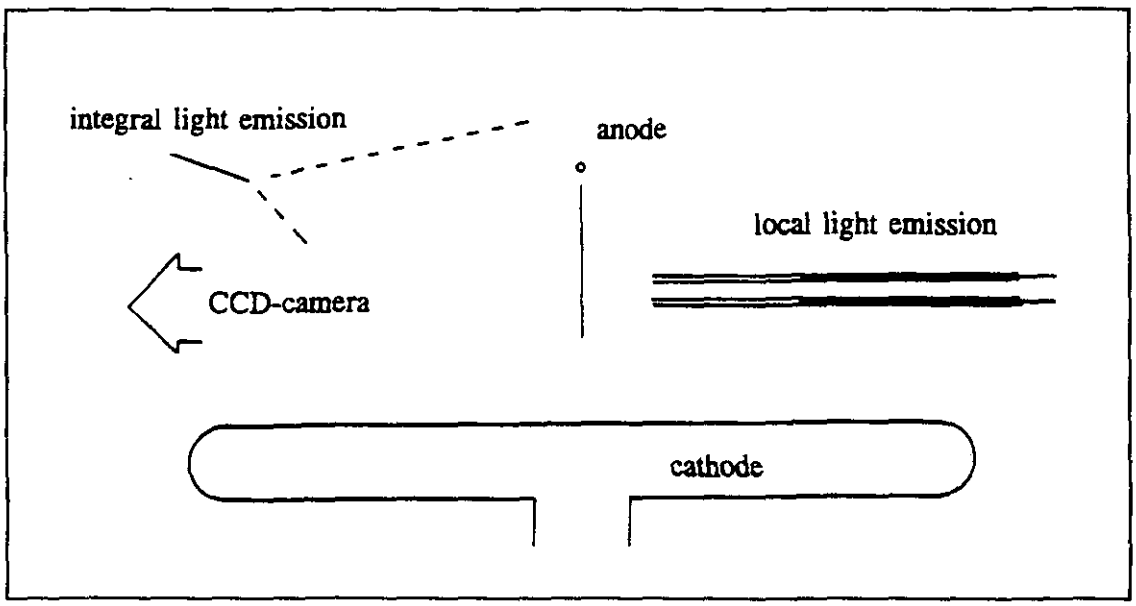

Fig. 4.1: Experimental arrangement for the measurement of the streamer propagation velocity.

4.3 CCD detector (WP1, A1.1)

In order to detect spatially resolved light emission a Charge Coupled Device (CCD) detector is used (EG&G model 1430-P). A 60 mm lens (Nikon) forms an image of the discharge on the detector. The detector contains 576x-384 light sensitive pixels having a size of 23x23 μm each. The pixels are sensitive in the range 400-1100 nm with a maximum quantum efficiency of ~38 % at 750 nm.

The corona configuration used is either point-plane or wire-plane. The electrode configuration is placed in a closed box (150x150x150 mm) which is gas tight and made of celeron. Different point radii or wire diameters can be used. The corona point or wire is placed in the center of the box. The gap distance can be easily varied upto 50 mm by displacement of the cathode plate (100x100 mm). Several optical windows are provided in order to perform optical measurements with photomultipliers simultaneously. The box containing the corona configuration is placed against the inner wall of a larger metal box, which provides the necessary electromagnetic shielding of the power supply. The "gas tight box" containing the corona can be displaced in a sense perpendicular to the optical axis of the CCD detector, see Fig. 4.2. Light is recorded by the CCD detector when the shutter is opened. The shutter minimum opening time is 50 ms. Single shot discharges are recorded by triggering the high voltage circuit with a synchronisation signal which corresponds with complete opening of the shutter. Also the light from a series of discharge pulses can be obtained by opening the shutter during an externally triggered repetitive discharge. A gated intensifier is available which can be used for low level signals or for short exposure times, 34 ns is the shortest opening time.

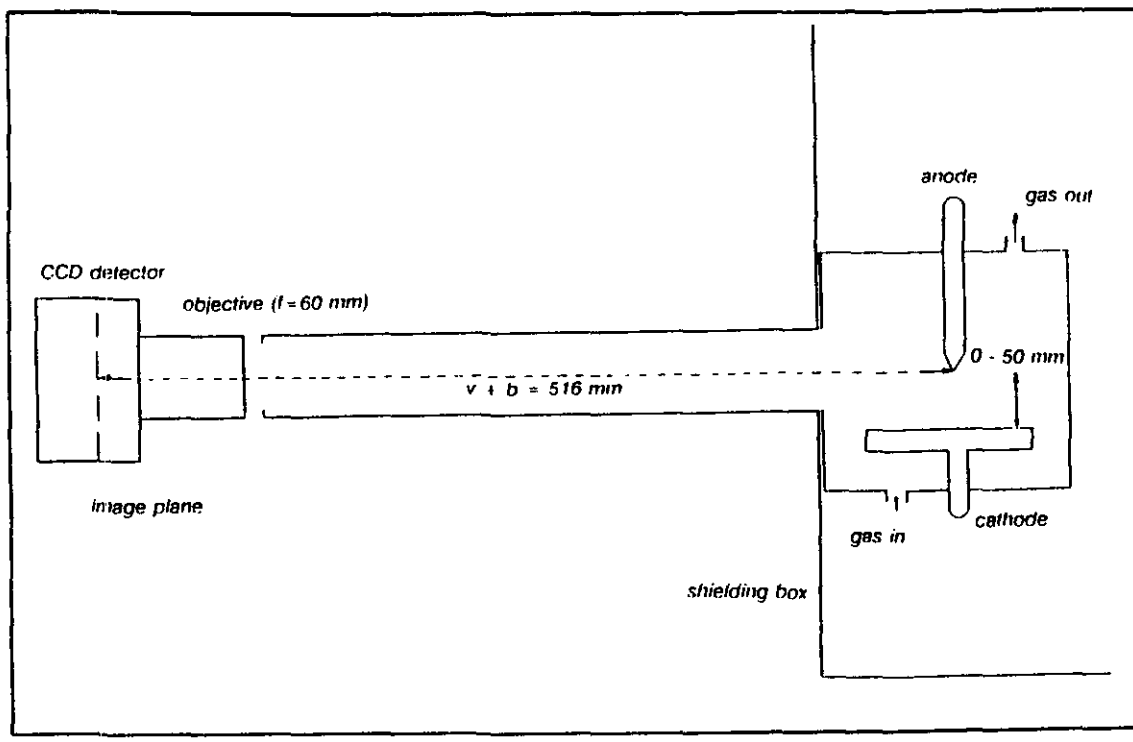

Fig. 4.2: Experimental set-up for CCD-detector

4.4 Schlieren photography (WP1, A1.1)

4.4.1 Introduction

Schlierenphotography has been used often to study the transition from a primary streamer to a spark (see for example Domens et al., [29]). In fact three different types of Schlieren techniques can be used to study gas discharges [30]. In the Toepler method the displacement of the beam, refracted in regions whith a density gradient dn/dx, is recorded. Interferometric methods depend on the value of the refractive index n, since the velocity of light in the discharge region is c/n. The Shadow Schlieren method is such that only regions of large d^2n/dx^2 are visible. Schlieren techniques are rarely used to study the primary streamer itself, without transition into a spark. This is probably due to the low energy density and small diameter of the primary streamer requiring both high sensitivity and high spatial resolution.

G. A. Woolsey et al. [31] investigated primary streamers of a positive DC corona discharge in air at atmospheric pressure using the shadow method. They measured the angular deflection of a laser beam as function of radial distance from the streamer axis with good time resolution. A quantitative analysis, including Abel inversion, appeared to be possible. They calculated a maximum decrease of neutral density in the residual streamer channel up to 13.5 %.

The primary aim of the present Schlieren study is to determine the discharge structure of the positive streamer corona discharges produced by fast rising pulses along a wire in a wire-plate configuration. In order to visualize the streamers having small diameters (≤ 100 μm) and low energy density the use of a set-up with good spatial resolution and good sensitivity is necessary. Some geometrical optical considirations for attaining high resolution in a Schlieren experiment, as proposed by J.W. Hosch and J.P. Walters [32], are used.

4.4.2 The Schlieren set-up

The Schlieren set-up is schematically drawn in figure 4.3. The light emitted by a flashlamp (EG&G, FXQS-850 with UV bulb) is focused using a quartz lens on a quartz fiber with a diameter of 600 μm. The fiber is positioned in front of a slit with a width of 60 μm. With a parabolic mirror a parallel light beam is produced. After passing through the discharge gap the light beam is focused by an identical mirror on a knife edge. The second mirror produces also an image of the discharge gap on a photographic film in a camera (Mamiya M645) without objective. The demagnification factor is 0.64. The camera shutter is used to trigger the spark gap of the high voltage pulse circuit. Black-white films (Kodak TMY120) upgraded to 3200 ASA are used. The flashlamp, which produces a light pulse with 15 μs duration, is triggered after an adjustable delay time (Δt = 2 - 2000 μs) following the start of the high voltage pulse.

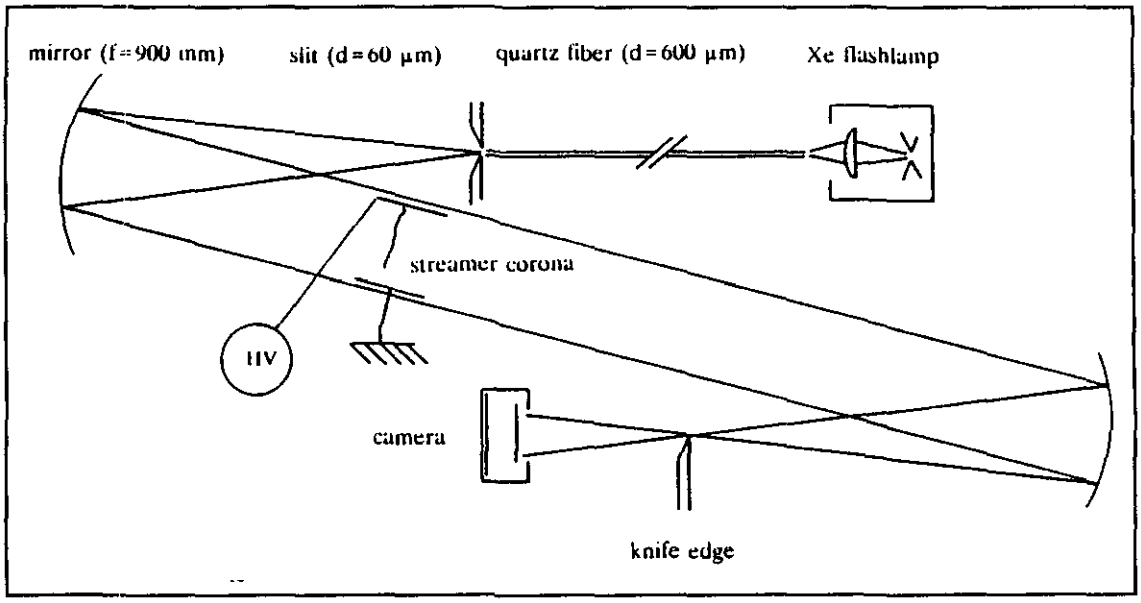

Fig. 4.3: Schematic diagram for Schlieren photography

Optical aberrations (astigmatism and coma) are minimized using small mirror angles ($\sim$ 0.17 rad). The two mirrors have the same focal length (f = 900 mm). They are operated at the same off-axis angle. The major advantage of this Z configuration is the fact that coma is canceled in the plane of the knife-edge. The knife edge is set in the middle of the focus parallel to the slit. Adjustments of the knife edge position are made using intensity measurements with photodiodes positioned off axis at the image plane. In absence of the discharge 50 % of the light intensity is allowed to pass the knife edge barrier. The films are developed such that the non perturbated background is grey.

The intensity profile of the source image at the knife-edge plane has been measured (Fig. 4.4). The width of the intensity profile is nearly the same as the slit diameter showing that a good image of the source (slit) is produced at the knife-edge plane.

4.4.3 Sensitivity and interpretation

The distance from the mirror to the knife edge was chosen to provide a compromise between light intensity and sensitivity. The sensitivity is defined as the minimum deviation angle α_{min} that can be detected. This angle depends also on the number of grey tints that can be distinguished or measured from the Schlieren picture:

$$\alpha_{min} = h/(N\,d)$$

where h is the height of the image, N is the number of grey tints and d is the distance between knife edge and discharge. In our set-up $\alpha_{min} = 2.6/N\ 10^{-5}$ rad

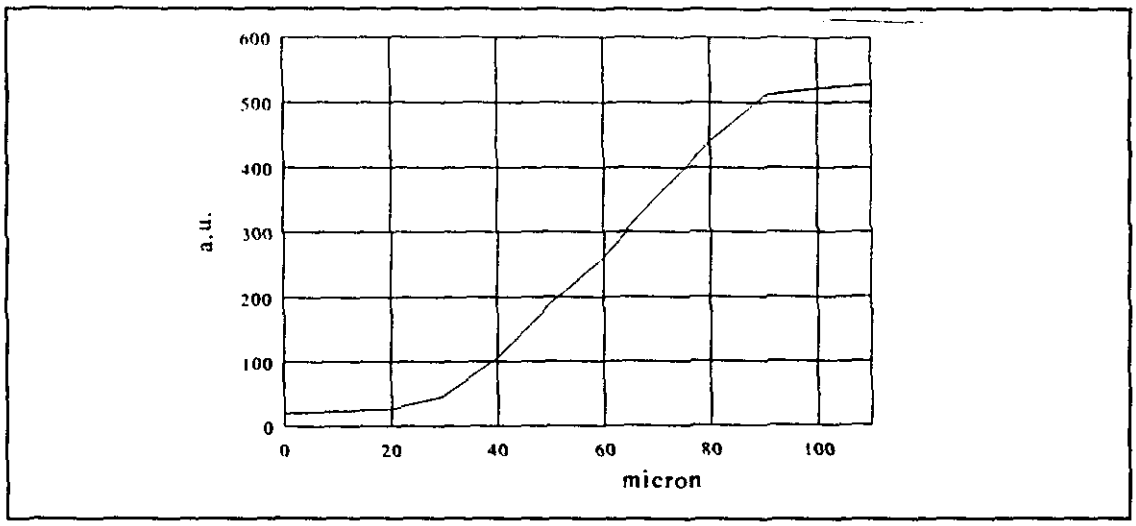

Fig. 4.4 Intensity profile measured at the knife-edge plane

or taking N = 10 as a reasonable value, $\alpha_{min} = 1.3\ 10^{-6}$ rad.

A mathematical treatment of the observed pictures is in principle possible. The deflection of light passing through a neutral gas density perturbation with cylindrical symmetry (which results from gas heating after a streamer has passed through the gas) is schematically illustrated in figure 4.5.

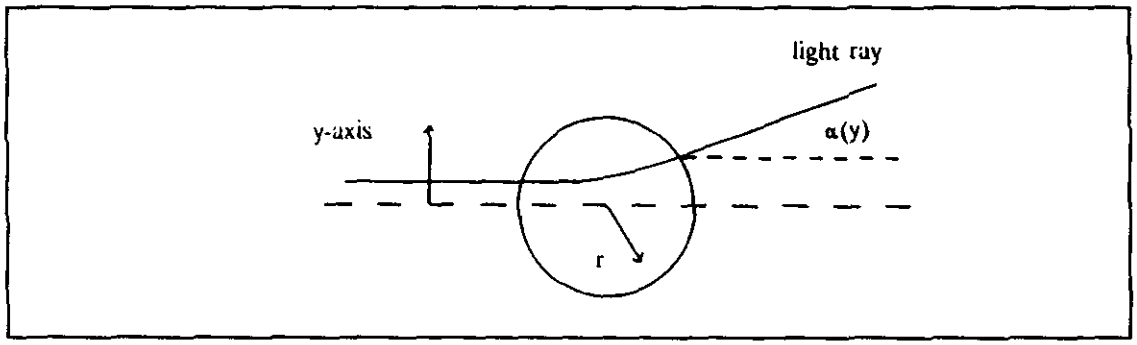

Fig. 4.5: Deflection of light passing a cylindrical symmetric density perturbation

The deflection angle can be expressed as described in [33]:

$$\alpha(y) = 2y \int_{y}^{R} \frac{1}{n(r)} \frac{\partial n}{\partial r} \frac{dr}{\sqrt{(r^2 - y^2)}}$$

A density perturbation having positive and negative gradients causes dark and light patterns at the image plane. The interpretation of the image is rendered difficult by the fact that light at one position at this plane can originate from more than one positions in the density perturbation, each having different local

density gradients. This "covering" of light rays originating from different radial positions complicates the calculation of density profiles from the observed images.

This problem can be avoided by using a second slit instead of the knife edge. However the range of density gradients that can be observed is then limited by h/d. Furthermore, the slit width must be much smaller than the characteristic diameter of the density perturbation. This condition can not be realised because a minimum slit width of 60 μm is necessary in order to obtain enough light. This width is of the same order as the total streamer diameter.

On the other hand, the inverse procedure, calculation of the intensity profile at the image plane can be easily done. This calculation needs an assumption or a calculation for the neutral density profile, the angular deflection formula and the measured intensity profile in the knife-edge plane. Simulated Schlieren photographs can be compared with experimental results. This approach is actually considered.

4.5 Emission spectroscopy (WP1, A1.2)

The optical emission obtained with a lens-fiber system directed along the wire is also spectrally resolved with a monochromator (Jarell-Ash, 16 Angstrom/mm). Larger lenses, 10 mm diameter, are used in this case to obtain a sufficient signal-to-noise ratio. Two radial position of the optical axis of this lens are possible: 6 mm from the wire or 6 mm from the cylinder wall. From the ratio of intensities of a nitrogen ion and neutral line the characteristic energy of the electrons is determined, using the method described by Hartmann [34].
The used emission lines are:

$N_2{:}C^3\Pi_u \rightarrow B^3\Pi_g$ at 337 nm and $N_2^+{:}B^2\Sigma_u^+ \rightarrow X^2\Sigma_g^+$ at 391 nm.

The excitation cross sections of the upper levels of the excited states have different thresholds, at 12 and 20 eV respectively. The non radiative de-excitation of both upper levels depends on the nature of the quenching molecule.

The fraction of molecules that radiate is:

$$f = 1/(1 + \alpha N \tau)$$

where α is the de-excitation rate constant, N is the number of quenching molecules per unit volume and τ the natural radiative life time. Literature data for τ, $\alpha(N_2)$ and $\alpha(O_2)$ are summarized in table 4.1. De-excitation rates for quenching by CO_2 were not found.

The ratio of the initial populations (without quenching) is expressed by:

$$\Pi(B)/\Pi(C) = I(B)/I(C) * f(C)/f(B)$$

where I(B) and I(C) are measured line intensities and f(B) and f(C) weighted averages based on the data for O_2 and N_2.

Table 4.1 *Radiative life time and de-excitation constants of N_2 levels*

state	τ (ns)	$a(N_2)$ (10^{-10} cm^3/s) [37]	$a(O_2)$ (10^{-10} cm^3/s) [37]
N_2: $C^3\Pi_u$ [35]	41 ± 2	0.11	3.12
N_2^+:- $B^2\Sigma_u^+$ [36]	60 ± 1	4.53	7.36

The available time resolution (10 ns) and spatial resolution (10 mm) of the diagnostics do not allow to measure the changes of electron energy along the streamer. For the measurements only the peak value of the optical signal is used. The measured value is thus an average of the characteristic electron energy in the region of the streamer front. The transmission of the optical system is calibrated with a Tungsten ribbon lamp.

4.6 Absorption spectroscopy (WP2, A2.1)

The OH radical is an intermediate state in many processes. It has therefore been studied in great detail. The theoretical fundamentals of its structure are given in the famous book by Herzberg [38]. A large amount of spectroscopic data is summarized in the well known tabels of Dieke and Crosswhite [39], additional information can be found in the book of Huber and Herzberg [40].

Emission of OH radicals has been observed in flames and discharges already in the 1920's. The most intense part of the spectrum is in the ultraviolet, with the band head at 306.4 nm. This has turned out to be the A-X transition. The spectrum is analysed with the theory of quantum mechanics. The total angular momentum, K, is the main quantum number in this case. By taking into account the electron spin and the nuclear spin, the selection rules lead to a system of 12 rotational branches which fully account for the complex spectrum as it is observed.

The oscillator strength of the transition is also known (f = 0.001). It is therefore possible to determine absolute densities of OH radicals in the ground state with an absorption experiment. The emission spectrum intensity is related to the population of the upper level of the molecule. This level is, however, populated by electron collisions with water molecules and it is deexcited by radiation and by collisions with several molecules. It is therefore virtually

impossible to relate this intensity to an absolute density of the upper level since it would require a very sophisticated model including all these mechanisms.

There are several complicating factors in the absorption experiment. The first is the velocity of the molecules which leads to a thermal distribution. If this distribution can be described by a Boltzmann function, it results in absorbed frequencies with a Gaussian profile around the centre frequency of an individual rotational line. A second broadening mechanism, due to pressure, gives a Lorentzian profile. The combination of these two profiles is called a Voigt function. Other broadening mechanisms exist but can be neglected in the present case. Many absorption measurements have been performed in flames and the Voigt profile for this case is determined by Lezberg [41]. It turns out that for a pressure of 1 bar and a temperature of 400 K the Gauss and the Lorentz width are the same. This means that the Voigt function must be used.

The second problem is that the wavelength separation of the rotational lines is mostly very small. The ideal solution for this problem is a apparatus with extremely high wavelength resolution. A high resolution, in practise, leads to a low signal intensity so an optimum must be found. There are a few lines in the spectrum that are somewhat isolated [42]. The extra criterium to choose one of them is related to the distribution of the OH radicals over the different rotational states. At a temperature of 400 K the maximum of this distribution is at K = 2 or 3. The final criterium is to select the strongest branch, which is here the P- or the R-branch. The choise is now made for the R_2^3 rotational transition, also because in Ref. 16 the data are carefully selected for this line.

Another problem is that it cannot immediatly be assumed that a Boltzmann distribution for the ground state radicals is valid. This depends again on the rates of the involved collisional processes. OH can be formed in the ground state or in the A-state. The A-state is depopulated by emission, its radiative lifetime is given to be 700 ns [40]. The collisional deexcitation of the A-level by several molecules is measured by Wysong e.a. [43]. From these measurements its follows that both the deecitation of the A-level and the rotational redistribution of the X-level occur well within 1 ns for the conditions of our experiment.

The formation and destruction of the OH itself must also be considered. No direct measurements are available, but there are extensive models that deal with the physico-chemical processes in flue gas [44]. The major sources of OH are dissociative attachment of H_2O producing OH and H^-, dissociation of O_2, followed by hydrogen abstraction from H_2O, and from H_2O^+ ions forming H_3O^+ and OH. The time scale for these processes is roughly 10 μs. The decay of OH in this model is by reactions with SO_2 with a reaction time of about 50 μs. These times are much slower than the redistribution time. This leads to the important conclusion that the OH radicals are always in the ground state and have a thermal distribution in our experiments. This makes it possible to use the standard methods for the calculation of the OH density as in [38] and [39].

The lifetime of the OH is less than 100 μs, so the measurement must

have a much higher time resolution. The signal-to-noise ratio of the measurement depends, however, strongly upon the number of photons that reach the detector in this time interval. This number is determined by two items. First, the number of photons that are emitted by the lamp and its imaging optics, Second, the resolution and the efficiency of the wavelength selecting device.

An economic source of high intensity is a flash lamp. The lamp is described in section 4.4. At the maximum of its pulse it has ten times more intensity than a 1 kW DC Xe-lamp in the wavelength region around 300 nm. The light of this lamp is focussed on a quartz fiber of 600 μm. This fiber can be coupled into the EMC cabinet without causing electromagnetic interference problems. The light coming out of the fiber is shaped into a parallel beam by a quartz lens of 12 mm diameter. This beam traverses the discharge volume along the wire and falls than onto a mirror with a curvature radius of 0.9 m. This mirror reflects the beam onto a second quartz lens that focusses the light into a second fiber that transports the light to the monochromator. The lenses and the mirror are suspended with stainless steel wires of 1 mm. This will cause no problems with the gas flow because the flow is already very turbulent.

A 0.5 m Jarrel Ash monochromator is used with slits adjustable from 10 to 400 μm. The light is detected at the output slit with a Hamamatsu R666 photomultiplier with GaAs cathode. The electrical signal is recorded with the LeCroy oscilloscope. The load resistor of the multiplier must be chosen high enough to provide a good signal and low enough for a high time resolution. The value of 10 kΩ turns out to be the optimum in most cases.

The triggering requires a special treatment in this experiment because the flash lamp has an unavoidable delay time and a rise time which depends on the pulse shaping network that feeds the lamp. The delay time is 4 μs and the rise time 3 μs. So the lamp must be triggered 7 μs before the corona, assuming that the corona has negligible delay, if the initial phase of OH formation is to be studied. The delay of the corona depends on the spark gap trigger and on the corona formation time which is largely determined by the pulse voltage. The total delay of the corona is well within 1 μs if the pulse tranformer described in section 2.7 is used and a pulse voltage well above corona inception is applied. Two trigger transformers are used which obtain their input pulse from a trigger unit of an image intensifier camera, which has two outputs with adjustable delay time fron 10 ns to 99 μs (model 46A Trigger Delay Generator, TRW Instruments, Inc.,USA).

4.7 Gas detection (WP2, A2.2)

The analysis of the flue gas is a major aspect of a study regarding flue gas cleaning. Two separate parts are to be considered: first the chemical components to be removed and second the overall composition of the flue gas since the cleaning process may depend on it. A different approach for the two

processes is required since the first concerns densities in the order of promilles to ppm's and the second deals with percentages. Two pieces of equipment are available: a gas analyser with electrochemical cells and a quadrupole mass spectrometer.

4.7.1 The electrochemical cell

The operation of the electrochemical cell is similar to a fuel cell. Gas is brought into contact with a (solid) electrolyte though a porous electrode. This leads to a potential difference with a reference electrode, which can be recorded as a measure for the amount of gas that has diffused through the electrode. This diffusion is linear with the concentration out side the electrode, so the electrode signal is also proportional to it. More details can be found in [45].

The electrochemical cell can be made sensitive for a specific gas by the right choise of the porous membrane and the electrolyte and it is easy to operate. Its sensitivity can also be regulated with the membrane. The cell is usually temperature controlled for a stable operation and a gas cooler/dryer is required when flue gas is analysed. A disadvantage of the cells is that cross sensitivity is likely to occur in complicated mixtures. The cells recover slowly from overload and the electrolyte degradates when the cell is used. There are also aging problems with the electrodes so that in general the life time of a cell is limited to two years.

A SONOX Rend-O-meter has been acquired from van Vught B.V., The Netherlands. This is an industrial piece of equipment for the analysis of flue gas of burners, including also items such as effiency and air/fuel ratio. This is a modular system and can be made on customer requirement. Tabel 4.2 gives the specifications of our system.

Tabel 4.2: Specifications of SONOX Rend-O-meter

detector	sensitivity
O_2	0 - 25 %
CO	0 - 2 %
NO	0 - 2000 ppm
NO_2	0 - 200 ppm
SO_2	0 - 2000 ppm
temperature	0 - 700 °C

The six signals are displayed on the front of the apparatus, but they are also led to analogous outputs through a buffer amplifier so that the signals range from 0 to 5 V for every channel corresponding to the numbers of the

tabel. These signals can than be tansferred to the measurement system described in section 2.4. The accuracy given by the manufacturer is 0.3% for O_2 and 2% for the other gases. The system should be checked with calibrated gas mixtures once or twice per year. The amount of CO_2 is calculated by an internal program from the SONOX. The measured amount of O_2 is combined with the type of fuel used. This method is not very accurate because natural gas is not purely CH_4. It also contains some C_2H_6 and the composition is varied during the seasons. This may lead to an error of ~10%.

4.7.2 The mass spectrometer

A common laboratory method for gas analysis is the quadrupole mass filter. The gas is let into a high vacuum chamber where it is ionized by an electron beam. The ions enter a radiofrequent field and only one specific charge/mass ratio has a stable path to the detector entry. This ratio can be scanned to make a spectrum of the ions created from the gas. See [46] for more details.

The quadrupole and the detector operate only under high vacuum ($< 10^{-5}$ Torr). The flue gas is sampled at a pressure of 1 bar, so a gas inlet system is required to reduce this pressure. This is done by means of a capillary tube and differential pumping. The capillar is a stainless steel tube with an inner diameter of 0.4 mm and a length of 4 m and is kept at a temperatur of 75 °C to prevent condensation of water vapour. It ends in a chamber that is pumped by a rotary vacuum pump to 10^{-2} Torr. A valve connects this chamber to a second chamber which is kept at 10^{-6} Torr by a turbomolecular pump. This chamber is directly connected to the quadrupole.

It is evident that only stable molecules are able to reach the quadrupole. Short lived radicals such as OH cannot pass the capillar because its transit time is several seconds. Even molecules such as O_3 are unlikely to get through also because of collisions with the wall. The complicated inlet system makes is virtually impossible to do absolute measurements. Absolute values can, however, often be obtained by using an external reference. In flue gas, for example, one knows that the N_2 density is something like 72% and the other signals can be related to this value.

A major disadvantage of the mass spectrometer originates from the necessity of the ionization. This process causes also dissociation, therefore different ions can be detected from one molecule, e.g. N_2^+, N^+ and N^{++} from N_2. A further complicating factor is that different molecules sometimes have the same mass, e.g. N_2 and CO are both 28 amu, and can therefore not be distinguished. This problem becomes even worse when the different isotopes of the atoms are taken into account, such as O^{16}, O^{17} and O^{18}, or N^{14} and N^{15}.

Only a very precise analysis of a measured spectrum can give reliable data. The cross sections of the ionization and dissociation processes must be known. Still it cannot be expected that a minor concentration of NO will be

detected since it coincides with the $N^{14}N^{15}$ molecule which has a concentration of 3000 ppm. SO_2, however is separated from other molecules due to its relatively high mass and also H_2O can be expected to be determined. Therefore the mass spectrometer is still considered as a worthwile extension of the gas analyser with the electrochemical cells.

The equipment used originates mainly from Balzers, BRD, and consists of a QMG-101 quadrupole, a QPG-101 scan unit, a GES-010 gas inlet system, a QMA-145 channeltron detector and a EVA-040 rotary pump. The turbomolecular pump is a TPU-250 from Pfeiffer, BRD.

5. Modelling

5.1 Introduction

A general review of streamer models published in literature up to now is first presented in this chapter. It is followed by a description of the main aspects of the streamer propagation model developed under WP1. Chemical models specifically created for flue gas cleaning are mentioned shortly in the next section, with a subsequent summary of the important features of the chemical model (WP2).

5.2 Streamer propagation (WP1)

5.2.1 Positive streamer concept

The original streamer concept emerged in the years 1935-1940 through the works of Flegler, Raether, Loeb and Meek. The positive or cathode-directed streamer concept including gas ionization, as proposed by Loeb and Raether, has proven to be necessary to explain the fast filamentary precursors to breakdown that are observed emanating from the anode in air coronas. This ionisation becomes very rapid only when the original field becomes highly distorted by positive ion space charge at the head of an avalanche. New electrons, created by photo-ionisation, are assumed to initiate additional avalanches near the head of the main avalanche, producing a rapid propagation of the avalanche across the gap. In relatively small gaps, or when streamers reach the cathode, photo-ions released at the cathode may also play a role.

5.2.2 Equivalent avalanche models

One of the earliest models for propagation of streamers in the low field region of non-uniform fields has been made by Dawson and Winn [47]. In this model it has been assumed that the growth of electrons is a property solely of the streamer head, uninfluenced by the channel conductivity. The successive creation of new series of avalanches is represented by one single equivalent avalanche. The condition for continued streamer propagation, is that each succeeding spherical region of positive charge must be exactly similar to the one preceding it, i.e. the radius and the charge density of the two spheres should be the same. This model is therefore also called "equivalent avalanche model". Calculations from the model indicate that the criterion for propagation of a streamer in a zero external field in atmospheric air is that the number of ions in the head is 10^8 and the radius about 30 μm.

The model of Dawson and Winn is further improved by Gallimberti [48]. In this model of Gallimberti the equivalent avalanche model is extended with an energy criterion. The loss of energy during the formation of new avalanches (due to ionization, attachment, vibrational and electronic excitation and dissociation) must be counterbalanced by the energy gain of the electrons in the applied

field and the gain of potential energy caused by the build-up of a new concentration of positive ions. In this model the increase of positive ions in the streamer front can be calculated. The potential energy gained in the high field region is consumed in the low field region. The model predicts that stationary streamer occurs whwn the applied external field is 20 Td ("stability field"). The calculated streamer characteristics for long air gaps are in accordance with experimental results [49].

5.2.3 Hydrodynamic approach and local equilibrium

The space-time evolution of a streamer discharge can be described using one-dimensional continuity equation for electrons and ions, coupled to the Poisson equation for the external and space charge electric fields. The equations contain macroscopic coefficients for ionization, attachment, diffusion (longitudinal and transversal) and drift velocity. This macroscopic model (also currently called hydrodynamic or fluid model) can only be used if local equilibrium exists between the electrons and the local value of the electric field in the discharge. Only in the case of local equilibrium the macroscopic coefficients are sole functions of the local reduced electric field.

The condition of local equilibrium can be assumed when the relaxation time for getting a steady state electron energy distribution function is short compared to the characteristic time of discharge development. The electron relaxation time can be calculated solving the Boltzmann equation, which describes the time evolution of the electron energy distribution function. Using a Monte Carlo method to solve the Boltzmann equation, the calculated electron relaxation time in nitrogen is $\tau_e \approx 1$ Torr ns [50]. This means that at atmospheric pressure the electrons are in equilibrium with the local value of the electric field within a few ps. The characteristic time for the field variation in a moving streamer front can be estimated from the ratio of the characteristic streamer head size and its propagation velocity: τ_E = (50 μm)/ (5 10^5 m/s) = 100 ps. Because of the fact that $\tau_e << \tau_E$ the assumption of local equilibrium is justified. The characteristic longitudinal streamer size in this approximation has been taken from a two-dimensional Monte Carlo simulation of streamer formation of Kunhardt (Ref.25). This is a microscopic discharge model in which no assumptions with respect to equilibrium conditions need to be made. However, the Monte Carlo method is much time consuming and therefore costly. The method is useful in order to find the range of applicability of the hydrodynamic approach. For this purpose the simulation of the discharge development during a short period (6 ns in [51]) is sufficient.

5.2.4 Macroscopic models

A number of macroscopic models describing the formation and propagation of streamers has been realised (for example [52-56]). Most of the models indicate that under atmospheric conditions the cathode directed streamer starts to propagate when the number of positive ions left by the anode directed electron avalanche exceeds the number 10^8.

In the early work of Davies and Evans [52] the solution of Poisson's equation is based on the representation of a space charge filament by a series of charged disks, with a fixed charge density on each disk. The continuity equations for electrons and positive ions were integrated by the method of characteristics. The method of disks was later improved by taking into account the finite radius of the streamer [53]. Charges are then supposed to be distributed over each disk with a Gaussian density profile. The width of the profile corresponds to the streamer diameter that must be treated as an input parameter. Using this method of disks the value of the electric field on the streamer axis is calculated.

The influence of unstable negative ions on current growth and streamer propagation speed in air has been demonstrated in calculations of Kline [54]. The detached electrons from O_2^- result in a faster growth of n_e than in case only stable negative ions are assumed. Kline used a similar numerical approach as Davies, Davies and Evans [53].

Another numerical technique, using the Flux Corrected Transport (FCT) algorithme, has been first used for streamer modelling by Morrow [57]. This technique is very efficient but will not be discussed here. The algorithme, which is is now widely applied for streamer modelling, has also been used by Gallimberti for calculation of streamer propagation in flue gas [58]. It should be noted that the models mentioned up to now are one-dimensional models where the streamer diameter is an input parameter for the model, rather than being determined self-consistently. Also the role of photoionization in front of the streamer must be represented by at least two input parameters describing the total amount and absorption of radiation in front of the streamer.

Also two-dimensional studies of streamers has been made. Dhali and Williams presented results of a two-dimensional computer simulation of streamer propagation in atmospheric N_2 [55]. Their calculations demonstrate that the streamer characteristics in steady state are roughly independent of the magnitude of the density of the initial ions used to create the streamer. However the diameter of the streamer is influenced by the diameter of the initial space charge distribution. It appears that streamers tend to propagate at their initial diameter and do not self- consistently find a certain diameter.

Recently different models for the formation and propagation of streamers in a uniform field in N_2 has been published by Kunhardt et al. [56]. Monte Carlo simulation results (streamer size, electric fields and electron densities) are the same as those results that are calculated using a two-dimensional hydrodynamic model.

In flue gas the gases that have an significant influence on the electron kinetics are: N_2, O_2, CO_2 and H_2O. The total concentration of the pollutants CO, SO_2, NO and NO_2 is less then 1% and can therefore be neglected. The macroscopic coefficents (ionization and attachment coefficients, drift velocity and diffusion coefficients) can be either obtained from calculation by solving the

Boltzmann equation and using cross sections for the individual processes, or from measurements (for example obtained with drift tubes or avalanche studies).

Steady state solutions to the Boltzmann equation can be used because the electrons are in equilibrium with the local value of the electric field. The most common technique used to solve the Boltzmann equation has been the *moment method*. A computer program that solves the Boltzmann equation for a partially ionized gas with several components is available [59]. The steady state Boltzmann equation for a flue gas mixture has already been solved by M. Yousfi [60].

Measurements of the macroscopic parameters have been done using a simulated flue gas mixture with the same composition as the mixture used for the calculation [61]. At a value of the reduced electric field of 100 Td the calculated attachment coefficient is higher than the measured attachment coefficient. Because this field is near the value of the critical field this difference in attachment coefficient causes a difference between the calculated critical field strength (117 Td) and the measured critical field strength (100 Td) in flue gas.

5.2.5 The IVTAN streamer propagation model

This section is devoted to mathematical modelling of the single positive streamer, the first step in the chain of events in the reactor. It is a summary of the report produced by IVTAN as their final report for the sub-contract under this project [62]. The positive streamer is observed in nonuniform electric fields as a thin conducting cylindrical channel moving towards the cathode with a characteristic velocity of 10^5 - 10^6 m/s. Streamer propagation is caused by ionization of gas molecules in the region of high electric field (near the streamer head). Theoretical investigation of streamers has been carried out on the basis of models of various levels of complexity. Rigorous analysis of streamer motion needs at least 2D models (and in some cases, e.g. to describe branching 3D models). More often 1D or quasi 2D models are used in which diffusion and drift only in the direction of the streamer propagation is considered. The finite transverse size of the streamer is taken into account by use of the method of disks [52] for the calculation of the electric field. Comparison of 2D and 1D results shows that the main features of the streamer are adequately described in the 1D approximation.

The most uncertain parameter in the 1D model is the streamer radius R_s which is assumed to be constant in time. Up to now no values are available from 2D or 3D calculations, and the results from experiments show a large variation from 15 to 85 μm [63,64]. In the model described is the streamer radius is an external parameter and has a constant value during a calculation, which is preferably taken from experimental values (see section 6.3.1).

Basic equations

The positive streamer is modelled by numerical solution of the coupled system of continuity equations for densities of different species N_j . Species taken into account are electrons, positive ions and negative ions. The neutral gas density is assumed to be constant because the degree of ionization is low. Electron diffusion is neglected because its contribution is very small at the discharge modelling time. The electric field is obtained in a self-consistent way by solving the Poisson equation with the method of disks (five reflections on both sides are taken into account).

Electrons and ions are produced by collisions and photoionization. All collisional processes are given as rate constants which are a function of the local, reduced electric field. Besides this there is a uniform, background electron density which is necessary for the initiation of the streamer. The current, I, in the external circuit is calculated using the Sato equation [65]:

$$I = \pi R_e^2 e \int_0^d (N_e V_e + N_p V_p + N_n V_n) E_l \, dx / V$$

where N_e, N_p and N_n are the densities of electrons, positive and negative ions, V_e, V_p and V_n their respective drift velocities, E_l is the Laplacian field strength, V is the applied voltage and d is the gap distance.

Elementary processes in streamers in air and flue gases

The characteristics of the streamer propagation and the plasma parameters in its head and channel are determined by a set of kinetical processes such as ionization, attachment, recombination, photoionization etc. The actual values are determined by the gas composition, including temperature. For flue gas not all data are available, therefore in some cases estimates are used.

The processes taken into account are:

-ionization, given as a coefficient, α, as a function of E/N:

$\alpha/N = [1 + 6 \cdot 10^6 / (E/N)^3] \, 5 \cdot 10^{-16} \exp[-1010/(E/N)]$,

for air and flue gas the same equation can be used [66,61].

-electron drift velocity, V_e:

$V_e = 3.2 \cdot 10^5 \, (E/N)^{0.8}$ cm/s

-three-body attachment coefficient η_3:

$\eta_3/N^2 = 1.6 \cdot 10^{-37} \, (E/N)^{-1.1}$ cm^5

for flue gas a correction is made on the basis of the mole fractions, the coefficient for H_2O is taken to be 7 time higher than O_2, for CO_2 this is 1.5 times

-two body attachment η_2:

$\eta_2/N = 4.3 \cdot 10^{-19} \exp(-1.05 \, | 5.3 - \ln(E/N) |^3)$ cm^2

for flue gas a relative coefficient of 2 is taken for water

-ion-ion recombination β_{ii}:

$\beta_{ii} = 2 \cdot 10^{-6} \, (T/300)^{-1.5}$ cm^3/s

-electron-ion recombination β_{ei}:

β_{ei} = (3-6)·10^{-8} cm^3/s for two-atomic ions and
β_{ei} = (2-4)·10^{-7} cm^3/s for four-atomic ions

-volume photoionization, Q_{ph}:
this process provides generation of electrons in front of the streamer head by absorption of far UV photons emitted from the streamer head. The formulas for this process are given in [62].

Excitation and dissociation of molecules

Excited molecules and radicals, generated by electron collisions directly and by ions in streamer head and channel, are chemically active particles which clean flue gases, produce ozone, etc. These particles also react with negative ions which may lead to the release of electrons, thereby influencing the conductivity at later stages of the streamer development. The experimental data on these processes are limited. The following reactions are taken into account:

$e + O_2 \rightarrow e + O_2(a^1\Delta)$
$e + O_2 \rightarrow e + O + O$
$e + O_2 \rightarrow e + O(^1D) + O$
$e + N_2 \rightarrow e + N_2(A^3\Sigma)$
$e + N_2 \rightarrow e + N + N$
$e + CO_2 \rightarrow e + CO + O$
$e + H_2O \rightarrow e + OH + O$

These reactions are represented as a first order reaction with a reaction rate, K, of the shape:

$$K = A \exp[-B / (E/N)],$$

where A and B are constants.

Gas heating and vibrational excitation are described with empirical formulas [62]. This is of interest for the dissipation of the energy among the different processes and to find the decay times of these processes. A final property that is calculated is the amount of radiation that is emitted by specific nitrogen states, in order to compare it with the optical measurements. This radiation does not depend only on the density of the upper level, but it is strongly influenced by collisional deexcitation of this level, i.e. quenching.

Numerical techniques

The general equations are solved numerically by using a moveable nonuniform mesh. A very fine mesh must be used in order to resolve the streamer field structure at the head and to avoid numerical instabilities due to the strong multiplication of electrons. The flux corrected transport algorithm (FCT) provides a small numerical diffusion and is used to solve the continuity equations on a non-uniform mesh [67]. The kinetic terms and the photoionization are computed straigtforward, as in [68].

For fast moving transient phenomena such as a streamer front the use of a moving computational mesh is necessary [67]. The disk method for the calculation of the electric field requires the calculation of the influence matrix for each mesh. Therefore a continuous movement of the mesh is undesirable. So the mesh is taken with a very fine, uniform step in the region of the streamer head, and with expanding steps outside. When the head comes near the border of the fine mesh, this mesh is repositioned and the matrix is recalculated. At the anode fall region the mesh must be fine enough to obtain a stable solution. The total number of mesh points can be up to about 1000. Beyond this value this model can no longer be used on a personel computer due to limitations of memory size and computational speed.

5.3 Radical production and chemical reactions (WP2)

5.3.1 Existing models

Several chemical kinetics studies for the removal of NO_x and SO_2 with electron beam have already been carried out. One of them is made in Karlsruhe [69] and another in Pittsburgh [70]. Both studies make use of the evaluated data for atmospheric chemistry of Baulch et al. [71]. The chemical reactions for the e-beam process which are selected in these reports can in principle also be used as a basic set of reactions for the pulsed corona process. The main differences between the processes are caused by the different initial ions and radicals concentrations. In the e-beam process the electrons are monoenergetic and typically 100 eV. In a streamer discharge the electron energy is distributed over the electrons according to an electron energy distribution function with a characteristic electron energy which is a function of the local space charge field in the streamer. So at every point along the streamer the characteristic electron energy is different. The maximum value of the electron energy in the streamer front is according to measurements and model calculations $\sim$10 eV. The characteristic electron energy in the streamer channel is $\sim$1 eV.

In the Pittsburgh study calculations are compared with the interesting experiments of Tokunaga in relatively simple gas mixtures [72-73]. The most important radical which converts SO_2 and NO_x into acids, is the OH radical. The chemistry for NO_x removal is complicated by the fact that also N_xO_y compounds are produced in the discharge. NO is converted to NO_2, eventually to NO_3, before nitric acid is formed. However in the calculations for e-beam treatment the production of radicals like $O(^1D)$ and OH by direct dissociation of oxygen and water is considered as small compared to the production of OH by ions. Because of the fact that in a discharge the average electron energy is lower, the relative contribution of direct dissociation is supposed to be higher. The main direct OH production process is dissociative attachment to water molecules producing OH and H^-. The production of $O(^1D)$ metastables is also important. A model study which deals with the chemistry in flue gas induced by a dielectric barrier discharge [74] predicts that at low O_2 concentration the SO_2 removal, is limited by the lack of generation of OH due to insufficient production of $O(^1D)$.

The essential chemistry for SO_2 and NO_x removal is represented at table 5.1 and 5.2 respectively.

The Pittsburgh study for a flue gas mixture (69% N_2, 8% O_2, 10% CO_2, 13% H_2O, 520 ppm SO_2 and 203 ppm NO) contains about 150 reactions for 60 different species. When taking into account reactions with NH_3 (which can be added to the flue gas before energization) at least 15 reactions should be added ([70], p. 81). The Karlsruhe study includes about 739 reactions, but the first 515 reactions are reactions with or between ions and also a large number of reactions with N_xH_y are included. The largest part of those reactions with ions is probably unimportant as far as they concern the charge transfer to particles with minor concentrations. It is expected that ions play only a role in the removal process via the formation of OH radicals. This reaction path is likely to proceed through fast charge transfer processes of the type as mentioned in table 5.1. Not exactly the same charge transfer processes are taken into account in [69] and [70]. Therefore more details on the reaction paths via positive ions will be looked for, for example in [71c] and contacting the authors of [44].

The ions selected in the Pittsburgh study seem to be sufficient in predicting the behaviour of electron beam experiments under several experimental conditions. The most important positive ions are H_2O^+, H_3O^+ and ions like N_2^+, N_4^+, O_2^+ which can all be hydrated. Obviously the negative ions must be included, as they determine detachment and recombination with the positive ions. The most important negative ions are O_2^- and O^-.

In a model for ozon generation from air in dielectric barrier discharges [74] it is demonstrated that most of the O radicals are produced by reactions with the $N_2(A)$ metastable. Dissociation of water molecules by this metastable is probable but not known. Of course there is a high probability that radicals like OH, O and H form other more stable compounds as HO_2, H_2O_2 and O_3 before they can react with SO_2 and NOx. Various reaction paths with these "secundary" radicals have been included in the model studies of [69] and [70].

Most SO_2 removal occurs via:

$$\mathbf{OH} + SO_2 + M\,(H_2O) \rightarrow HOSO_2$$

$$HOSO_2 + \mathbf{OH} \rightarrow H_2SO_4$$

In e-beam treatment (electron energy ~ 100 eV) most OH is procuced by hydrated ions:

- Hydrated clusters are formed by charge exchange:

* $N_2^+ \rightarrow O_2^+ \rightarrow O_2^+.H_2O$

$$O_2^+.H_2O + H_2O \rightarrow H_3O^+ + O_2$$

$$H_3O^+.OH + H_2O \rightarrow H_3O^+.H_2O + \mathbf{OH}$$

* $N_2^+ \rightarrow H_2O^+ + H_2O \rightarrow H_3O^+ + \mathbf{OH}$

* Further build up of hydrate clusters

- Ions recombine to form H $\rightarrow$ HO_2 $\rightarrow$ OH:

* $H_3O^+(H_2O)_n + NO_3^-(H_2O)_m \rightarrow (m+n+1)H_2O + NO_3 + H$

$$H + O_2 + M \rightarrow HO_2$$

$$HO_2 + NO \rightarrow NO_2 + \mathbf{OH}$$

$$HO_2 + O_3 \rightarrow 2O_2 + \mathbf{OH}$$

In electrical discharges, with an average electron energy in the range 5-10 eV, also direct water dissociation is probably important:

* $e + H_2O \rightarrow H^- + \mathbf{OH}$ ($\sigma = 7.10^{-18}$ cm^2 at 6.5 eV)
* $e + H_2O \rightarrow H + OH^-$ ($\sigma \sim 10^{-19}$ cm^2 for 6-12 eV)

Metastables also produce OH:

* $e + O_2(X) \rightarrow O_2(B) + e \rightarrow O(^1D) + O(^3P) + e$ ($\sigma \sim 2.0.10^{-17}$ cm^2)

$$O(^1D) + H_2O \rightarrow 2\mathbf{OH}$$

Table 5.1: Essential chemistry for SO_2 removal. Hydrated ion reactions are taken from Ref. 37, p. 14. Cross sections (σ) are taken from Ref. 44.

NO and NO_2 are removed by HO_2, O_3, OH, O and N

- N and $N_2(A)$ produce O:
  - * $N + NO \rightarrow N_2 + O$
  - * $N_2(A) + O_2 \rightarrow N_2 + 2O$
- O is removed by NO_2 and produces O_3:
  - * $O + NO_2 \rightarrow NO + O_2$
  - * $O + O_2 + M \rightarrow O_3 + M$
- HO_2 is formed by H:
  - * $H + O_2 + M \rightarrow HO_2 + M$
- NO and NO_2 react with HO_2, O_3, OH and N:
  - * $HO_2 + NO \rightarrow NO_2 + OH$
  - * $O_3 + NO \rightarrow O_2 + NO_2$
  - * $OH + NO_2 + M \rightarrow HNO_3 + M$
  - * $N + NO \rightarrow N_2 + O$

Table 5.2: Essential chemistry for NO_x removal

5.3.2 The IVTAN model "KINEL"

This section presents a description of the work performed under the subcontract devoted to the development of the chemical kinetices computer code adopted to the conditions of the pulsed corona setup of the EUT and to the development of the computer code of the coupled chemical kinetics and gasdynamic decay in the vicinity of the streamer trail with inclusion of transport processes. It is a summary of the final report written by IVTAN under this subcontract [75]. The connection with the modelling work on the streamer propagation (section 5.2 and [62]) is that the streamer model provides the initial data on the chemical species and the energy supply from the electric field to the streamer.

Chemical kinetics modelling

Plasma-chemical processes are being considered nowadays in different purification systems (see chapter 1). The role of the discharge state is to produce chemically active radicals, ions and excited molecules. These active species take part in chain reactions resulting in the removal of toxic components. The typical composition of the flue gas under consideration is:

N_2: 70 - 74%
O_2: 1 - 5%
H_2O: 6 - 18%
CO_2: 8 - 15%
CO: 10 - 100 ppm
NO: 200 - 600 ppm
SO_2: 400 - 2000 ppm

The substances to be removed are NO and SO_2, NO will convert spontaneously into NO_2 for a small fraction when O_2 is present. SO_2 removal is strongly coupled to NH_3 addition, this will be discussed later in this section. The main reaction channels involved in the removal of NO are:

$$
\begin{array}{llll}
N + NO & & \rightarrow N_2 + O \\
OH + NO_2 & + M & \rightarrow HNO_3 + M \\
HO_2 + NO & & \rightarrow NO_2 + OH \\
H + O_2 & + M & \rightarrow HO_2 + M \\
O_3 + NO & & \rightarrow O_2 + NO_2 \\
O + O_2 & + M & \rightarrow O_3 + M \\
O + NO_2 & & \rightarrow NO + O_2 \\
N_2^* + O_2 & & \rightarrow N_2 + 2O
\end{array}
$$

There is a competition between forward and reverse reactions which defines the final concentration of NO. For the complete description of the chemical conversions behind the streamer head the reaction scheme from [69] was adopted. Parameters of several elementary reactions were checked and

taken from [76]. The total reaction scheme consists of about 1000 elementary stages [75]. Among them are 210 positive ion-neutral reactions, 70 negative ion-neutral reactions, 450 ionic recombination reactions, 60 reactions of excited species and 165 reactions among ground state neutrals. It is important to note that all these reactions are in the gas phase and may therefore not describe all the processes occuring in flue gas cleaning. This topic will be adressed later.

The solution of the chemical kinetics equations has been accomplished by the program KINEL using GEAR's method for the solution of stiff ordinary differential equations. The computer code package KINEL has been developed to solve gas phase chemical kinetic problems for large reaction systems. The specific advantage of KINEL is that programming experience is not required to use the system succesfully.

Gasdynamical decay of the streamer channel

Under the typical conditions of the pulsed corona discharge, used in flue gas cleaning, the characterictic gasdynamic time, t_{gd}, is defined as the ratio of the streamer channel radius, R_s, to the local sound velocity, c_{str}. It is in the order of 10^{-6} - 10^{-7} s, i.e. much less than the time required for many important chemical reactions which take place in the chemical relaxation of the pulsed corona discharge [69]. This means that the gasdynamical decay of the streamer channel can influence the actual chemical reaction rate and, consequently, the heat delivered by the reaction which again has a back influence.

For this reason the gasdynamical processes are coupled with the chemical behaviour of the gas mixture. The streamer head propagates with a velocity of 10^5 - 10^6 m/s, so a gas volume located in the streamer path is subjected to high electric field and the accompanying excitations less than 1 ns. A large fraction of the energy will be dissipated in this short instant, so the gas is heated locally much faster than the gasdynamical decay time. This results in a pressure increase and a consequent gasdynamical wave propagation in radial direction. The wave propagation is accompanied by temperature and density fluctuations and consequent chemical rate changes. (This wave causes also the sound which can be heard when a pulsed corona discharge is in operation.)

The gasdynamic expansion and diffusive decay of the streamer channel is treated as an expansion of a cylindrical volume of chemically reacting gas placed into an inert gas. Variations of chemical and gasdynamical parameters along the streamer are neglected, diffusion coefficients of all species are assumed to be equal to each other. Under these assumptions the expansion process is described with a set of one-dimesional equations for gasdynamics, heat/mass transfer and chemical kinetics [75]. The numerical solution of the equations is accomplished with a full conservative implicit finite difference scheme. The set of corresponding finite difference algebraic equations is solved by Newton's method []. This algorith for numerical simulation of the streamer expansion and decay has been realized in the computer code HYDRO.

The KINEL reaction analyser

A system of 1000 reactions is difficult to handle in terms of which reactions are important and which are not. A low concentration of a certain species does not mean that this species is unimportant, this can also occur if its production and destruction rates are (almost) equal. A dedicated module is added to KINEL for the analysis of these aspects. It can create time dependent curves of the concentration of all species in the model and also the time derivative. But its most powerful feature is to create histograms of a certain species which shows at a given moment the integral contribution of a reaction path to this species as either a production or a consumption. This gives a very good overview of the dominant pathways for a specific molecule.

Modelling of the thermal NH_3-SO_2 reaction

Addition of ammonia into flue gas without any external activation effects like corona discharge or e-beam leads to rather effective SO_2 removal from the gas phase by aerosol formation. Aerosol droplets contain various products like $(NH_3)_2SO_2$, $(NH_4)_2SO_3$, $(NH_4)_2SO_4$, $(NH_4)HSO_4$, etc. [69]. If a flue gas/ammonia mixture is also affected by e-beam or corona discharge then nitrogen/ammonia compounds can be found in a condensed phase. Ammonia therefore seems to represent a "connecting link" between gas phase and heterogeneous chemistry of the cleaning process. Unfortunately the detailed physical/chemical mechanisms of the aerosol/heterogeneous processes are not well know yet. Experimental data are scarcely available but only for the conditions of acid rain in the upper atmosphere. Flue gas cleaning programs only contain fitting parameters for these processes up to now [69].

Experiments with NH_3 and SO_2 in humid air at 1 bar and 300 K show a characteristic time constant for aerosol formation containing the above mentioned substances of 0.1-1 s [77,78]. It was found that the reaction has a first order dependence on the gas phase densities of ammonia and sulphur dioxide. This leads to a reaction rate constant, which unfortunately differs considerably from experiment to experiment, it value is found to be: $2 - 13 \cdot 10^{-15}$ cm^3/s. Nevertheless as a first attempt this reaction rate is used in KINEL to calculate the influence of ammonia addition.

6. Results and discussion

6.1 Introduction

This chapter gives a summary of the main experimental result that have been achieved with a short discussion at each item. Several examples of the model calculation are presented, when possible they are compared with the measurements.

6.2 Electrical parameters (A1.0 and A2.0)

6.2.1 Pulse shapes

The high voltage pulse can be characterised by several parameters: a) rate of rise, b) maximum voltage, c) duration, d) DC bias and e) repetition rate. The typical time for a streamer to cross the gap is in the order of 100 ns, therefore rise times much longer than this value will not be considered. In our set-ups the voltages range from 20 kV, which is near the inception value for the small setup, to about 100 kV, which may lead to breakdown in the large setup. This gives a lower value for the voltage rate of rise of 0.2 kV/ns and a maximum desirable limit of 10 kV/ns. It will depend on the impedance of the discharge and of the circuit wether or not this maximum is obtained.

In the course of the experiments it has turned out that there are only two forms of voltage pulses which are fundamentally different. All other forms are inbetween mixtures. One shape is a constant voltage pulse, an example is given in fig. 6.1a, with its current in fig. 6.1b. The first current peak is purely capacitive and the time duration of the corona current is rather long, more than 200 ns. The second pulse type is shown in fig. 6.2, it is created by including a DC bias and a much smaller coupling capacitor is used. This leads to a fast decrease of the voltage and in fig. 6.2b it is shown that the total current duration goes down to zero in 20 ns. The capacitive and discharge current are mixed in this case. This second pulse has the advantage that it automatically avoids breakdown because it limits its own duration. This implies that there is no energy loss as is the case with a second spark gap. These measurements are made with the small setup. The second pulse shape can be obtained at both setups and is always used in cleaning experiments.

Another interesting feature of the voltage pulse is shown in fig. 6.3. It shows four curves with DC bias changing from 0 to 30 kV and the same voltage setting of the pulse of 80 kV. Fig. 6.3a shows that at maximum bias the total voltage of 110 kV is not reached, probably there are increasing voltage losses in the circuit due to the high current with added bias. At maximum current the voltage always has its minimum, but after that the voltage returns to a stable level for 300 ns. This level is almost independent of the value of the DC bias, so the discharge has a strong stabilising effect on the voltage in this period, in which the current decreases more than one order of magnitude. The

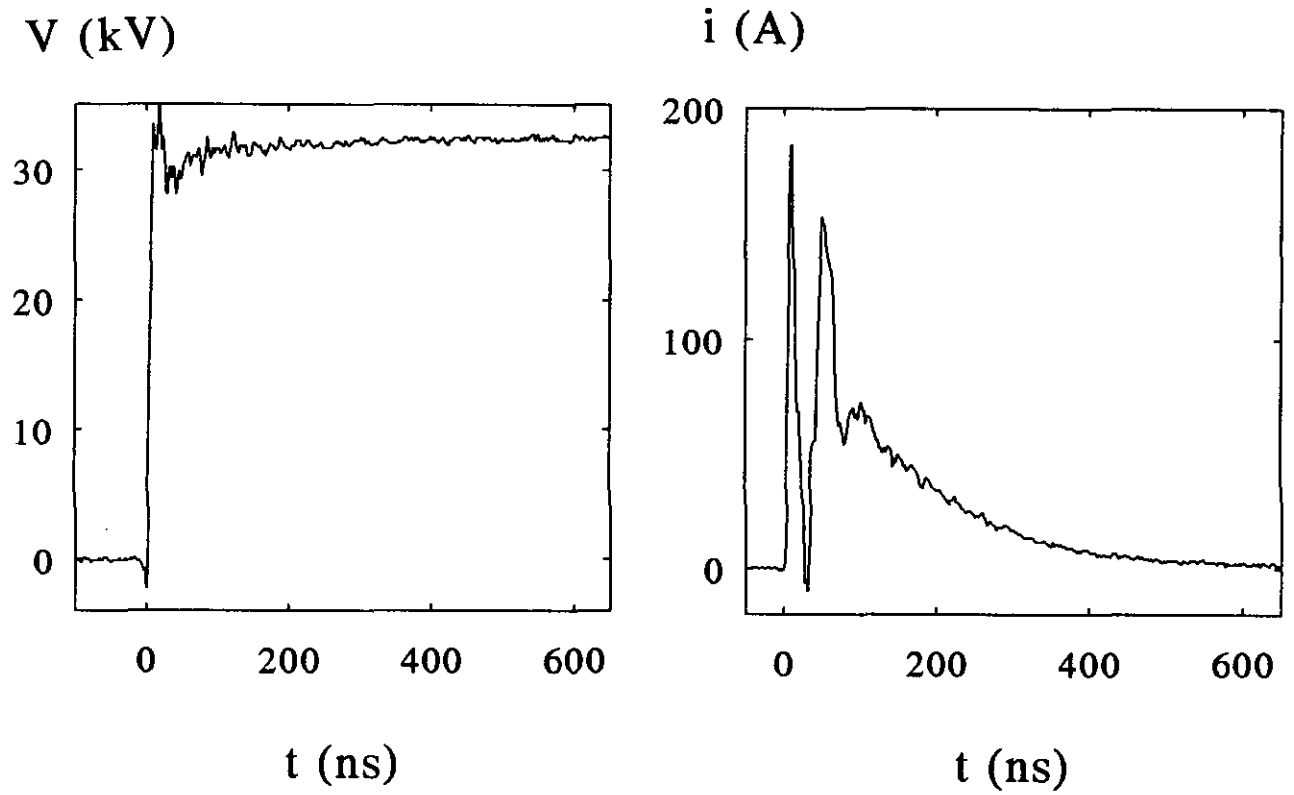

Fig. 6.1: Example of voltage (a) and current (b) pulse with a relatively large coupling capacitor to obtain a "constant voltage" source.

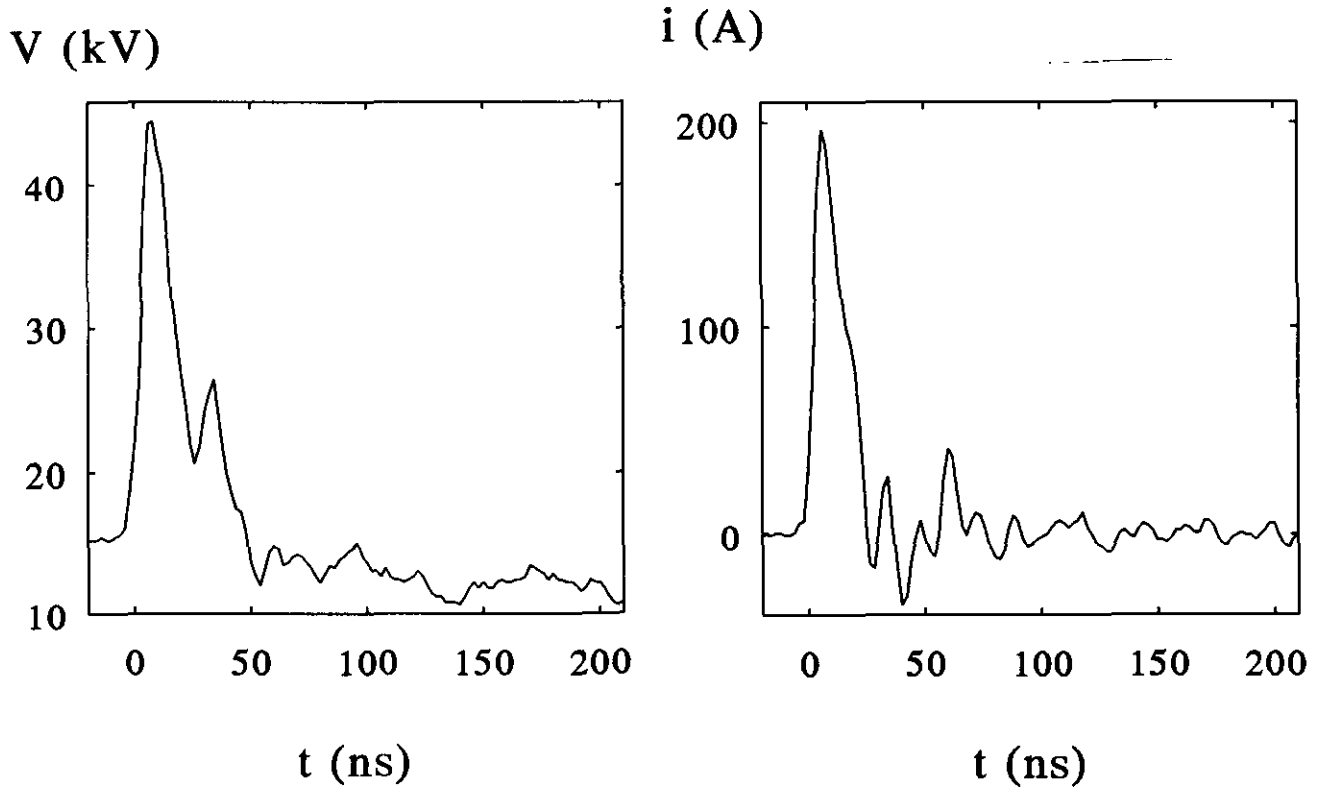

Fig. 6.2: Example of voltage (a) and current (b) pulse obtained with a small coupling capacitor to obtain the shortest possible current pulse.

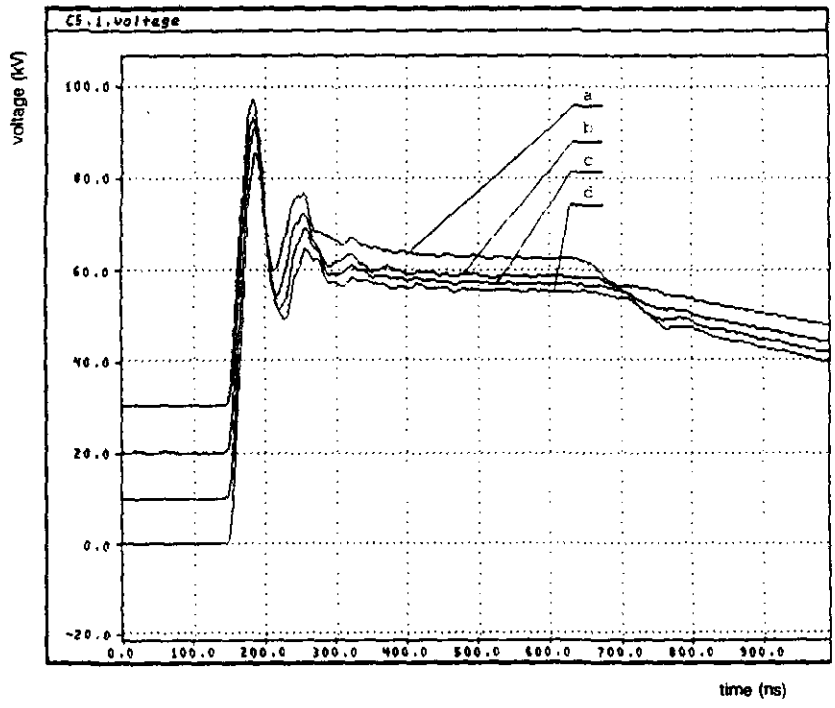

Fig. 6.3: Voltage waveforms obtained with different values of DC bias (a: 0, b: 10, c:20 and d: 30 kV). Between 300 and 700 ns the discharge has a strong stabilising effect on the voltage.

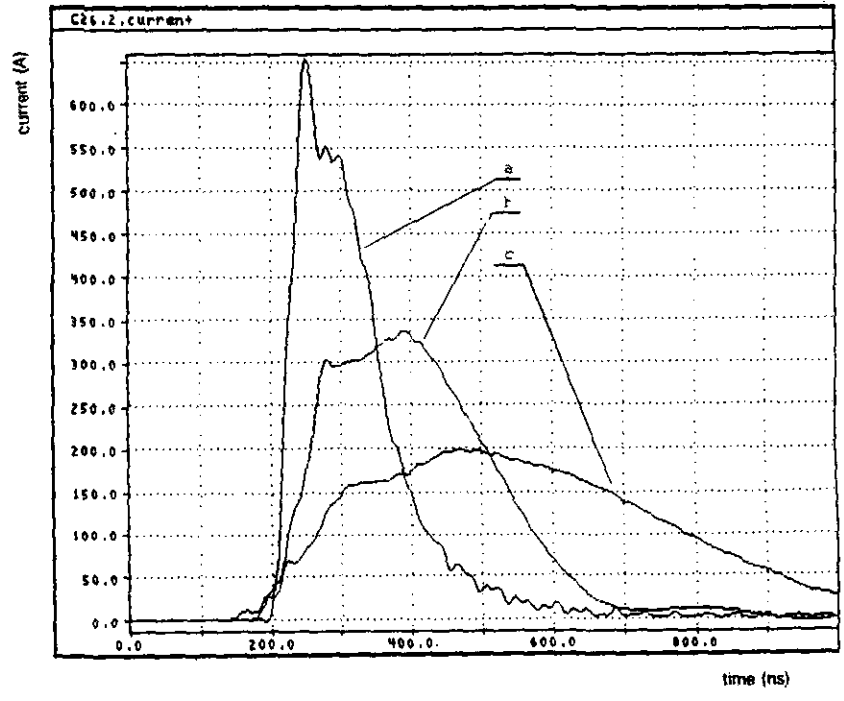

Fig. 6.4: Current waveforms obtained with different additional inductances (a: 0, b: 17.5 and c: 55 μH). The integrated current of the three curves is almost the same.

average field strength in the gap during this period is rather high, 60/7.5 = 8 kV/cm. These measurements were made without a second spark gap.

Figure 6.4 show the effect of an additional inductance between coupling capacitor and corona reactor. Values of 0, 17.5 and 55 μH have been used. Fig. 6.4a shows that the oscillation in the voltage becomes slower with increasing inductance. Also the current duration becomes much longer, as shown in fig. 6.4b. It turns out that the total energy in these three pulses is almost constant. The behaviour of total circuit can be represented quite well with an LCR network model using a time dependent resistor to describe the discharge. This model is described in detail in [79].

6.2.2 Induced energy

Figure 6.5 shows four cases of the energy obtained per pulse in the small set-up, but normalised to a wire length of one meter. In fig. 6.5a the peak voltage is along the horizontal axis, in 6.5b the rise time, in 6.5c the repetition rate and in 6.5d the anode radius. The results have been obtained in the wire-plane geometry with a distance of 35 mm, the anode radius is 0.3 mm, except in 6.5d. From fig. 6.5a it is concluded that the dependence of the energy on the pulse voltage fits very well a quadratic shape, starting at the inception value of 15 kV. In fig. 6.5b it is clearly seen that rise time and DC bias both have considerable influence on the energy input. By increasing the repetition rate the energy input per pulse decreases, as is demonstrated in fig. 6.5c, however, the total power dissipation still increases with increasing repetition frequency. This decrease is much less pronounced in the presence of a DC bias, but the overall values are lower in this case. The energy increases with the radius of the anode, this can be explained by the fact that at a thin wire the streamer propagates in a lower electric field strength in the gap. The effects of DC bias and repetition rate must be coupled with space charge but are not straigthforward explainable.

With the large set-up the energy per pulse has been measured as a function of the peak voltage and the DC bias. Variation of the repetition rate is limited in this case by the available DC supplies and changing the anode radius is more complicated. Fig. 6.6 shows results for three values of series inductance: 0, 17.5 and 55 μH. This inductance does not have much influence on the input energy when the peak voltage is changed (fig. 6.6a) or the DC bias (fig. 6.6b). The maximum value obtained is 9 J per meter wire length. With zero DC bias the energy input is much lower with this set-up, up to 1.0 J/m at 80 kV pulse voltage. This result seems contradictory with fig. 6.5b, but they cannot be compared directly, since the voltage level in fig. 6.5b is 25 kV, i.e. not much above inception, whereas in fig. 6.6 the voltage is far above the static breakdown voltage (of around 60 kV).

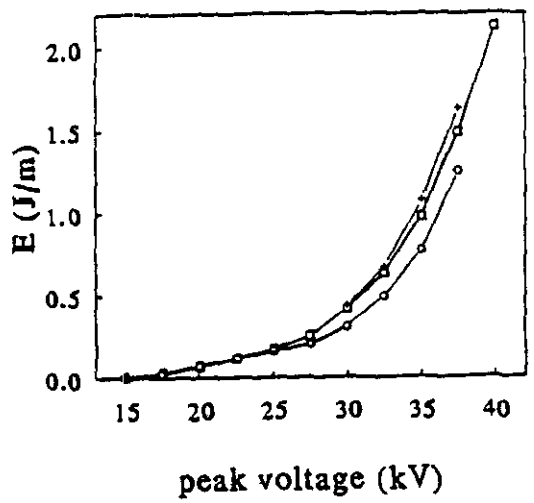

Fig. 6.5a: Energy vs. peak voltage (a) and energy density vs. rise time (b) for the small set-up with a wire-plate configuration. (□ rise time 40 ns, ○ rise time 160 ns, both pulse width 800 ns, +: rise time 40 ns, pulse width 1600 ns).

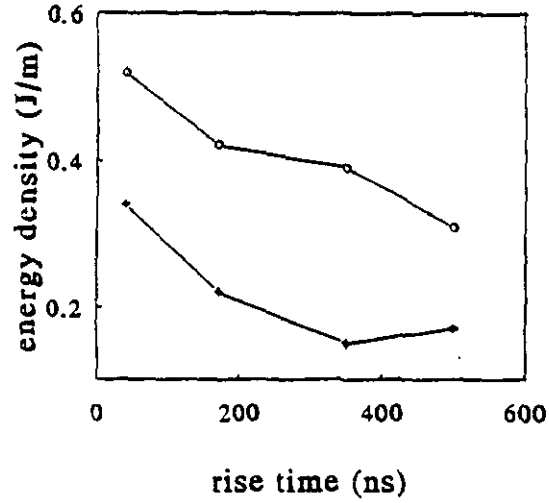

Fig. 6.5b: Energy density for two bias voltages (pulse 25 kV, 40 ns, ○: 0 kV bias, +: 5 kV bias).

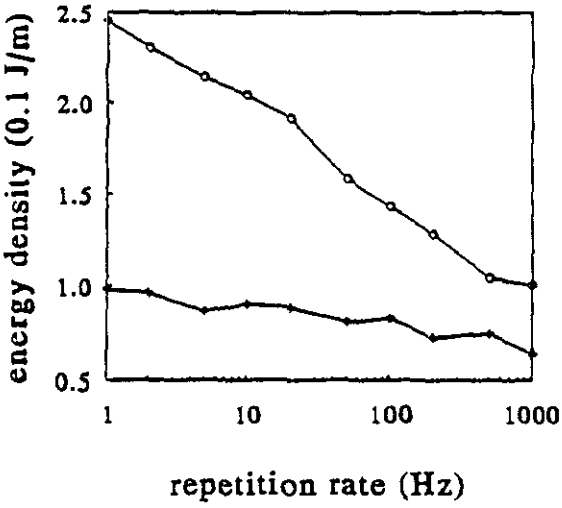

Fig. 6.5c: Influence of repetition rate on energy density. (Pulse 25 kV, 40 ns, ○: 0 kV bias, +: 5 kV bias).

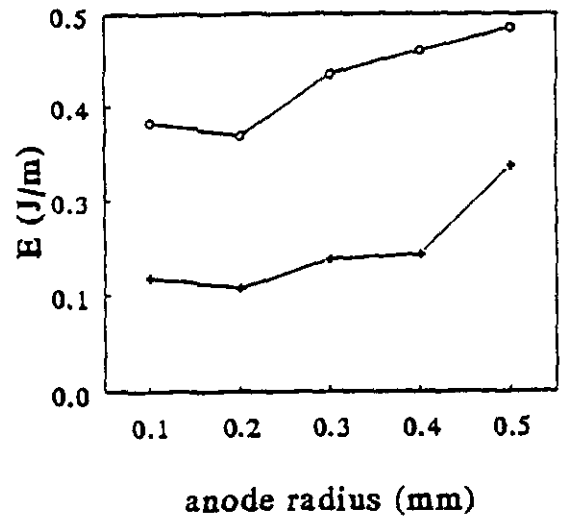

Fig. 6.5d: Influence of anode radius on energy. (Pulse 25 kV, 40 ns, ○: 0 kV bias, +: 5 kV bias).

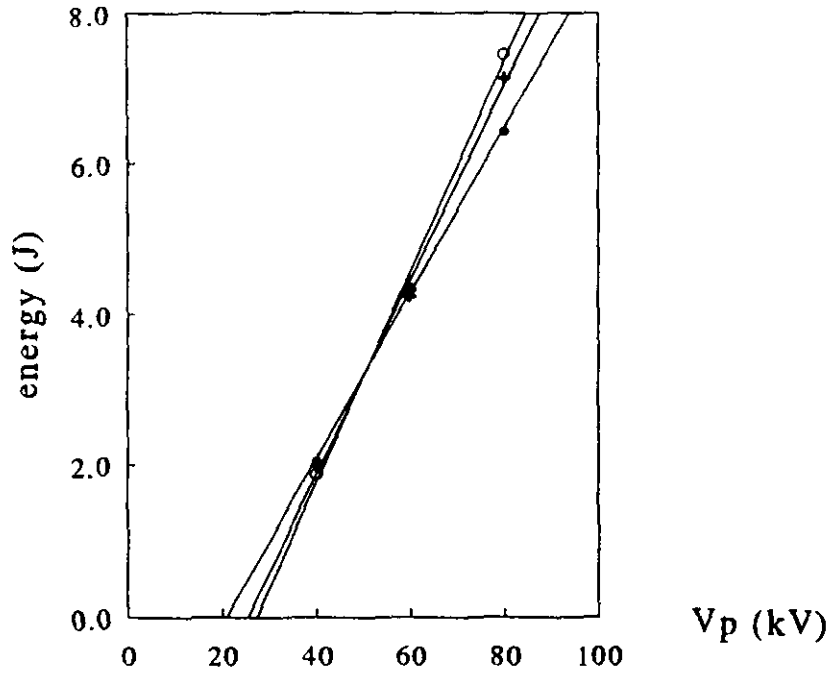

Fig. 6.6a: Energy per pulse vs. peak voltage of corona discharge in air, obtained at the large set-up, for different additional inductances. DC bias 30 kV, ●: 0 μH, +: 17.5 μH and ○: 55 μH.

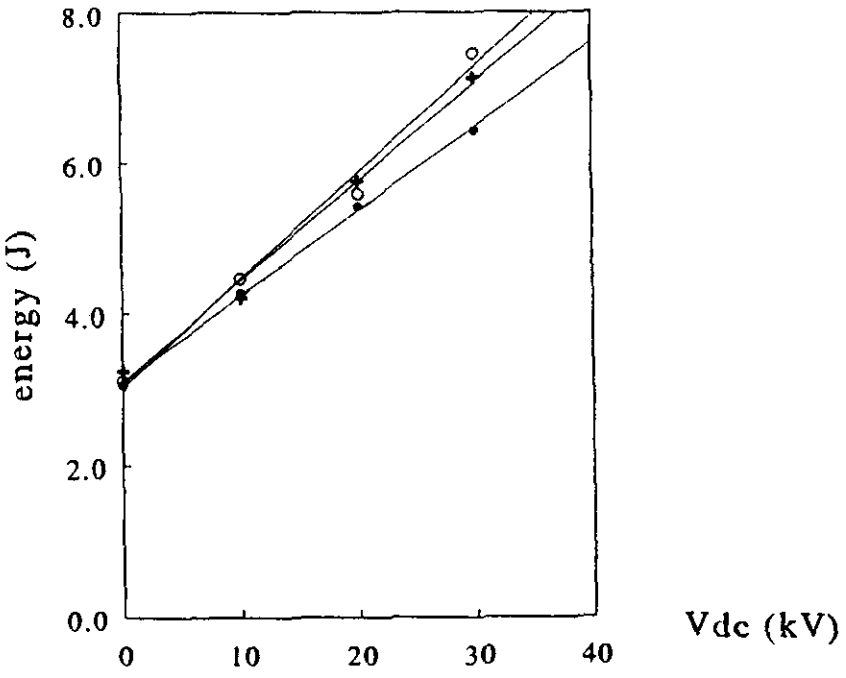

Fig. 6.6b: Energy per pulse vs. DC bias of corona discharge in air, obtained at the large set-up, for different additional inductances. DC bias 30 kV, ●: 0 μH, +: 17.5 μH and ○: 55 μH.

6.3 WP1

6.3.1 Discharge structure (A1.1)

The Schlieren photo's are made in a wire-plane gap with a distance of 50 mm, a wire length of 100 mm and a wire radius of 0.4 mm. The reference pulse condition is 40 kV peak voltage, 5 kV DC bias and 30 ns rise time, the gas is always ambient air. As described in section 4.4 the photo's can be taken with different delay times after the corona pulse. It turns out that the visibility of the streamers on the photo's is the best after 50-100 μs. Fig. 6.7 is an example of such a case. Two different types of channel are clearly observed. Relatively thick channels cross the whole gap while a greater number of thin short channels are also clearly visible, but only upto 1 cm from the anode wire.

The average number density of the streamers (determined from 10 photo's) is 7 cm^{-1}. There are about three times more thin, short channels than long, thick channels. Near the anode the thick channels demonstrate sharp contrasts, which means that in this region the deflection angle is larger than α_{lim}. Density gradients are thus relatively large and the lateral displacement of the beam makes straigthforward determination of the channel diameter impossible. The diameter of the Schlieren pattern, ~1 mm, is a maximum value for the channel diameter. Because $\alpha > \alpha_{lim}$ in this region, the density reduction factor f is at least 2%. However farther away from the anode the contrast in the channel pattern is much lower, allowing determination of the channel diameter. Midplane the channel diameter is ~2 mm and near the cathode it is ~4 mm. From a comparison of the patterns observed at midplane with calculated profiles (fig. 4.4), the maximum reduction of the neutral density can be estimated at 0.5 ± 0.3%.

When the delay time between the discharge and the flash lamp is made shorter, the residual streamer channels show up less clearly. Thus delayed energy transfer to the gas is clearly demonstrated. Heat transfer along the channels as a function of time is not observed. The delayed energy release is likely to be due to transfer of vibrational energy from metastable nitrogen molecules to translational energy. However, when no delay time is used (i.e. photographs are illuminated up to a time of 10 μs after the front of the voltage pulse) thick channels are already observed. Their diameter is hardly smaller than those observed 100 μs later. This observation leads to the conclusion that the thick warm channels are formed by a radially expanding cylindrical shock front. (This was assumed beforehand in section 5.3.2). The initial temperature and pressure rise of the streamer channel is followed by gas dynamic expansion at about the velocity of sound. So the channels are broadened to a diameter of 2 mm in about 3 μs. This cannot be resolved with the present measurement system. At delay times larger than 200 μs, Schlieren patterns show less contrast because of heat diffusion. The channels are still visible after delay times up to 2 ms.

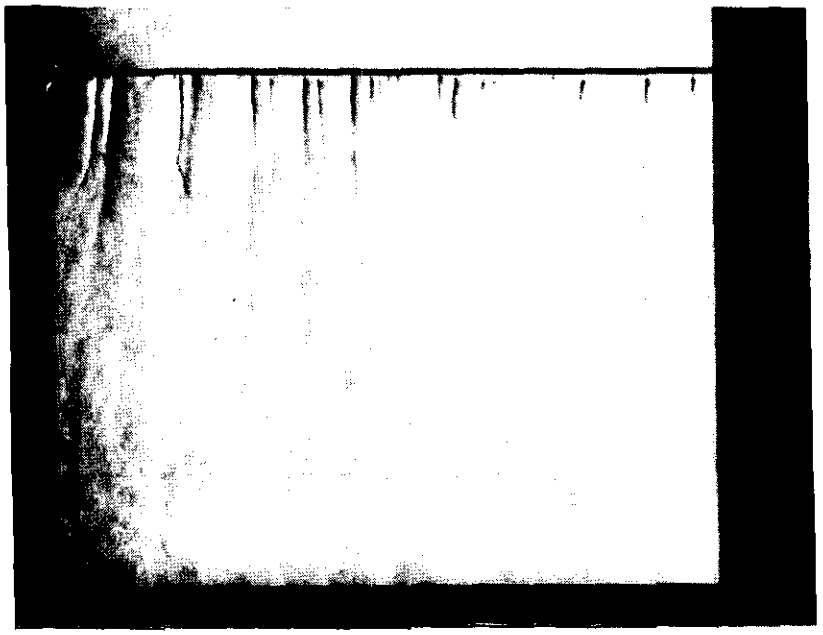

Fig. 6.7: Schlieren photo of a wire-plate discharge, gap distance 50 mm, peak voltage 40 kV, 40 ns rise time.

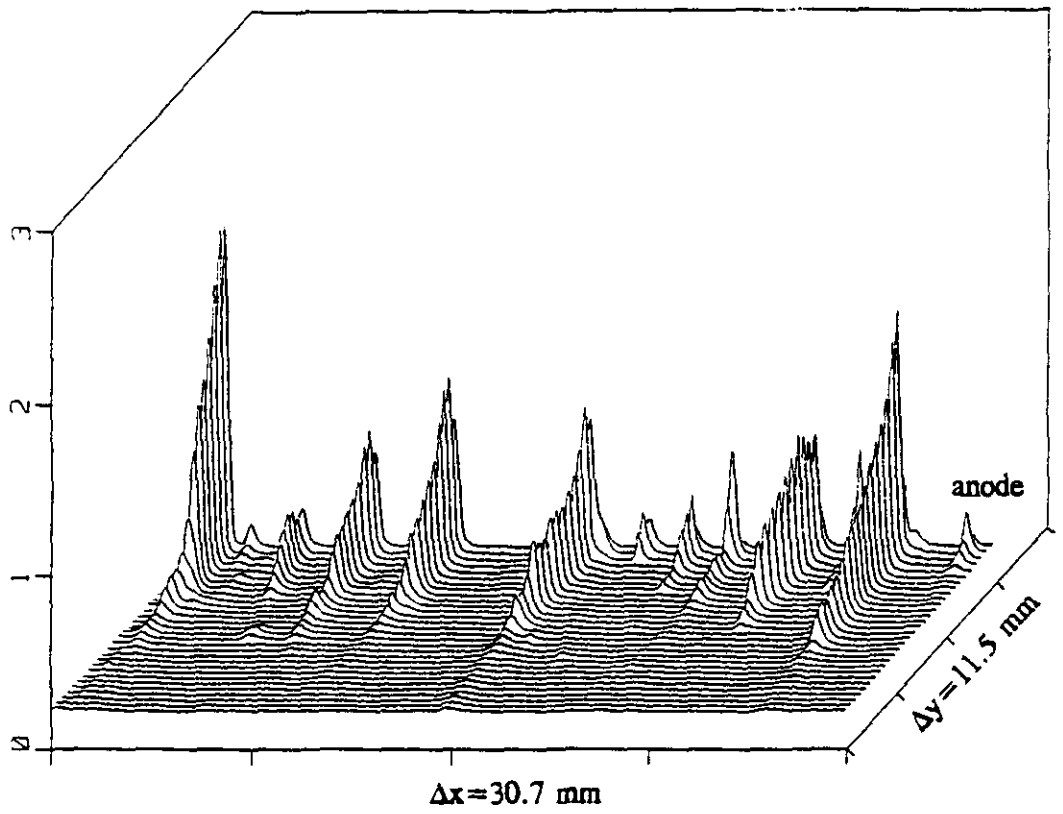

Fig. 6.8: CCD picture giving a two-dimensional emission profile of a wire-plate discharge, gap 35 mm, peak voltage 25 kV, rise time 40 ns.

It should be noted that the thick long channels are observed only with peak voltages in the range of 35-40 kV. For the gap distance used, 50 mm, these values are close to breakdown. When lowering the voltage from 40 to 37.5 and 35 kV, the total number density decreases from 7.2 to 6.6 and 4 cm^{-1} resp., and the charge per streamer decreases from 17 to 16 and 13 nC. The influence of the voltage rise time is very similar to the lowering of the peak voltage. For a longer rise time the charge per streamer decreases and the number decreases as well. DC bias voltages up to values of 10 kV, keeping the total voltage constant, have no influence on the observed Schlieren patterns.

The anode structure has been changed by inserting a thin saw blade in stead of a wire. This saw blade has 12 pins per cm. Under identical conditions as fig. 6.7, a streamer is observed at every pin. The long thick channels are not observed and the individual streamer channels appear more identical. However, the total injected charge per unit length is the same. This clearly shows that the anode shape influences the discharge structure.

A picture of the discharge structure as it is observed by the CCD camera is shown in fig. 6.8. It shows only a fraction of the gap, which had a wire-plane distance of 35 mm, and an anode radius of 0.3 mm. At $V_p = 25$ kV strong emission is observed near the wire but no streamers are observed in the cathode region. At $V_p = 30$ kV, streamers bridging the whole gap are observed. The emission is detected without time resolution. Time resolved photomultiplier signals show that the light emitted by the primary streamer front has a very short duration. The luminosity of the streamer channel is very low, until the secondary streamer extends from the anode along the primary streamer channel. The strong signal seen up to distances of 6 mm from the anode is due to the secondary streamer phenomenon. This strong signal is not caused by a high intensity of the emission but by its much longer duration! The streamer number density measured from the CCD pictures agrees very well with the number density obtained from the Schlieren pictures. However, comparison with space and time resolve photomultiplier measurements reveals that neither the Schlieren photo's nor the CCD images are sensitive enough to detect all streamers far from the wire at relatively low peak voltages (< 25kV).

The use of the CCD camera is extended by combining it with a gated intensifier. This enhances the sensitivity of the system several orders of magnitude and it allows the use of a time frame with a minimum frame width of ~ 34 ns. Pictures obtained with such a gate time show that the channel left by the primary streamer remains dark until the moment that the catode is reached. After this, the secondary streamer is seen as a partial re-illumination of the residual primary streamer channel near the anode. This is shown in fig. 6.9 which is taken 106 ns after the start of the voltage pulse. The signal of the primary streamer is completely vanished and the extend of the secondary streamer can now be observed clearly. This secondary streamer becomes less visible when the O_2 concentration is decreased and it is not observed in N_2-CO_2 mixtures. These observations confirm the theory that attributes the secondary streamer phenomenon to the attachment properties of oxygen at low field

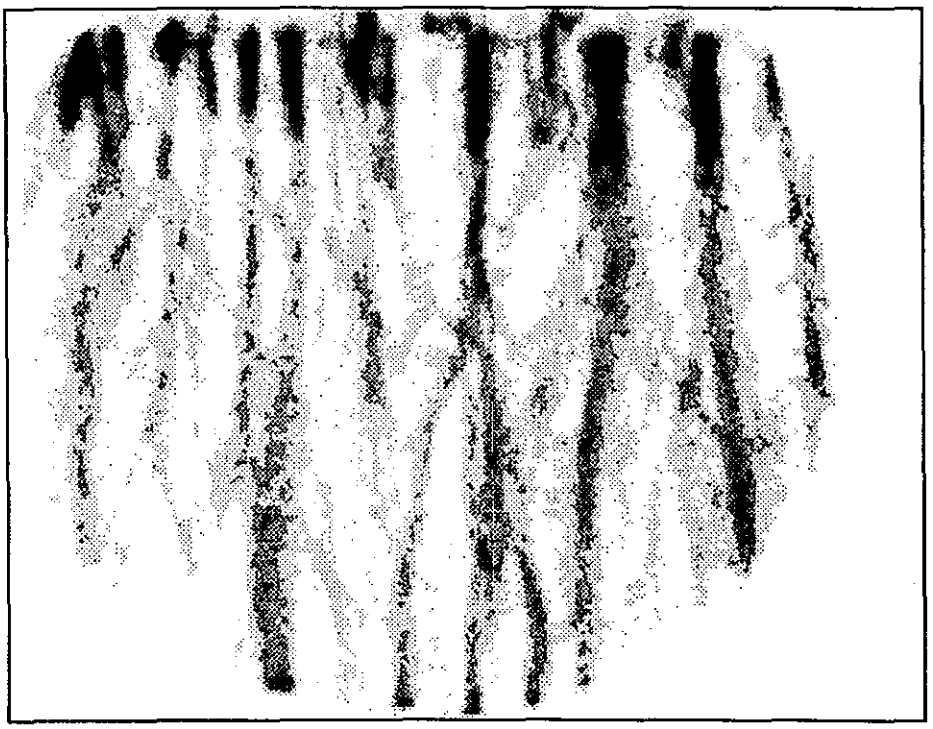

Fig. 6.9: CCD picture obtained with intensifier showing the whole gap, the picture is taken 106 ns after the start of the voltage pulse. At the anode the secondary streamers show up.

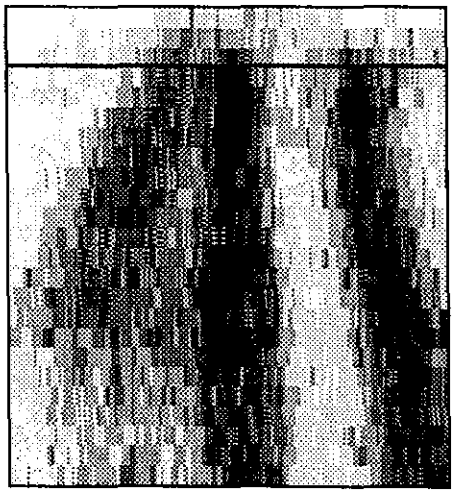

Fig. 6.10: CCD picture obtained with image intensifier of a small part near the anode. The streamer diameter obtained from these images is 200 μm.

strengths [80]. With the intensifier it is observed that also at a low voltage, $V_p = 20$ kV, some streamers cross the entire gap. Only at a voltage just above inception, 17.5 kV, no streamers reaching the cathode are observed. When the cathode-plate is covered with glass the discharge structure remains unchanged and the secondary streamer is still seen. However, at places where streamers reach the dielectric, a bright surface discharge is observed.

Another way to use the increased sensitivity due to the intensifier is to magnify the image in order to determine the streamer diameter. Fig. 6.10 shows an example of such a picture. It has been taken near the anode with a gate time of 34 ns, so no light of the secondary streamer is observed. The streamer diameter determined at 50% of the maximum intensity is approximately 200 μm and remains fairly constant during the propagation across the gap. In this picture it is also seen that two streamers start at almost the same position, but the left one stops after ~1 mm. This is probably due to the mutual influence of their electric fields.

6.3.2 Electron energy (A1.2 and A1.4)

In figure 6.11a, made at the large set-up, an example is given of the optical emission of the discharge in air from a cylindrical volume of 10 mm diameter along the wire. The signal is obtained with the monochromator tuned to the maximum of the N_2 337.1 nm line. It is given as a function of time for three different pulse voltages, 40, 60 and 80 kV and 30 kV DC bias. The two maxima in the curves correspond to the primary and secondary streamer. The rise of the secondary streamer gives the moment when the streamer arrives at the cathode. This instant was also determined with a fiber that collects light only from a small region just above the cathode. Fig. 6.11b gives the emission near the anode of the N_2 ion line at 391.4 nm under the same pulse conditions.

Fig. 6.12 shows emission as a function of the wavelength in the region of the N_2 ion line, at $V_p = 80$ kV and $V_{DC} = 30$ kV. The maxima at 389.5 and 393.9 nm are from the neutral N_2. In this figure two conditions are indicated, a) is for the primary streamer and b) for the secondary. They can be measured separately by using a time window on the oscilloscope signal, the separation point is chosen at the minimum of fig. 6.11b. It can be seen from the figures 1 and 2 that the ion line is much weaker than the neutral (The sensitivity of the detection system hardly changes between 337.1 and 391.4 nm). This is to be expected because the excitation and ionisation processes have cross sections with different threshold values (12 and 20 eV, resp.) and both processes occur in one electron collision as can be estimated from the small size of the streamer head (~100 μm) and its high velocity (~10^6 m/s). A second aspect is that the ion line is much weaker in the secondary streamer (background signal intensity must be taken into account). This indicates that the average electron energy is lower here. Under the conditions of our experiment a Maxwellian electron energy distribution function is generally assumed [81]. Combined with the Burns

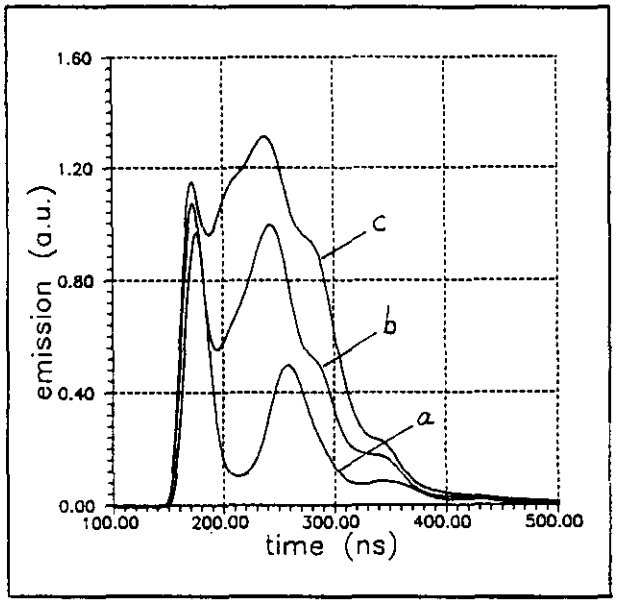

Fig. 6.11a: Emission of the N_2 line in air at 30 kV bias and a pulse voltage of a: 40, b: 60 and c: 80 kV.

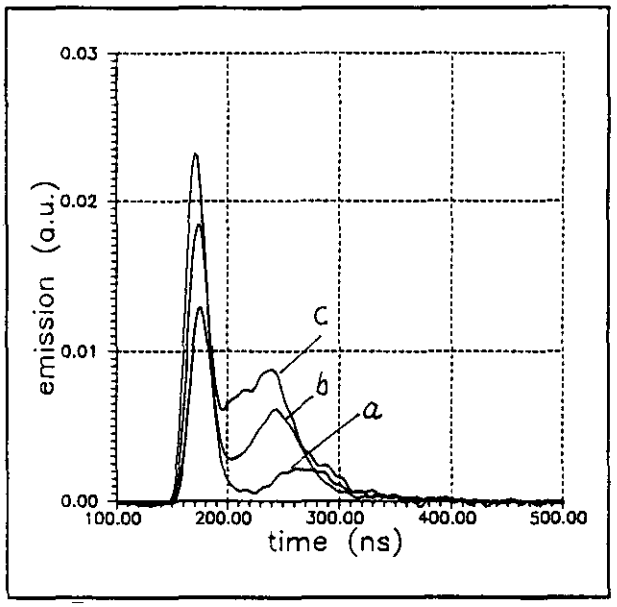

Fig. 6.11b Emission of the N_2 ion line in air at 30 kV bias and a pulse voltage of a: 40, b: 60 and c: 80 kV.

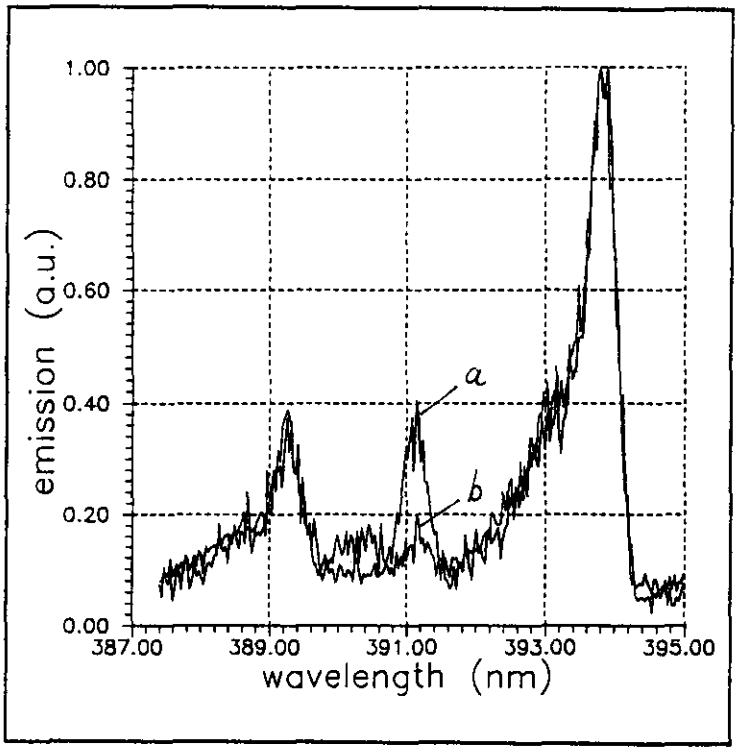

Fig. 6.12: Emission vs. wavelength for primary (a) and secondary (b) streamers, pulse voltage 80 kV and bias 30 kV.

cross sections as described in [82] it is found that the electron energy for primary streamers in air is in the order of 10 eV. It increases with ~2 eV when the pulse voltage is raised from 40 to 80 kV, but only with the highest rate of rise, i.e. 3 kV/ns, otherwise it is constant. It is also constant during the streamer propagation. It is difficult to estimate the absolute error in this result but the trend is realistic. In the discharge channel behind the streamer head the emission intensity is very low. The electron energy cannot be derived here, also because the method becomes inaccurate and the electron distribution function is no longer Maxwellian. The electric field in the channel left behind by the primary streamer is the so-called stability field [66,83]. Experiments show that 20 Td is the field strength in the streamer channel [83]. This gives an electron energy of 0.3-0.6 eV from Boltzmann calculations [66,81,84]. This value is also found in other experiments [85].

The length of the secondary streamer is estimated to be 1-2 cm from visual observation. It is limited in length, because the integrated field strength across the gap must be equal to the applied voltage. With 20 Td in the channel this leads to ~100 Td for the field strength in the secondary streamer, which is similar to earlier observations [80]. The length of the secondary streamer obtained with the image intensifier at the small set-up leads to practically the same value for the field strength. The relation between average electron energy and reduced field strength given in [81,84] gives a value of 1 eV in this case. The line ratio method gives 4 eV and 300 Td here. There are two reasons why this result can be expected to be too high. First it is difficult to subtract the background density precisely and second there can be new primary streamers in the signal. This makes the method inaccurate for this part of the experiment.

For the streamer head 10 eV electron energy yields a field strength of 900 Td. The formula in [81] is for pure N_2, but the Boltzmann calculations [84] have been carried out in mixtures of N_2, O_2, H_2O and CO_2 and leads to a similar result. The value of 900 Td found here agrees with calculated values for the streamer head [66,72].

In flue gas the secondary streamer hardly appears and is always much shorter than in air. This leads to the conclusion that the electric field is higher in the discharge channel in flue gas, i.e. ~30 Td [8], so there is less voltage remaining to build up a secondary streamer. The attachment coefficient of flue gas is different, due to the presence of H_2O and CO_2 and a much lower O_2 concentration. There are also strong excitational collisions of H_2O and CO_2 molecules. Because these (de)excitations are not well known quantitatively it is not possible at this moment to derive values of the average electron energy in the case of flue gas. Considering the calculations [84] they will not differ much from air.

6.3.3 Gas temperature (A1.2)

The gas temperature in the residual streamer channel after the primary streamer has passed is derived from the well-resolved rotational emission spectrum of the light emitted by the secondary streamer. The strongest emission peak of the nitrogen emission spectrum, the 0-0 vibrational transition of the second positive system at 337.1 nm, has been used. A simulation program determines the wavelength positions and intensities of all possible transitions between rotational levels of the different electronic states. The method is based on the well-known theory of molecular spectra and structure [38]. The rotational temperature is obtained by comparison between the experimental spectrum and the simulated spectrum for which the rotational temperature is an input parameter.

The time scale of the exchange of translational and rotational energy is in the range of picoseconds at atmospheric pressure. Therefore the rotational temperature may be used for the determination of the gas temperature. Light of the secondary streamer is used to determine the gas temperature in the residual streamer channel. This can be done because it is well separated in time from the emission of the primary streamer (see 6.3.1 and 6.3.2).

The best fit between the experimental and the simulated spectrum is obtained for a temperature in the range of 300-350 K. This means that, 100 ns after the passing of the primary streamer, the gas in the residual channel is not much heated. It should be noted that the peak voltage which is used for the spectroscopic measurement is 25 kV. This voltage is far below breakdown voltage. The voltage at which the breakdown probability becomes non-zero is 30 kV for the gap of 35 mm that is used for the spectroscopic measurements. On the Schlieren pictures significant gas heating by streamer channels is only seen at voltages just below breakdown (40 kV for 50 mm gap).

6.3.4 Streamer inception (A1.3 and A1.4)

The optical signals from quartz fibers are used to determine time differences between the inception of different streamers. This is done by using one fiber with a very large opening angle so the it sees the whole discharge volume (including the first streamer). A second fiber has a very limited angle of view and is positioned so that it sees a volume close to the anode with only one streamer at most. The time difference between the first fronts of both signals is the delay between the very first streamer and an arbitrary one. This delay time is put into a histogram and after many pulses this histogram gives the distribution function of the delay times of different streamers in one electrical pulse. Fig. 6.14 shows two such histograms, using 25 and 30 kV peak voltage and 40 ns rise time. Both lines show that the delay times are always shorter than 15 ns and there appear to be two groups, one with a maximum at 2 ns and the other at about 8 ns. There is only one process which is fast enough to initiate an avalanches over a distance of several centimeters, i.e. photoionisation. The light

can travel 30 cm/ns and the avalanche takes about 1 ns to develop into a streamer head so this explains well the first maximum in the histogram. The second maximum must also be related with these effects because all other processes are orders of magnitude slower, a detailed explanation however is not yet known.

Fig. 6.15 shows how the energy in one pulse varies along with the voltage of the inception. It is clear that the energy in a pulse increases with the inception voltage. This effect is probably due to the fact that the avalanche develops in a higher field, when the inception voltage is higher, and this will lead to a higher streamer current. The higher current is caused by an increasing number of ions in the streamer head, but also by its higher velocity (see next section).

6.3.5 Streamer propagation velocity (A1.3)

The time delay of the multiplier signals from the two fibers is recorded on the oscilloscope and stored real time in the memory of a computer. (Interchanging of the fibers establishes the overall difference in transit time of the two channels). The delay times are displayed in histograms which show a symmetrical distribution with a standard deviation of up to 20%. This deviation is mainly due to the stochastic variation of the streamer velocity. The average streamer velocity is deterimined from 1000 measurements at 20 Hz repetition rate of the discharge.

In fig. 6.16a the velocity is displayed for two voltages in the 35mm wire-plane gap. The velocity has its maximum value towards the anode, but the closest point is already 4 mm away, due to the method chosen. Making the distance between the fibers smaller would result in a much larger error, since the measurement is already on the limit of the photomultiplier and the oscilloscope capabilities. A slight increase in the velocity is observed from the middle of the gap until the cathode. Fig. 6.17a show the result of a variation of the oxygen content in a N_2-O_2 mixture. The velocity decreases with increasing O_2 concentration. Figs. 6.16b and 6.17b show the results of model calculations to be described in the next section. For ease of comparison they are already placed along each other.

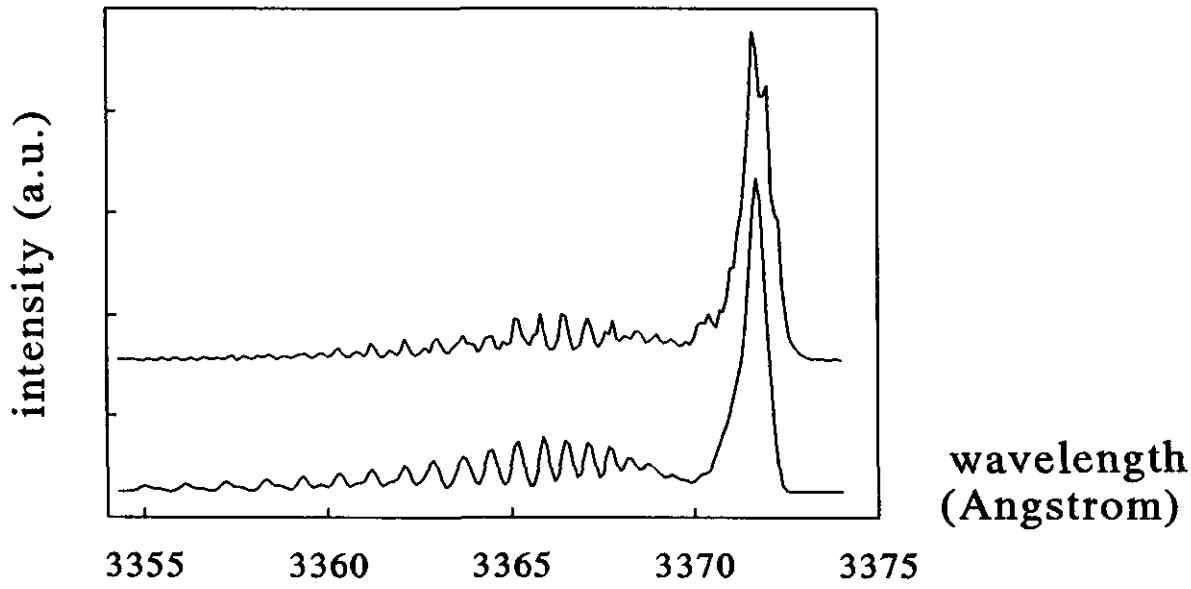

Fig. 6.13: Measured and simulated spectrum of the N_2 337.1 nm line, the gas temperature in the simulation is 300 K.

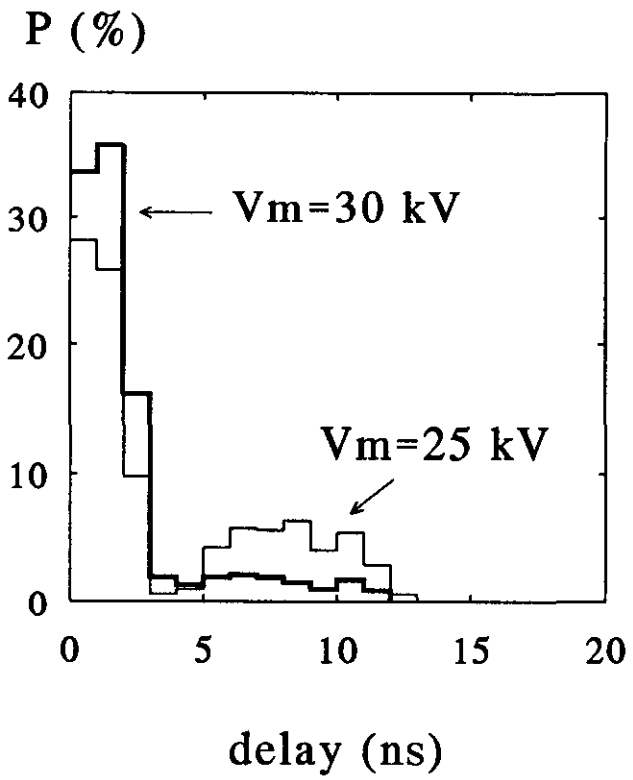

Fig. 6.14: Distribution of inception delay times for two pulse voltages.

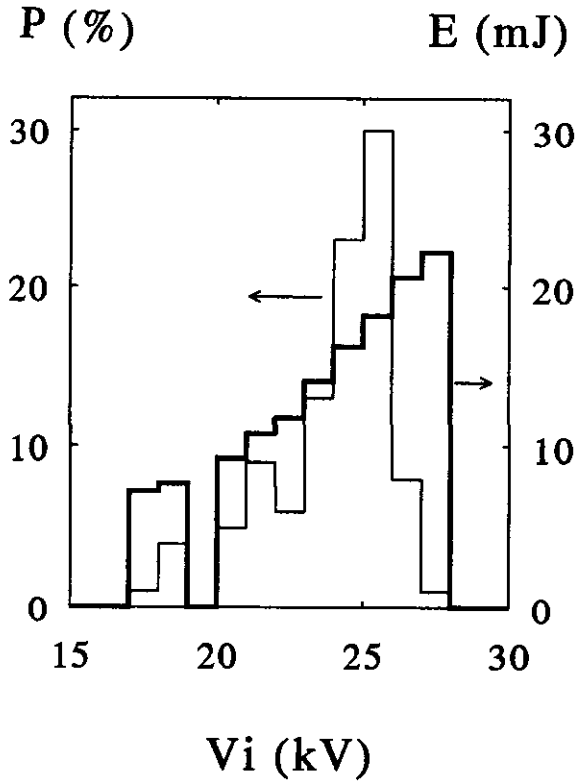

Fig. 6.15: Inception distribution and simultaneously determined energy content vs. inception voltage.

6.3.6 Model results and comparison with experiments (A1.5)

The streamer propagation model made at IVTAN has a variety of parameters, mainly for the gas composition and the voltage pulse. Further it contains several parameters for the numerical procedures and some physical processes of which the value is estimated or approached by an analytical function. This makes it very complex to test the computer program for its correctness both in a numerical and in a physical sense. So, in practise, the best way to work is to choose a standard condition and take parameter values as much as possible from experimental results. The first choise to make is the setting of the numerical parameters which is maintained at the recommended values [72]. The second is the discharge configuration. Most calculations are made with a wire-plane gap of 35 mm distance and an anode radius of 0.3 mm because most of the experiments have been performed with this condition. Then the gas is chosen to be dry air mainly, i.e. 80% N_2 and 20% O_2, with a temperature of 300 K and a pressure of 1 bar. The standard voltage pulse has an amplitude of 30 kV with an exponential shape and an 1/e-rise time of 10 ns. The time required by a 486-33MHz PC to calculate the crossing of the gap by the streamer head under these conditions is in the order of 4 to 20 hours.

The results produced by the program are divided in a time dependent part and a position dependent part (at certain moments). Fig. 6.18a shows the current that is calculated for the standard condition. The streamer starts after 12 ns, at a voltage of 21 kV. This is a sort of automatic inception mechanism, but it is only based on the dependence of the ionization on the electric field. The current has its maximum at 18 ns, which is before the maximum voltage, and it stops at 38 ns, i.e. when the streamer head reaches the cathode. The program cannot continue the calculation because other boundary conditions must be implied. The total charge is obtained by integrating this current and gives 2.36 nC. Fig. 6.18b shows the electric field which is obtained at $t = 35$ ns, i.e. when the streamer has almost crossed the gap. The maximum of the field is 260 kV/cm, i.e. 800 Td. At earlier instants, when the streamer head is close to the anode, this maximum is somewhat higher, up to 320 kV/cm. Fig. 6.18c shows the densities of ions and electrons, also at $t = 35$ ns. The positive ion density is always a little higher than the electron density, and the values found here are in good agreement with previous estimates [64,66,80]. The negative ion density is almost 20 times lower throughout the gap, execpt for a small region near the anode. The coarse steps near the anode can be avoided by choosing a finer anode mesh. However, the global results are very similar in that case but the program stops after 1 cm of propagation due to insufficient memory and also the calculation time increases considerably. The remaining net charge is also indicated in the figure. It has a maximum value of $1.1 \cdot 10^{14}$ cm^{-3} at the streamer head. The halfwidth of this maximum is 40 μm, this leads to a total positive space charge of $2 \cdot 10^8$ in the streamer head. This is also in good agreement with other models [47-58].

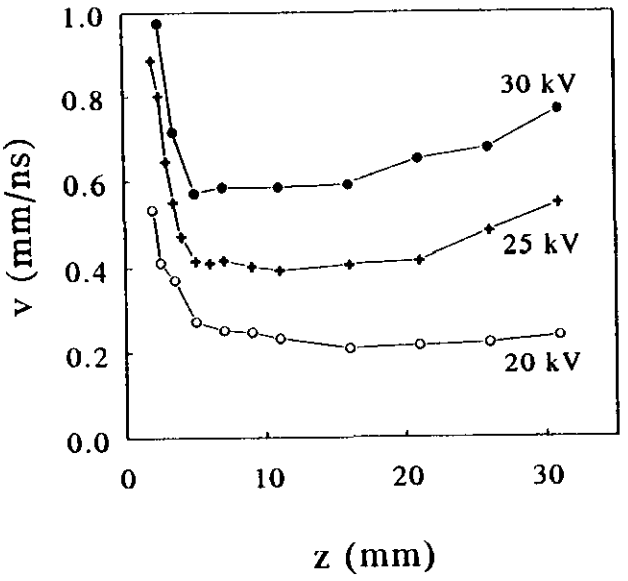

Fig. 6.16a: Streamer velocity vs. gap position for 20, 25 and 30 kV pulse voltage obtained from experiment, rise time 40 ns.

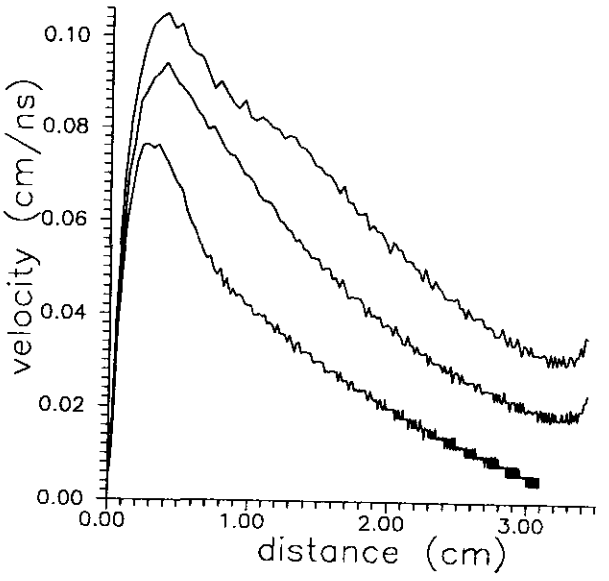

Fig. 6.16b: Streamer velocity obtained from theory, same conditions as fig. 6.16a.

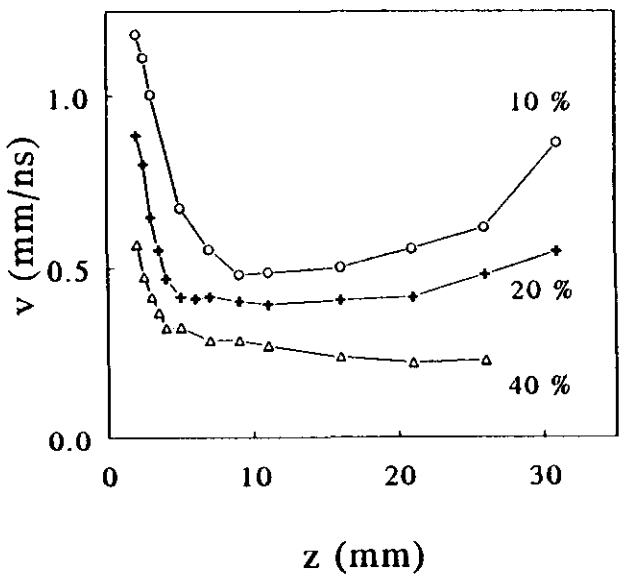

Fig. 6.17a: Measured streamer velocity vs. gap position at 25 kV and 40 ns at three values for the O_2 concentration in N_2.

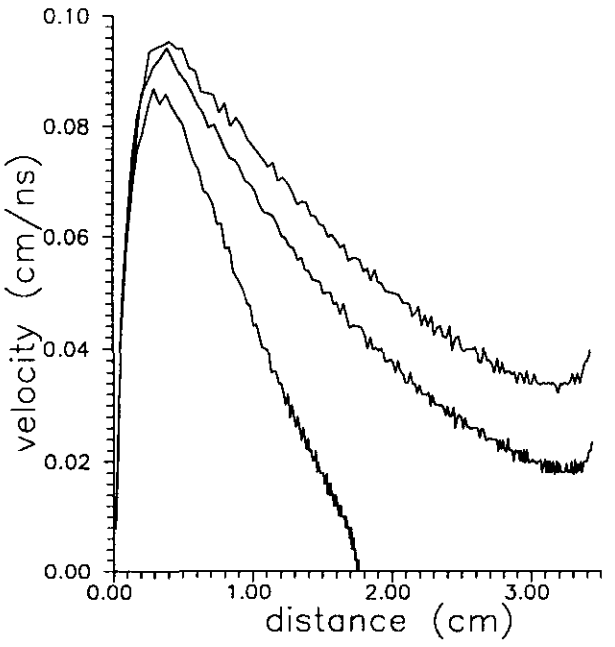

Fig. 6.17b: Calculated streamer velocity, same conditions as fig. 6.17a.

The position of the streamer head is calculated and written into a data file at regular instances (e.g. every 0.2 ns). The streamer propagation velocity is calculated by dividing the change in this position by the time interval. By plotting this value as a function of the streamer head position figures are obtained such as 6.16b and 6.17b. Some general features of these figures are described in section 6.3.5. It is seen that several general features of the model agree well with the measurement results. The velocities have quite similar values, the maximum velocity is near the anode and the trends with changing voltage and oxygen contents are identical. In detail there are also differences, the shape of the velocity curve is rather different, the anode and cathode effects are not alike, the charge calculated by the model is too low. Some of these deficiencies can be ascribed to limitations of the model. For instance the calculated charge is for the primary streamer only. Further the anode and cathode region require more sofistication in the model.

Nevertheless there are still many parameters that can be changed in order to fit the model to the experiments. In some cases this is almost a requirement due to the inaccuracy of the data contained in the model. One example will be demonstrated here with the process of photoionization. This process provides free electrons in front of the streamer head and thereby creates continuously the possibilitiy to start new avalanches. In some models a uniform background electron density is assumed for this purpose. But if a voltage is applied across the gap these electrons disappear if the Poisson equation is solved properly. The factor calculated for photoionization has been manipulated artificially to trace its influence. The propagation stops after a few millimeters if it is made very low and this moment is exactly the moment when the electrons of the background have drifted to the streamer head. When the photoionization is made very high (100x its standard value) several changes occur in the propagation process. It becomes much slower, which is seen in fig. 6.19a, it takes 170 ns now to cross the gap. The shape of the figure, with an almost exponential decay, differs considerably from 6.18a. The velocity also decreases much more, see Fig. 6.19b, which is of course in agreement with the longer transition time. Another remarkable feature is displayed in fig. 6.19c. The electric field is plotted here at $t = 170$ ns and it is seen that somewhere in the gap a region has emerged with a field strength of 30 kV/cm. The start of this region was already observed at $t = 50$ ns where some oscillations occured at this position. Fig. 6.19d shows the electron density at the same moment. The low electron density at the same location leads to a higher resistivity of this part of the plasma of the streamer channel, so a higher electric field is necessary to keep the current going. The observed field strength is equal to the critical field strength [64]. This description is almost identical to previous explanations of the secondary streamer [80], although it is mostly observed that this starts at the anode, after the primary streamer has crossed the gap.

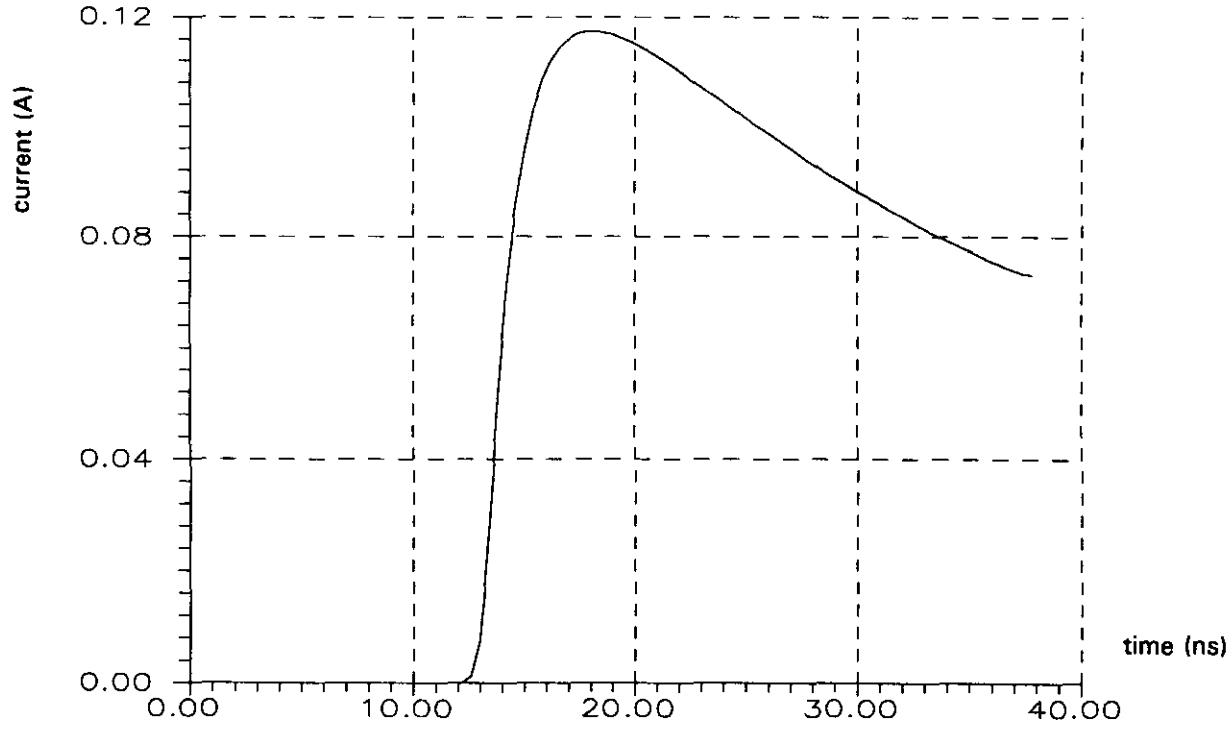

Fig. 6.18a: Current calculated for a wire-plate gap (35 mm) in air with 30 kV pulse voltage and an 1/e rise time of 10 ns.

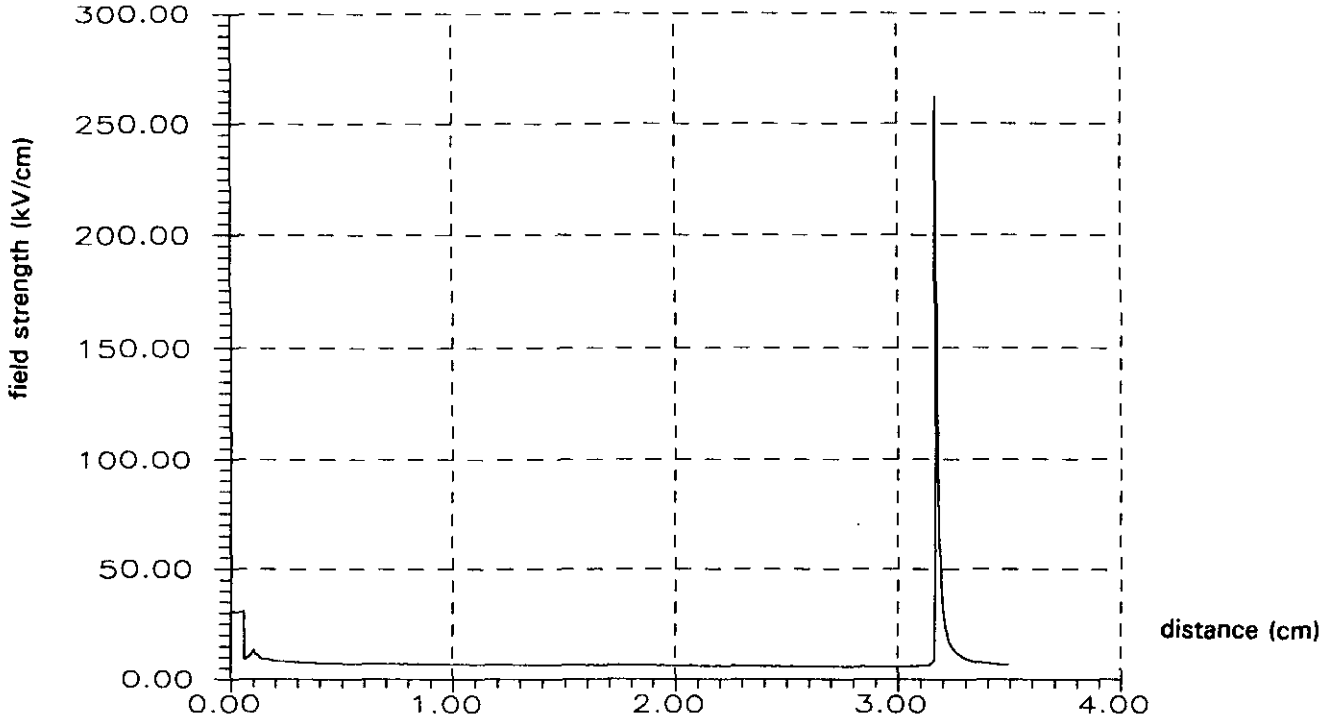

Fig. 6.18b: Electric field obtained at 35 ns, when the streamer head has almost crossed the gap, conditions as 6.18a.

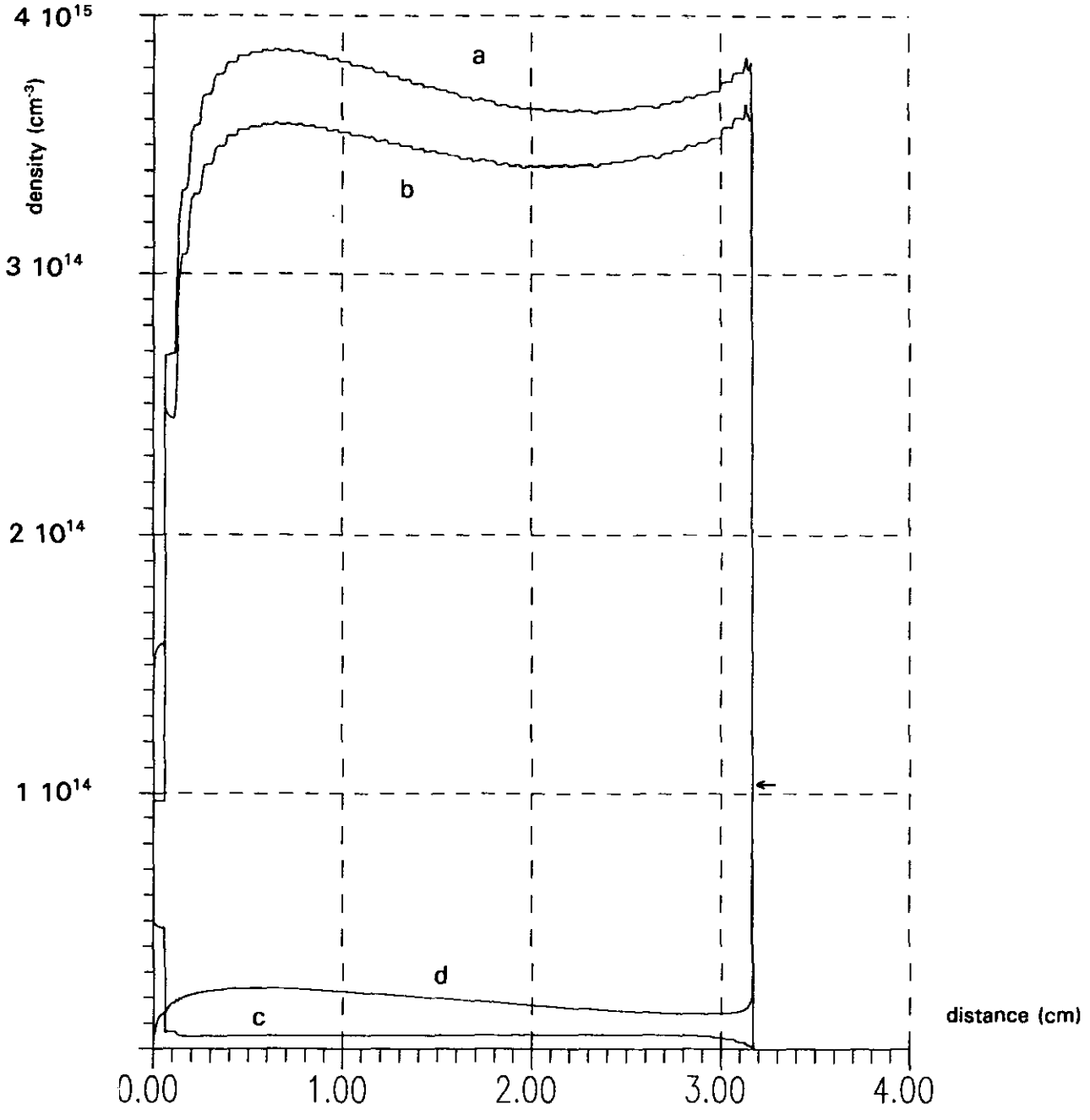

Fig. 6.18c: densities of positive ions (a), electrons (b), negative ions (c) and the net space charge (d), which turns out to be positive. The maximum net charge in the streamer head, 1.05 10^{14}, is indicated by the arrow.

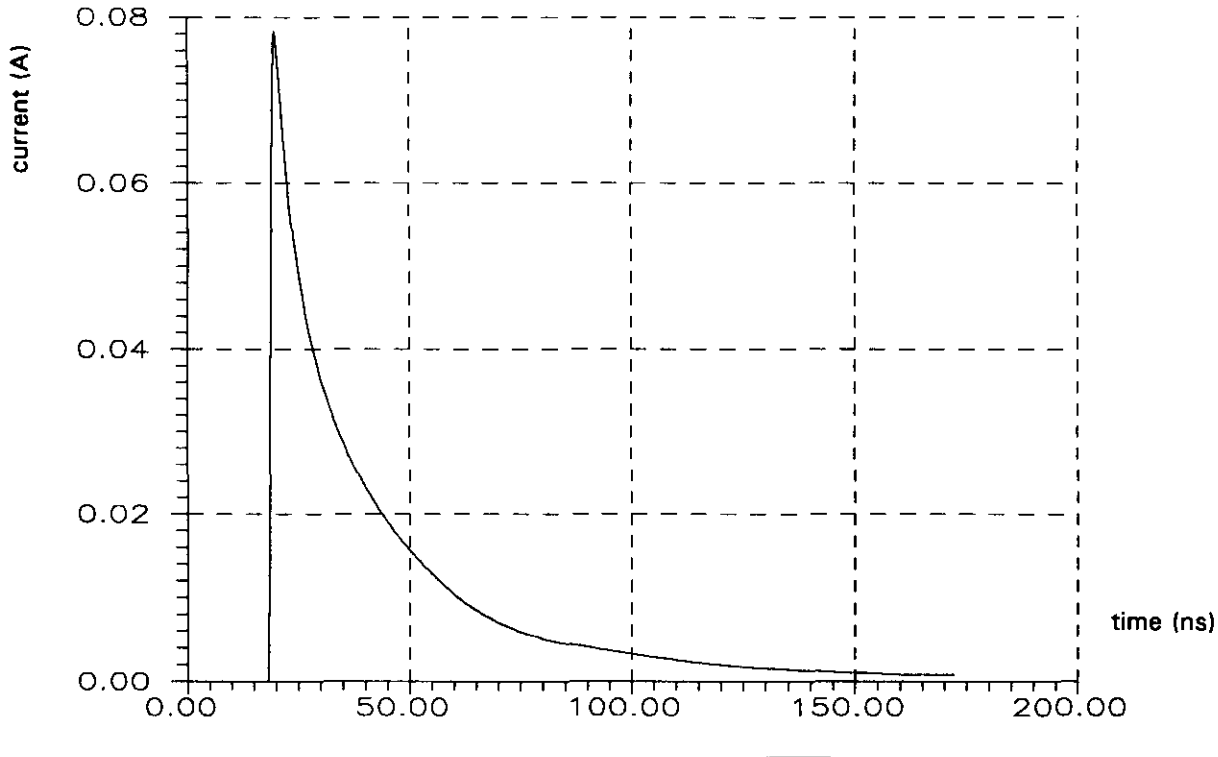

Fig. 6.19a: Current calculated under the same conditions as 6.18a, except for a 100x stronger photoionisation.

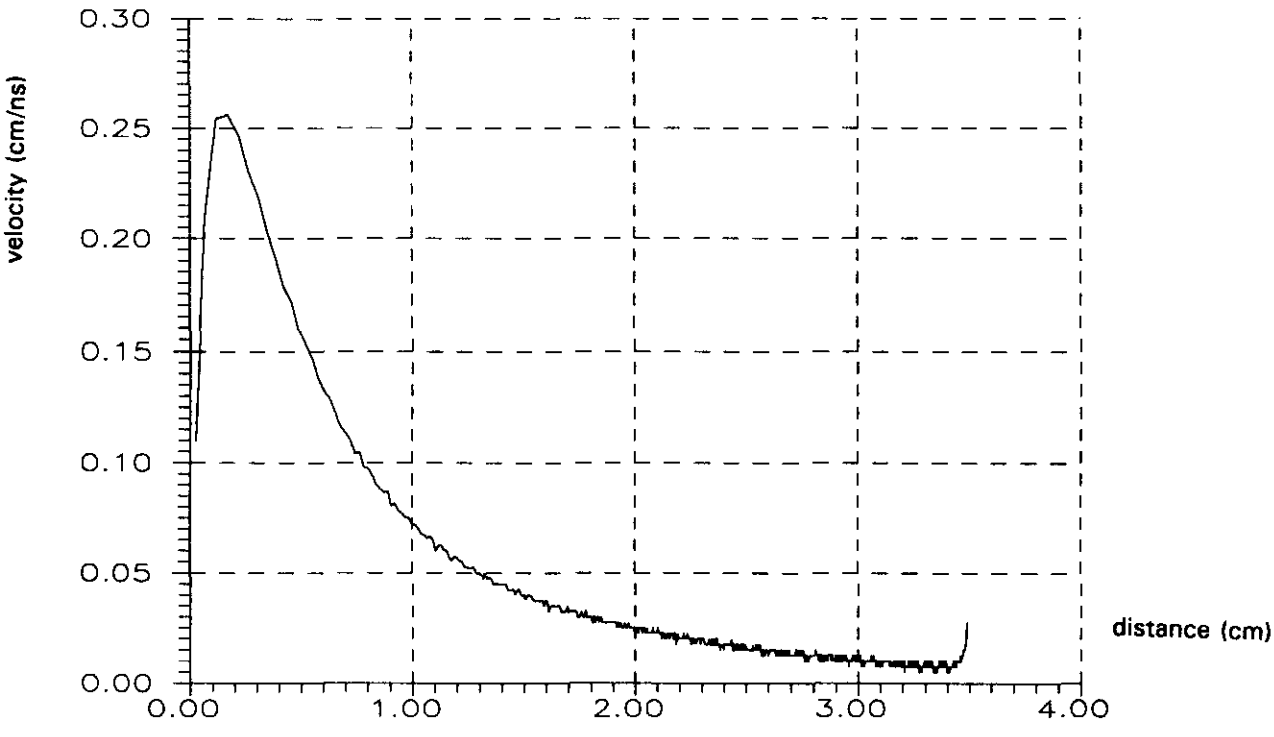

Fig. 6.19b: Streamer propagation velocity for the conditions of 6.19a.

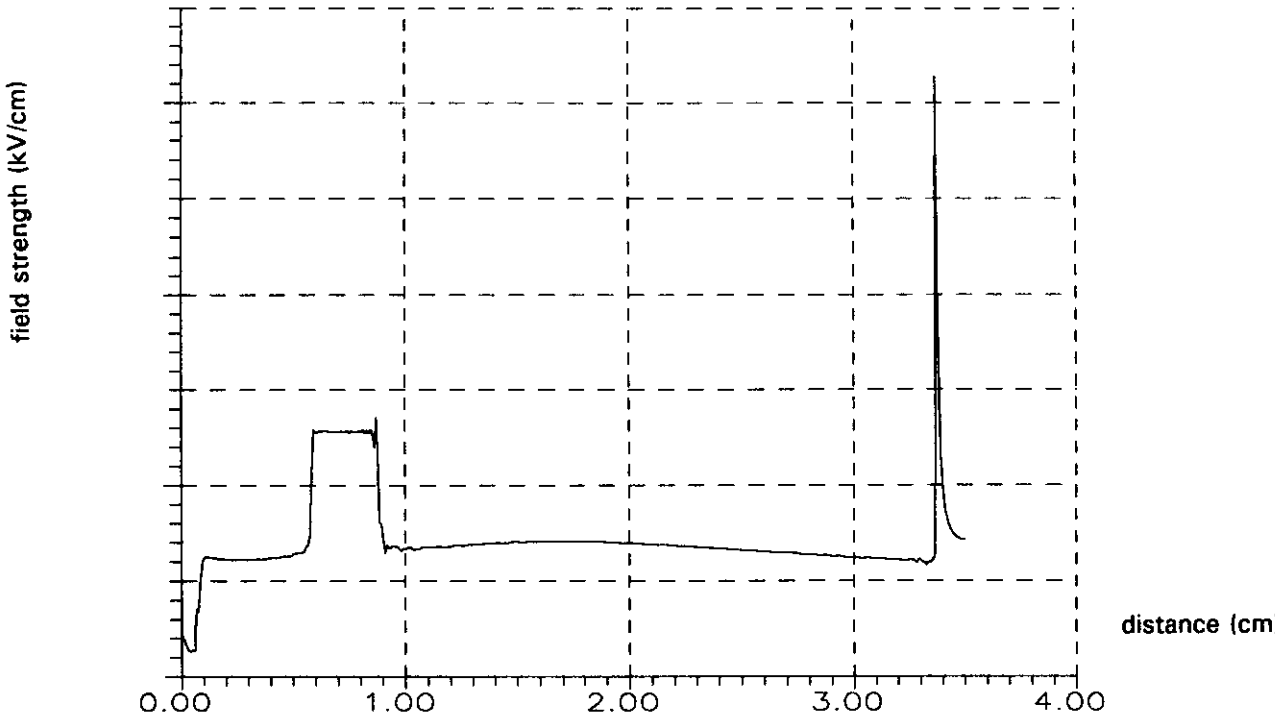

Fig. 6.19c: Electric field for the conditions of fig. 6.19a.

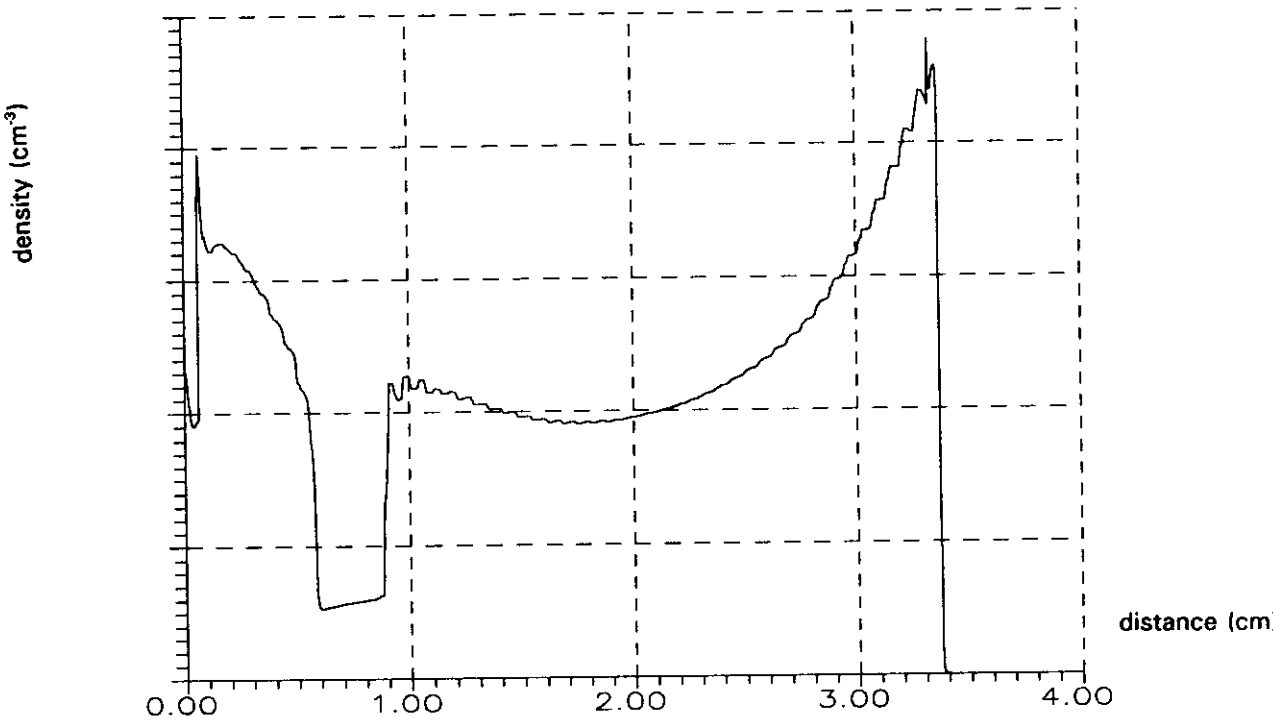

Fig. 6.19d: Electron density for the conditions of fig. 6.19a.

6.4 WP2

6.4.1 OH-emission (A2.1)

The presence of OH radicals is indicated by its emission near the bandhead of 306.4nm and another region of strong emission peaks around 308 nm. Fig. 6.20 shows a part of the spectrum obtained at the small set-up with a spectral resolution of 0.2 nm. Also indicated in the figure are two wavelengths at which there are peaks of the nitrogen SPS. In fig. 6.21 the same spectral range is given, but this one is obtained with the large set-up and with a spectral resolution of 0.5 nm. Two lines are indicated in this figure, one for air and one for flue gas. The flue gas has a high humidity (11%) so a relatively higher intensity of the OH peaks is expected. The two lines are normalised for ease of comparison. Here also the same wavelength regions of OH show up in the case of flue gas. These spectra have been obtained with averaging over approximately 100 corona pulses for each spectral point to obtain the optimum signal-to-noise ratio. It shows that the OH signal is very weak as could be expected from its very short life time by deexcitational collisions and chemical reactions.

6.4.2 Ozone concentration (A2.1)

Ozone is radily detected from its smell as soon as a corona discharge in air is operated (the smell may also be originating from the spark gaps). With the absorption technique described in section 4.5 the absolute concentration of ozone has been established in a cylinder of 450 mm length and 50 mm diameterin the small set-up. The result is shown in fig. 6.22, the steps are due to different flow velocities. The efficiency which is obtained with long-tailed pulses in dry air is ~20 g/kWh, which is equivalent to about 50 eV/molecule.

The ozone concentration in the large set-up is measured with a closed gas system with air or flue gas. This would lead to a linear increase of ozone as long as there are no losses. In fig. 6.23, which is the ozone concentration in air, this linear increase is observed only for a short time (~20 seconds). The energy consumption in this case is in the order of 100 eV/molecule, this higher value is due to the presence of water vapour because ambient air is used here. In both cases no attempts were made to optimise the electrical pulse shape to find the maximum energy efficiency since ozone generation is not considered as a goal in itself.

The amount of ozone measured in flue gas is very low. It is estimated to be 500 times lower than in ambient air. There are two clear reasons for this effect: the much higher temperature of the flue gas leads to strong back reactions and the high water concentration leads to chemical conversions of ozone. In both cases this does not mean a loss of the excitational energy since the products can still be used in reactions. Wether this leads to an overall increase or decrease of the efficiency of the cleaning process cannot be readily concluded.

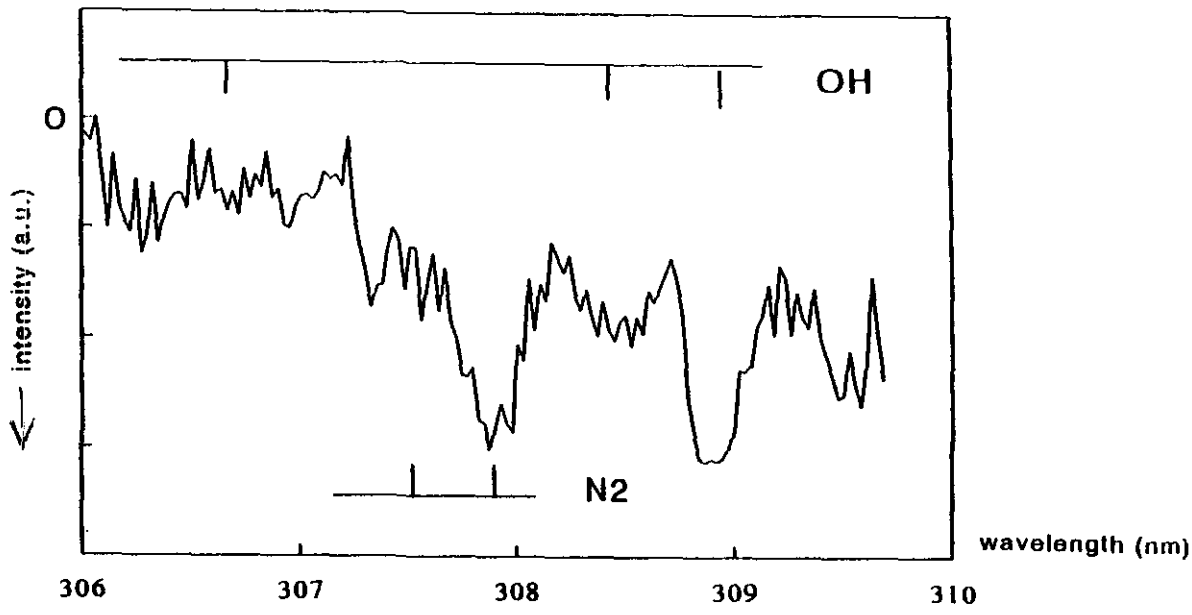

Fig. 6.20: Emission spectrum obtained at the small set-up in humid air revealing two peaks of OH emission, spectral resolution 0.05 nm.

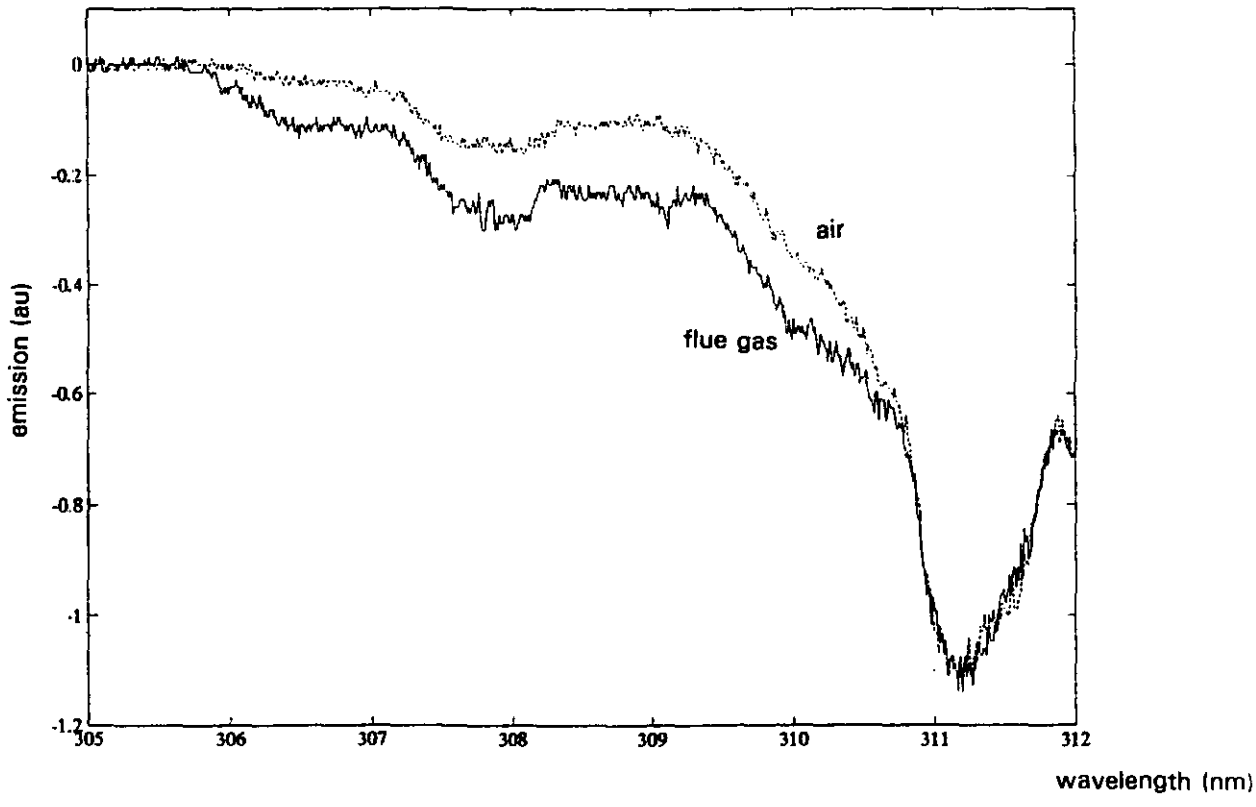

Fig. 6.21: Emission spectrum obtained at the large set-up in air and flue gas, showing OH peaks at 306.4 and 308.0 nm, spectral resolution 0.2 nm.

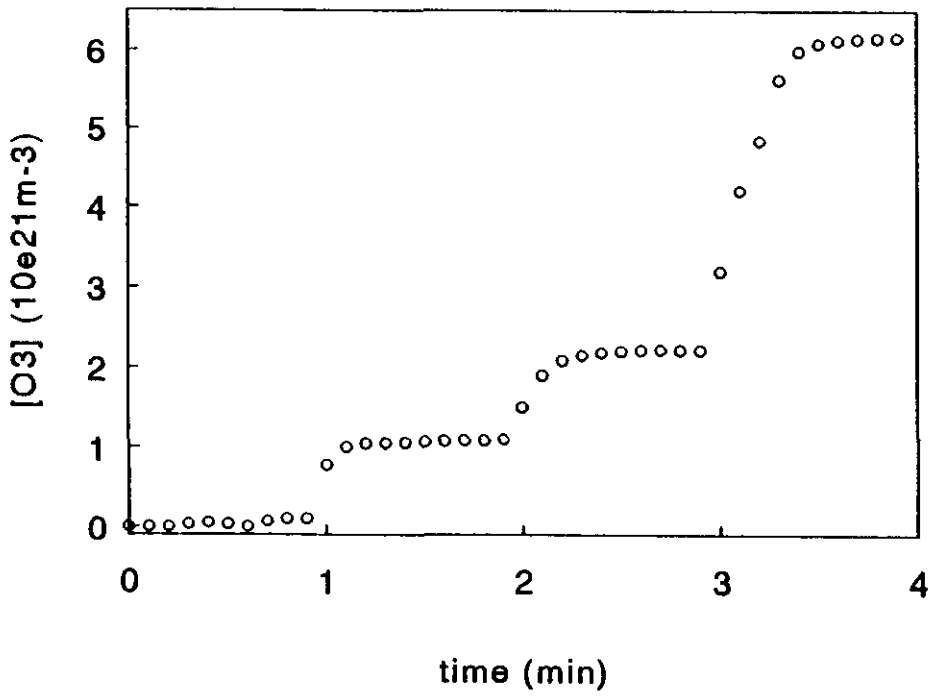

Fig. 6.22: Ozone concentration in dry air determined in the small set-up, the steps indicate a change in the repetition rate.

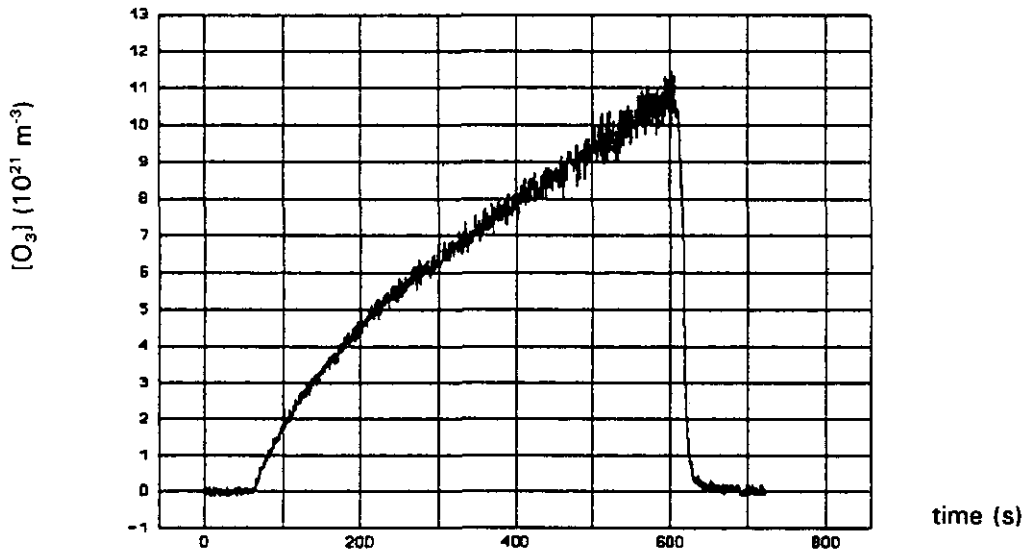

Fig. 6.23: Ozone concentration in the large set-up in ambient air.

6.4.3 Cleaning effects (A2.2)

In the small set-up several tests have been performed to obtain the removal efficiency of NO. These measurements have also been performed in a cylinder of 450 mm length and 50 mm diameter. The temperature of the cylinder and the incoming gas is controlled by electrical heating. The gas can be led trough water to increase its humidity. The temperature of this water is used to control this humidity. The cleaning efficiency is measured with two types of pulses: the constant voltage pulse and the short pulse (see fig. 6.1 and 6.2). Fig. 6.24a gives the NO and NO_2 concentration as a function of the input energy. This input energy is regulated by means of the repetition rate, where the voltage is adjusted each step to ensure constant pulses. The repetition rate can be increased up to 1000 Hz, which is equivalent to 33 Wh/Nm^3. The figure indicates the result for both pulse shapes and it is observed that NO decreases faster with the short pulses. The initial concentration of 250 ppm is decreased to 50% at an energy input of 6 and 8 Wh/Nm^3 for the short and long pulse resp. This result is very similar to previous data [23]. The influence of the humidity is shown in fig. 6.24b. It shows that an increase of the humidity leads to a higher cleaning efficiency. In this case the long pulse has been used. The combination of short pulses and high humidity probably leads to an even lower energy consumption for 50% removal. As has been shown before the NO_2 concentration increases at low energy input, showing that the cleaning process is indeed oxidative. The total balance of NO is far from complete. Other products are probaly formed and NO_2 can easily be absorbed by water clusters or droplets.

Experiments have also been undertaken in the large set-up using short current pulses only, as in fig. 6.2. In this case the power supply is limited to 30 Hz due to the limited current of the 100 kV supply. The flow of the flue gas therefore has to be reduced considerably to obtain a reasonable energy input. The best result is obtained with a flow of 9 m^3/hr, yielding a maximum power input of 6 Wh/Nm^3. In this case, using flue gas of 70 °C with 4% O_2, 9% CO_2, 18% H_2O, 69% N_2 and 310 ppm NO. At this low flow rate additional heating is used to keep the corona cylinder at the desired temperature. A reduction of 55% of the NO is obtained. This result is very much the same as what is expected with the small set-up, using short pulses and high humidity. Here also ammonia addition has been applied. It is found that this has no effect on the removal of NO.

SO_2 is also added to the flue gas under the same conditions. Its removal is only a few percent. The experiment is repeated in dry air, this gives a slightly better result. With a starting concentration of 625 ppm, a decrease of 28% is observed at 6 Wh/Nm^3, starting at 190 ppm this removal becomes 67%. With ammonia addition the SO_2 disappears completely under all condition when the amount of ammonia is more than stochiometric.

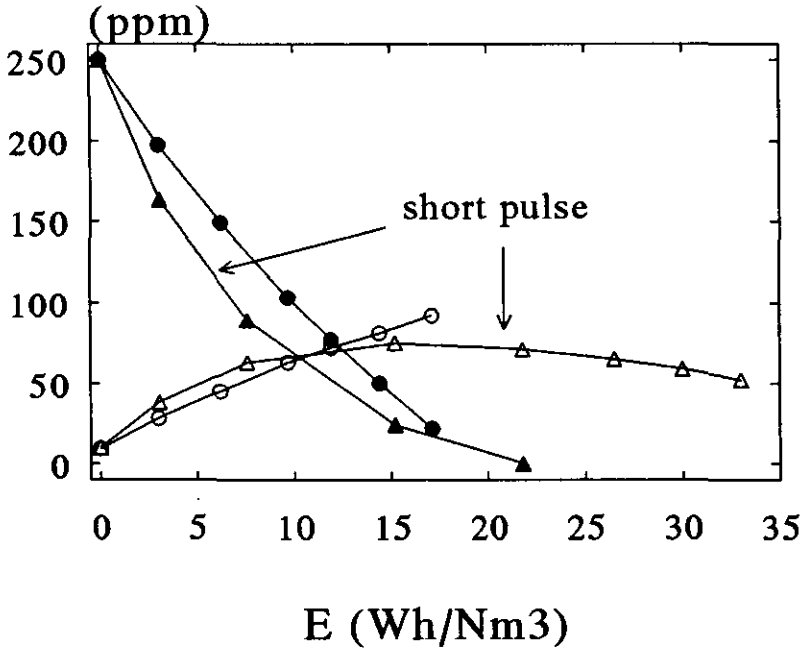

Fig. 6.24a: NO removal as a function of power input for standard and short pulses, NO_2 is formed in this process.

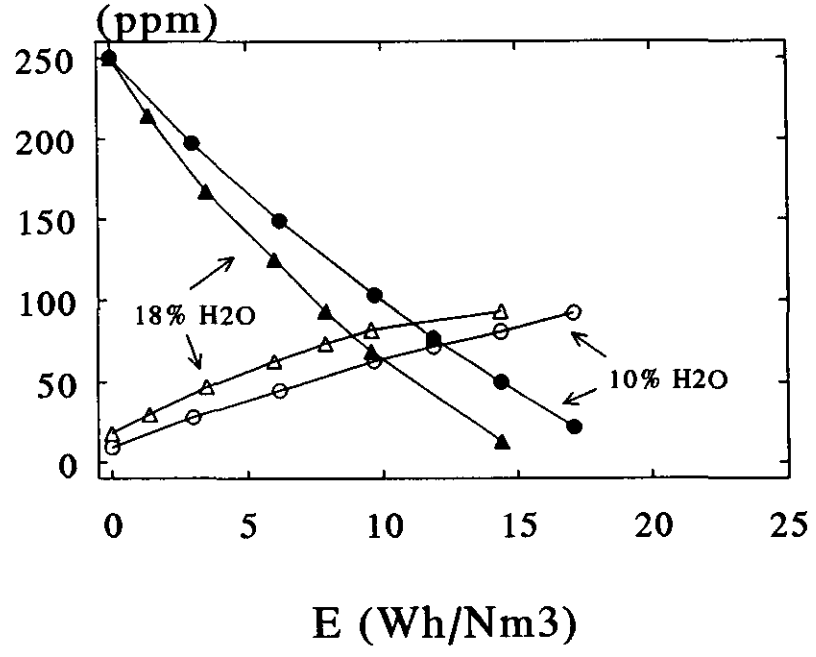

Fig. 6.24b: as fig. 6.24a for two values of the relative humidity

6.4.4 Solid deposition (A2.2)

The addition of ammonia offers the possibility for the formation of salts. Details of the processes involved, such as nucleation and growth, are largely unknown for the conditions of the experiments described here and also flue gas in general [69]. In the case of NO and NH_3 no salt formation is observed either in air or flue gas. With SO_2 however, a mist of white particles formes immediatly in both cases. The corona discharge causes large turbulences in the flow of these particles. The powder which is obtained from experiments in ambient air is analysed by dr. Claessen of the Department of Chemical Engineering of the EUT and it is found to be a very pure form of ammonium sulphate. Several of these results are surprising. One would expect NO or at least NO_2 to react with ammonia. The spontaneous reaction of NH_3 with SO_2 was supposed to form ammonium sulphite. The questions arising from the results obtained have not been answered up to now.

6.4.5 Model results (A2.3)

The calculation of the chemical kinetics with KINEL starts with a set of initial concentrations. Preferably this set is taken from the streamer propagation model which provides besides electron and ion densities also the concentrations of N and O atoms and N_2 and O_2 in excited state. All these values can be changed arbitrarely in the calculation to investigate the sensitivity of certain reaction paths or species [75]. Most calculations have been performed with flue gas conditions: 70% N_2, 6% O_2, 8%CO_2 and 16% H_2O and initial concentrations of 400 ppm NO and 1000 ppm SO_2. An example of the result for removal of NO and SO_2 is shown in fig. 6.25a. It shows the concentrations versus the logarithm of time. It is seen that the removal of NO has two time constants. This is most clearly recognised by looking at the major product NO_2. The first time constant is of the order of 10^{-4} s, the second one is about 10^{-2} s. The second product is HNO_2, and HNO_3 has only a small contribution. SO_2 is hardly converted in this case and its only endproduct is H_2SO_4. In fig. 6.25b the main cleaning radicals for this case are shown and it can be seen that the first time constant is due to OH and HO_2. This second radical is formed preferably and very rapidly from the H atoms which are formed simultaneously with OH from the dissociation of water. Further it is seen that the second time constant is caused by reaction with ozone.

The dependence of the cleaning effect on the initial OH density is investigated. It shows a more or less exponential curve as a function of the initial OH/NO ratio. This indicates that this reaction is a first order chemical process and that the cleaning effect per OH is the highest at the lowest ratios. If the OH concentration is high concurrent reactions occur, including radical-radical interaction.

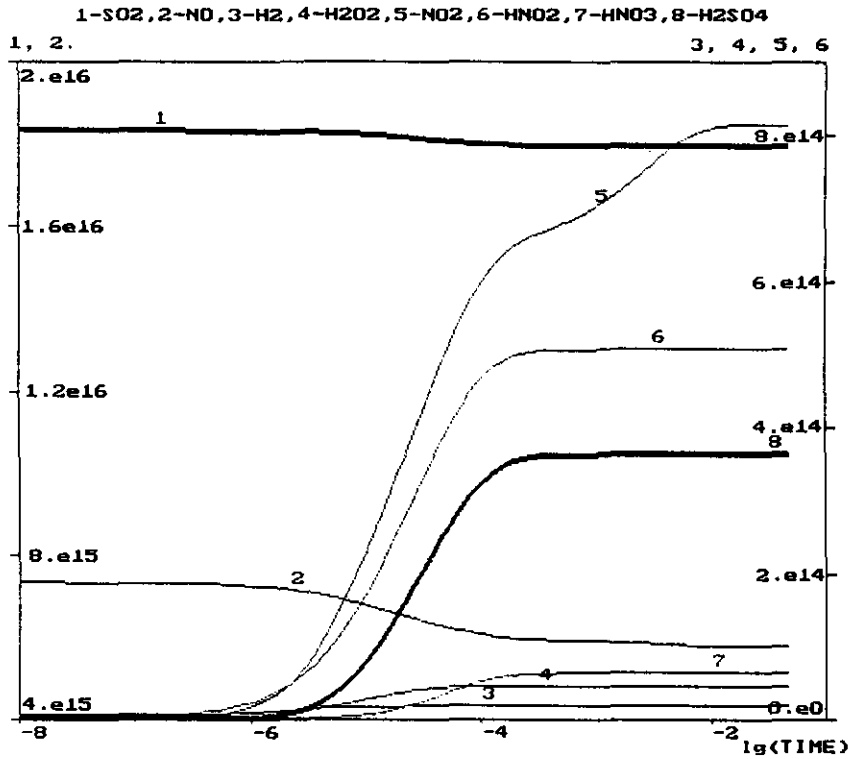

Fig. 6.25a: Calculated time dependence of the pollutants NO and SO_2 and the products formed in the cleaning reactions.

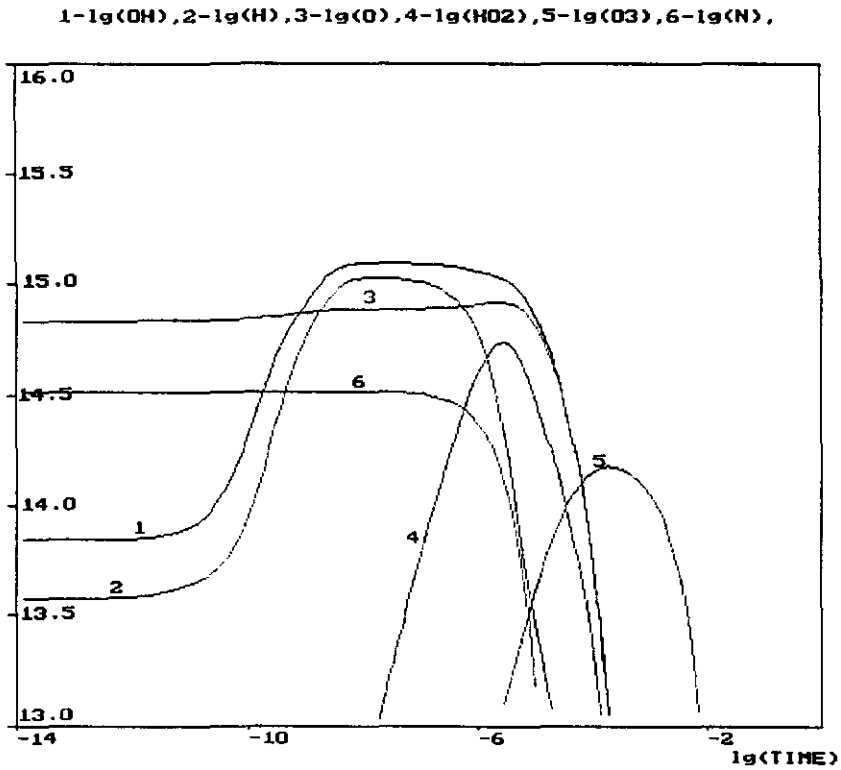

Fig. 6.25b: Calculated time dependence of the major radicals involved in the cleaning reactions.

The reaction analyser is used to verify which reaction paths are and are not important. Fig. 6.26 gives an overview of the radicals that play a role in NO conversions. On the left side of the center line are the reaction that consume NO and on the right side are the back reactions which produce NO (Note: the scale is logarithmic). The length of the bars shown in the figure is proportional to the total number of NO molecules that have passed the reaction, integrated in space and time. The gas condition for this calculation is 71% N_2, 16% H_2O, 5% O_2, 8% CO_2, 400 ppm NO and a temperature of 100 °C. Four oxidising reactions are important for NO removal, with OH, HO_2, O and O_3, in order of importance. One reducing reaction is significant NO + N, which contributes about 10% to the removal of NO. Other reaction contribute less than 1%. Three back reaction appear to be important: NO_2 + O, N + OH and NO_2 + H. Their total number is about 20% of the removal reactions, so it is certainly not negligible. In case of SO_2 the oxidation is for 90% by OH and for 10% by O and only one back reaction, SO_3 + O, contributes 3%. So for SO_2 the situation is far less complicated.

Fig. 6.27 shows two similar histograms for OH radicals, also integrated up to 0.08 s. Fig. 6.27a gives the reactions with radicals and fig. 6.27b the reactions with ions. There are several radical reactions that form OH, using N_2^*, O and HO_2. One ion reaction contributes significantly: H_2O^+. The total number of OH radicals is about one order of magnitude higher than the number due to direct electron impact during the streamer propagation. From the three OH consuming reactions only one is used for NO conversion to HNO_2. The other two are radical-radical interactions, which means, in most cases, a loss of excitation energy. Reactions among radicals will be less effective at low radical concentrations, because these reactions depend quadratically on the radical density, whereas the cleaning reaction depends lineraly on it.

The results presented here are just one example. It is known from diverse experiments that the gas conditions have a strong influence. The question remains wether or not it is possible to get the reactions in a desired direction by choosing a certain set of conditions, including the addition of additives. It must however be reminded that the basis of the validity of this calculation is the values of the rate constants. A lot of these constants are taken from data bases, mainly from atmospheric chemistry, and are obtained at conditions far from the situation of flue gas cleaning. Further the model does not include the heterogeneous reactions, as already mentioned, the role of reactions with molecules in high vibrational states is largely unknown and the influence of the gasdynamic expansion is not taken into account. For a quantitative model all these aspects will need to be considered in the future.

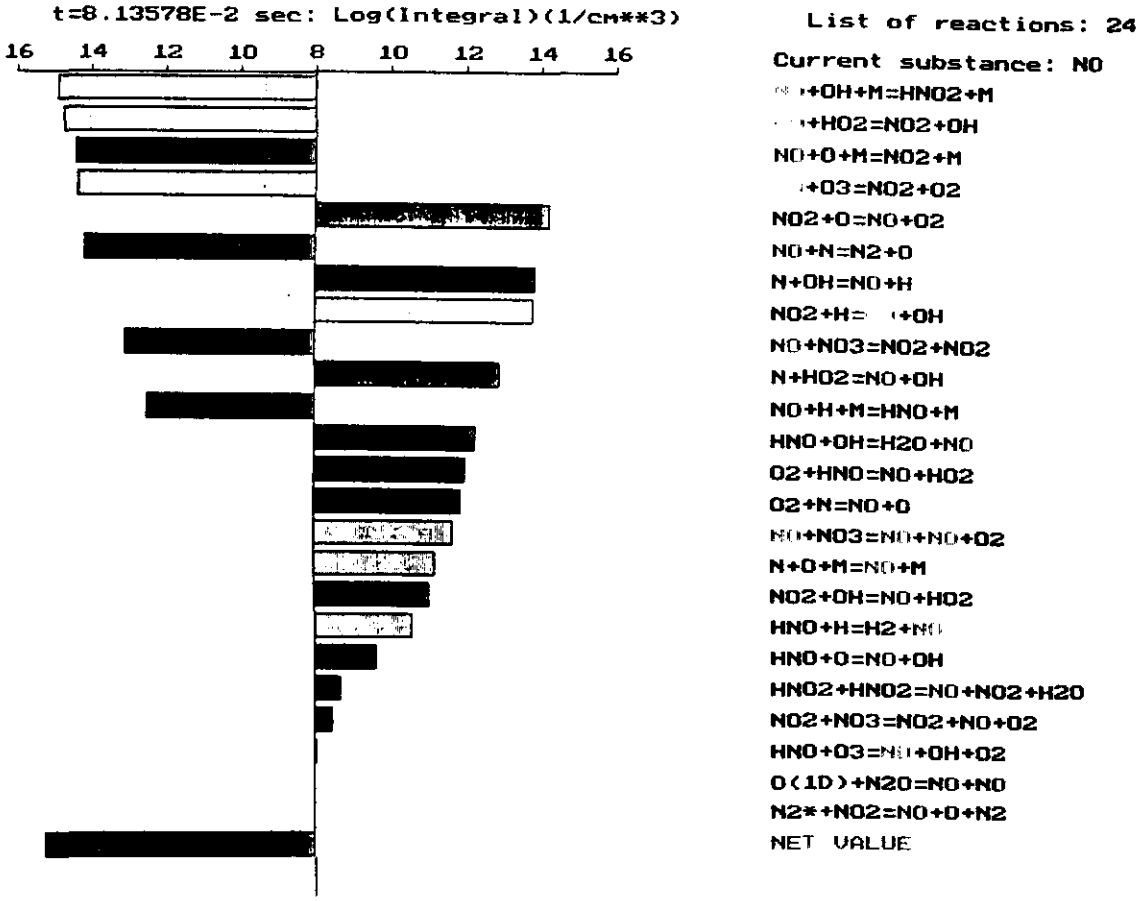

Fig. 6.26: Forward (left side) and backward (right side) reactions integrated up to 0.08 s for the NO molecule.

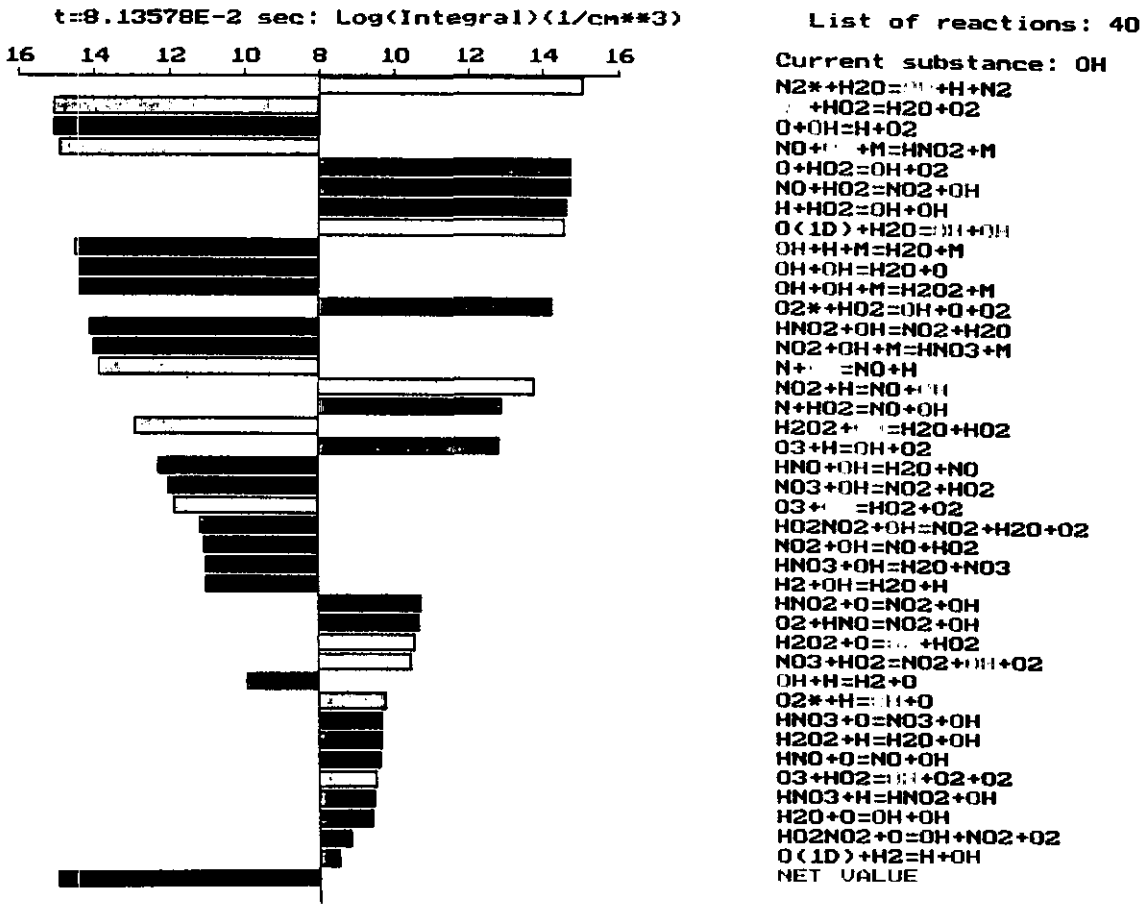

Fig. 6.27a: Integrated reactions up to 0.08 s for the OH radical with other radicals and molecules.

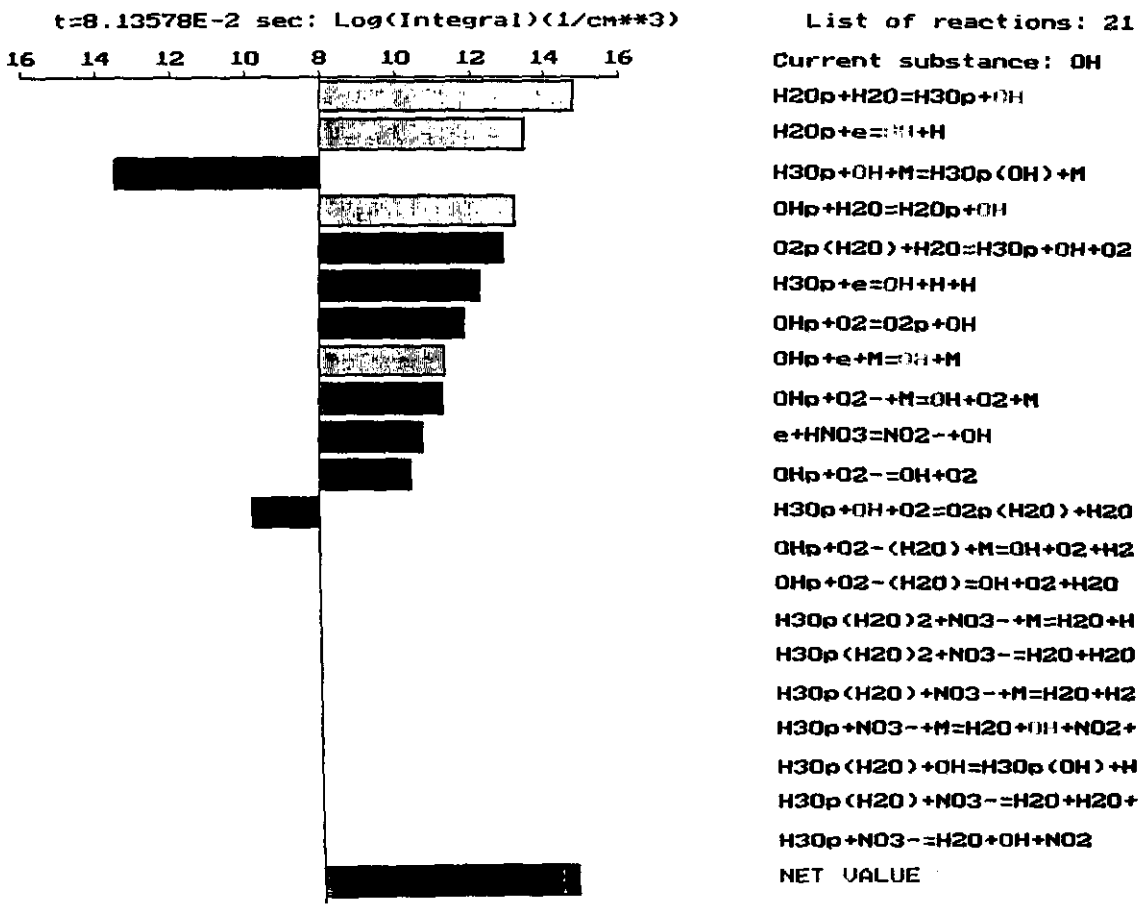

Fig. 6.27b: Integrated reactions up to 0.08 s for the OH radical with ions.

7. Conclusions

A brief overview of the main conclusions is presented here.

- Two experimental set-ups including a gas burner system, pulsed power supplies and EMC shielding are constructed and have been used for measurements on pulsed positive corona.

- Spark gap switched pulsed power supplies are a very good and versatile way to obtain pulses for experimental work. Their overall efficiency and long term reliability is possibly too low for industrial applications.

- Streamer corona is produced with high voltage pulses in air, flue gas and in N_2-O_2 and N_2-CO_2 mixtures. Charge and energy input are determined from voltage and current measurements. Measurement methods are developed and data are obtained for comparison with models of streamer corona discharge and chemical kinetics.

- An input energy of 1.2 J/m is obtained in a wire-plate corona with a gap of 35 mmm, at 40 kV crest voltage of short duration (500 ns). With a pulse of 100 kV and a 30 kV DC bias an energy input of upto 9 J per pulse and per meter corona wire is obtained in a cylinder of 150 mm diameter. The dependence of energy input on peak voltage, voltage rate of rise, DC bias and repetition rate is investigated in different gas mixtures.

- Other quantities of the pulsed corona discharge obtained from the experiments are the inception behaviour, the discharge structure and development, the characteristic electron energy and the streamer propagation velocity, all are derived from optical emission. Optical absorption is used to detect chemical species in the discharge reactor.

- From optical emission it is shown that streamers in pulsed corona start always simultaneously, within about 15 ns. In air primary they reach the cathode under all conditions where corona inception occurs. The secondary streamers start after the primaries have reached the cathode. The streamer full width at half maximum is 200 μm in the whole gap.

- At a voltage just above inception there is a statistically distributed delay time of about 1 μs. At voltages just below breakdown ignition occurs before the maximum voltage is reached and the jitter in the inception time lag becomes very low ($\leq$ 15 ns).

- The number of streamers per unit anode length is obtained from Schlieren photos and CCD camera images. In a wire-plate corona it is determined to be 2 cm^{-1} for channels that cross the gap and 4 cm^{-1} for thin channels of $\sim$10 mm length.

- The streamer propagation velocity, in air and gas mixtures, is obtained

from time delay measurements at several radial positions. The data agree well with the results of the model of the streamer propagation, which implies that the streamer propagation is well described by a 1-D time dependent model.

- A transition is observed in the streamer propagation both from velocity measurements and from CCD pictures. This transition occurs at a position where the applied electrical field is approximately equal to the critical field.

- The electron energy in the streamer head has a value of ~10 eV, which hardly depends on the pulse parameters. A decrease of this energy is observed when in nitrogen gas the oxygen content is increased from zero to 50%. The electron energy in the secondary streamer is ~1 eV and in the residual streamer channel it is ~0.5 eV, both values have been obtained indirectly by combining results from measurements and calculations.

- Emission spectra of air and flue gas have been recorded. They reveal emission of OH radicals from streamer channels in flue gas and a different vibrational behaviour of nitrogen in flue gas and in air.

- The rotational structure of a nitrogen emission line is observed. The gas temperature derived from it in the residual streamer channel is close to room temperature (between 300 and 350 K). This result confirmes the non-thermal nature of the pulsed corona discharge plasma.

- Taking the emission intensity as a (relative) measure for the electron concentration and also for the radical production, some conclusions can be drawn about the efficiency of the pulses. As expected the emission increases with the pulse voltage and its rate of rise. But if this emission is divided by the electrical energy input this trend reverses. This indicates that a high and fast pulse creates more electrons but with a lower efficiency. At low voltages or low rates of rise the energy deposition per unit volume is low and the capacitive current becomes relatively large, which leads to loss of power. This indicates that there should be an optimum inbetween.

- Absorption spectroscopy is used to determine ozone concentrations. In ambient air ozone is created at an energy cost of 50-100 eV per molecule. Its density in flue gas of 90 °C is 500 times lower compared to air. This is due to the strong deexcitation of ozone by the elevated temperature and collisions with water molecules. Ozone is not observed at higher flue gas temperatures.

- The detection limit of absorption measurement appears to be, up to now, insufficient for the observation of OH radicals.

- A low energy consumption of 6 Wh/Nm^3 to remove 125 ppm of NO is achieved by using short current pulses (100 ns).
  NO-removal increases with shorter pulses
  NO-removal increases with higher water concentration
  NO-removal increases with lower gas temperature

- SO_2 largely removed spontaneously and almost completely upon NH_3 addition under formation of pure ammoniumsulphate.

- The analysis of the chemical reaction paths shows that the largest part of the OH radicals is formed indirectly. The main topics for further research are the coupling of plasmaphysical and plasmachemical aspects, i.e. the influence of vibrationally excited species and the gasdynamic decay, and the inclusion of heterogeneous reactions .

8. Summary

This report, called "In-situ investigation of pulsed corona discharge", describes the activities which have been undertaken in the past three years at the EUT to obtain more information of the pulsed corona discharge in relation with the removal of SO_2 and NO_x from the flue gas of coal fired power stations (DeSOx/DeNOx). This work is a part of the activities of the JOULE project CLEAN, which has been performed in cooperation with ENEL in Italy and AEA Technology in the UK.

The work performed in Eindhoven has been largely devoted to experiments under a variety of well controlled conditions. For that purpose two experimental set-ups are constructed, a small one for measurements with different corona configurations and gas mixtures from cylinders and a larger one where air or flue gas from a methane burner can be treated in a 16 liter wire-cylinder reactor.

The power supplies for the experiments are capacitors switched with a spark gap. This type is esspecially suited for experimental work because the pulse shape can easily be changed. Two types of pulses are distinguished: a constant voltage pulse (after the initial rise) and a pulse that collapses after a short and intense current pulse. The fastest pulse that are created have a rate of rise of 5 kV/ns and the shortest (current) pulses are 20 ns. The maximum power input per pulse per meter corona wire obtained is 9 J. It is observed that the energy per pulse increases strongly with the initial rate of rise of the pulse. This effect coincides with an increase in the inception voltage. The voltage across the gap can be above static breakdown if the rate of rise is high enough ($\geq$1 kV/ns). This effect can be used to make pulses with high current, breakdown can be avoided by making a short pulse.

The discharge structure is observed with Schlieren photos and CCD camera images. The number of streamers for a smooth anode wire is 7 per cm anode wire for pulses just below breakdown voltage and 4 per cm for pulses just above inception. The structure can be influenced by the shape of the anode. The diameter of the streamer channel is determined with the CCD camera. It is found to have a luminous halfwidth of 200 μm, this value does not depend on the position in the gap, except for the cathode region where it appears to be larger. From pictures obtained at consequtive trigger instants it is observed that streamer cross the gap in 50 to 150 ns. The secondairy streamer appears at the anode after the primary streamer has reached the cathode, its length is limited to a fraction of the gap distance. The Schlieren photos show channels of 2-4 mm diameter, this is due to the gasdynamic expansion of the streamer channel in the first microseconds after the discharge.

Plasma parameters of the streamer discharge are determined with optical spectroscopy. The emission of the N_2 337.1 nm line can be used to determine the gas temperature from its rotational structure. The gas temperature is determined from emission of the secondairy streamer and is found to be

between 300 and 350 K, which implies a low consumption of energy for gas heating. The electron energy is determined from the ratio of the emissions of the 337.1 nm line and the 391.4 nm N_2 ion line. This leads to a characteristic electron energy of 10 eV for the primary streamer. This value is relatively insensitive to pulse conditions. The method is not applicable to the secondairy streamer because the assumptions of the analysis are not valid in this case and not for the residual streamer channel also because here the emission intensity is too low.

Several chemical species have been determined using in-situ spectroscopy. The major lines of the OH radical have been observed in emission at 306-310 nm. The ozone concentration inside the discharge reactor is determined quantitatively with absorption spectroscopy. The yield of ozone is found to be one molecule per 50-100 eV energy input, which is a few times higher than commercial ozonisers, but no attempts have been made to optimise this value. OH radicals have not been observed with absorption spectroscopy. Its life time ($< 1\ \mu s$) may be too short for observation with the present equipment.

Several investigations have been performed related to the question how the corona discharge reacts on parameter variations and wether or not it can be sent into a desired direction. For this purpose the inception behaviour of the discharge is examined. This shows that the streamer gets a higher current when the inception is at a higher voltage, in practise this implies a thick wire and a high rate of rise of the voltage pulse. The determination of the electron energy shows that the pulse shape is not capable of changing this energy, its only changes the number of charge carriers and their velocity. A DC bias is shown to enhance the maximum current into the discharge by almost an order of magnitude when this bias is close to the inception voltage. An increase of the repetition rate leads to a decrease in the energy per pulse but the to average energy continues to increase up to at least 1 kHz repetition rate.

The measurements performed at EUT are interpreted by comparing the results with model calculations. The two main models have been made at the Institute for High Temperatures (IVTAN) in Moscow. The first one is a plasmaphysical model for the development and propagation of the streamer discharge, the second one treats the chemical kinetics of the cleaning process. The plasmaphysical part is backed up by Boltzmann calculation performed at the University Paul Sabatier in Toulouse and the Institute for Electronics in Sofia. By combining the results of measurements and calculations it is concluded that the electron energy is 1 eV in the secondary streamer and 0.5 eV in the residual streamer channel. The value of 10 eV for the primary streamer is confirmed by these calculations. The calculated streamer propagation velocity is in fair agreement with the measured values. The trend in cleaning efficiencies is similar in experiment and theory. It must be reminded, however, that the chemical model must be considered as an initial one because important aspects such as heterogeneous reactions and vibrationally excited states are not included, nor the radical production in the secondary streamers after crossing of the gap by the primary ones. The model does give a good overview of the dominant

species and reaction paths in the gas phase. For the cleaning process the dominant radicals are OH and HO_2.

Cleaning efficiencies are determined in our set-ups to ensure that our work can be compared with result obtained by other experimentists. A decrease of 50% for NO from an initial value of 250 ppm is measured at an energy consumption of 6 Wh/Nm^3. A slightly better result can probably be obtained by using a higher humidity and/or a shorter pulse. NH_3 addition did not change this result, but this does react strongly with SO_2, under the formation of pure ammoniumsulphate leading to a complete removal of SO_2.

The work needs to be extended in the direction of the chemical reactions. The experimental conditions must be controlled and varied to a greater extend, maybe also with the introduction of other components. The inclusion of heterogeneous reactions into the model, with droplets as well as particles, is another important but gigantic challenge.

9. References

1. Creyghton, Y.L.M. et al., "*Progress Report no. 1-6*".
   JOULE project CLEAN, no. JOUF-0053-C, Brussel, 1990-1993.

2. Veldhuizen, E.M. van et al., "*High resolution Schlieren study of pulsed corona*".
   In: Proc. 4th Int. Conf. on Electrostatic Precipitation, Beijing, China, September 14-17, 1990. Ed. by Ruinian Li. Beijing: International Academic Publishers, 1991. P. 663-672.

3. Creyghton, Y.L.M. et al., "*Discharge structure and electron temperature of pulsed corona*".
   In: Proc. XV Int. Symp. on the Physics of Ionized Gases, Dubrovnik, September 3-7, 1990. Ed. by D. Veza. Zagreb: Inst. of Physics, 1990. P. 261-262.

4. Creyghton, Y.L.M. et al., "*Streamer characteristics of pulsed positive corona*".
   In: Proc. 10th Int. Symp. on Plasma Chemistry, Bochum, Germany, 4-9 August, 1991. Ed. by U. Ehlemann et al. Bochum: IUPAC, 1991. Section 3.2-5, p. 1-6.

5. Creyghton, Y.L.M. et al., "*Electrical and spectroscopic investigation of pulsed positive streamer corona in O_2-N_2 and CO_2-N_2 mixtures*".
   In: Proc. 3rd Int. Symp. on High Pressure, Low Temperature Plasma Chemistry, HAKONE III, Strasbourg, France, 3-5 September, 1991. Ed. by M. Lecuiller. Strassbourg: HAKONE, 1991. P. 153-158.

6. Veldhuizen, E.M. van et al., "*Measurements on pulsed corona in flue gas from a methane burner*".
   In: Proc. X Int. Conf. on Gas Disch. and Appl., Swansea, September 13-18, 1992. Ed. by W.T. Williams. Swansea, UK: Local Organizing Committee GD92, 1992. P. 631-634.

7. Creyghton, Y.L.M. et al., "*Streamer properties of pulsed positive corona discharge*".
   In: Proc. X Int. Conf. on Gas Disch. and Appl., Swansea, September 13-18, 1992. Ed. by W.T. Williams, Swansea, UK: Local Organizing Committee GD92, 1992. P. 302-305.

8. Keping Yan and E.M. van Veldhuizen, "*Flue Gas Cleaning by Pulse Corona Streamer*".
   Eindhoven: Eindhoven University of Technology, Faculty of Electrical Engineering, 1993. EUT Report 93-E-272.

9. Creyghton, Y.L.M. et al., "*Diagnostic techniques for atmospheric streamer discharges*".
Submitted for publication to IEE Proc. A., 1993.

10. Creyghton, Y.L.M. et al., "*Streamer corona for flue gas cleaning*".
In: Proc. XXI Int. Conf. on Phys. Ionised Gases, Bochum, September 19-24, 1993. Ed. by G. Ecker et al. Bochum: Arbeitsgemeinschaft Plasmaphysik, 1993. Vol. II, p. 120-121.

11. Keping Yan et al., "*Electron energy for primary and secondary streamers of pulsed corona in relation with flue gas cleaning*".
In: Proc. XI Int. Symp. on Plasma Chem., Loughborough, UK, August 22-27, 1993. Ed. by J. Harry. Loughborough: IUPAC, 1993. P. 609-614.

12. Rutgers, W.R. et al., "*Non-thermal plasma techniques for gas cleaning*".
In: Proc. IUE-ERE Research Seminar on Plasma Processing, Stockholm, June 21-22, 1993. Stockholm: International Union for Electroheat, to be published.

13. Veldhuizen, E.M. van et al., "*Electrical and spectroscopic investigations on pulsed corona for flue gas cleaning*".
Accepted for publication at IEEE/IAS Conf., Toronto, Canada, October 3-8, 1993. New York: IEEE, to be published.

14. Veldhuizen, E.M. van et al., "*Positive pulse corona in air and flue gas*".
Accepted for publication at 6th Asian Conf. on Electrical Discharge, Oita, Japan, November 24-26, 1993.

15. Frank, N. et al., "*EBARA electron beam process for flue gas cleanup: Plant test results and future development*".
Radiat. Phys. Chem. Vol. 31(1988), p. 57-82.

16. Civitano, L. et al., "*Free radical production by corona discharges in a DeNox-DeSox reactor*".
In: IX Int. Conf. on Gas Disch. and Appl., Venice, 19-23 September 1988, Padova: Benetton, 1988. P. 603-606.

17. Dahli, S.K. and I. Sardja, "*Dielectric-barrier discharge for processing of SO_2/NO_x*".
J. Appl. Phys. Vol. 69(1991), p. 6319-6324.

18. Chang, M.B. et al., "*Removal of SO_2 from gas streams using a dielectric barrier discharge and combined plasma photolysis*".
J. Appl. Phys., Vol. 69(1991), p. 4409-4417.

19. Eliasson, B. and U. Kogelschatz, "*Modelling and applications of silent discharge plasmas*".
IEEE Trans. Plasma Science, Vol. 19(1991), p. 309-323.

20. Braun, D. et al., "*Microdischarges in air-fed ozonizers*".
J. Phys. D: Appl. Phys. Vol. 24(1991), p. 564-572.

21. Cichanowicz, E., "*Engineering evaluation of combined NO_x/SO_2 technologies*".
EPRI, ESC Update, Vol. 20(1991), p. 4-10.

22. Book, H., "*Critical comments on EBARAS Final Report*".
Beta/Gamma, Vol. 1(1990), p. 41-43.

23. Civitano, L., "*Removal of toxic gases by corona discharge processing*".
In: Proc. "Plasma Technology: fundamentals and applications", Il Ciocco, Italy, July 5-7, 1991. Ed. by M. Capitelli and C. Gorse - London: Plenum, 1992.

24. Kanter, I.E., "*Research and development for advanced combined NO_x/SO_2 removal systems*".
Westinghouse R&D Center, Pittsburgh, USA, 1986. Springfield : NTIS, 1986. Report no. DOE/PC/60261--T23.

25. Finlayson-Pitts, B.J. and J.N. Pitts, "*Atmospheric Cemistry: fundamentals and experimental techniques*".
New York: Wiley, 1986.

26. Baranovich, E.I. et al., "*Plasma-catalysis oxidation of SO_2 in air by impulse corona discharge and relativistic electron beam*".
In: Proc. XX Int. Conf. Phys. in Ionized Gases, Il Ciocco, Barga, Italy, July 8-12, 1991. Ed. by V. Palleschi. P. 289-299.

27. Kloth, H.F.J. et al., "*Processes in pulsed electrostatic precipitators*".
In: V Int. Symp. on High Voltage Eng., Braunschweig, Germany, August 24-28, 1987. Ed. by H.C. Kärner. Braunschweig: High Voltage Institute, Technical University, 1987. Paper 91-05.

28. Spikings, C.R. et al., "*CLEAN*".
Final report CLEAN.135.R3. Culham, UK: AEA Technology, 1991.

29. Domens, P. et al., "*Large air-gap discharge and Schlieren techniques*".
J. Phys. D: Appl. Phys. Vol. 21(1988). P. 1613-1623.

30. Waters, R.T., "*Diagnostic Techniques for Discharge Plasmas*".
In: "Electrical Breakdown and Discharges in Gases". Ed. by E.E. Kunhardt and L.H. Leussen, NATO ASI Series B, Vol. 89b, New York, Plenum, 1983. P. 203-265.

31. Woolsey, G.A. et al., "*A quantitative laser Schlieren analysis of positive streamers in atmospheric air*".
Proc. R. Soc. Lond. Vol. A405 (1986). P. 355-367.

32. Hosch, J.W. and J.P. Walters, "*High spatial resolution Schlieren photography*". Applied Optics, Vol. 16(1977). P. 473-482.

33. Kogelschatz, U. and W.R. Schneider, "*Quantitative Schlieren Techniques Applied to High Current Arc Investigations*".
Applied Optics, Vol. 11(1982). P. 1822-1832.

34. Hartmann, G., "*Spectroscopie de la décharge couronne*".
Thesis no. 1783, University of Paris-Sud, Orsay (1977).

35. Carr, T.W. and S. Dondes, "*Direct measurement of the radiative lifetime and collisional quenching of the $C^3\Pi_u$ of nitrogen as studied by pulse radiolysis*".
J. Phys. Chem., Vol 81(1977). P. 2225-2228.

36. Smith A.J. et al., "*Measurement of the life times of ionic excited states using inelastic electron-photon delayed coincidence technique*".
J. Phys. B: Molec. Phys., Vol. 18(1975). P. 2869-2879.

37. Mitchell, K.B., "*Fluorescence efficiencies and collisional deactivation rates of N_2 and N_2 bands excited by soft X rays*".
J. Chem. Phys., Vol. 53(1970). P. 1795.

38. Herzberg, G., "*Molecular Spectra and Molecular Structure*".
Vol. I. Spectra of Diatomic Molecules, Van Nostrand, New York, 1950.

39. Dieke, G.H. and H.M. Crosswhite, "*The Ultraviolet Bands of OH*".
JQSRT Vol. 2(1962). P. 97-199.

40. Huber, K.P. and G. Herzberg, "*Molecular Spectra and Molecular Structure*".
Vol. V.: "*Constants of Diatomic Molecules*", Van Nostrand, New York, 1979.

41. Lezberg, E.A. et al., "*Comparison of Experimental Radical Profiles with Kinetic Calculations in Supersonic Nozzle*".
Washington DC: NASA, 1965. Technical Note TN D-2883.

42. Matschuk, G.G., "*Bestimmung der OH-konzentrationsverteilung in einer rotationssymmetrischen Methan/Sauerstoff Flamme*".
Dissertation, Technical University Aachen, 1972.

43. Wysong, I.J. et al., "*Quenching of A $^2\Sigma^+$ OH at 300 K by several colliders*".
J. Chem. Phys. Vol. 92(1990). P. 5218-5222.

44. Chang, M.B. et al., "*Removal of SO_2 from gas streams using a dielectric barrier discharge and combined plasma photolysis*".
J. Appl. Phys. Vol. 69(1991). P. 4409-4417.

45. Moseley, P.T. and B.C. Tofield, "*Solid State Gas Sensors*".
Adam Hilger, Bristol, 1987.

46. Maier, J.R., "*The Mass Spectrometer*".
Wykeham, London, 1977.

47. Dawson, G.A. and W.P. Winn, "*A model for streamer propagation*".
Zeitschrift fur Physik, Vol. 183(1965). P. 159-171.

48. Gallimberti, I., "*A computer model for streamer propagation*".
J. Phys. D: Appl. Phys., Vol. 5(1972). P. 2179-2189.

49. Gallimberti, I., "*The mechanism of the long spark formation*".
Journal de Physique Vol. 40(1979). P. C7-C193.

50. Boeuf, J.P., "*Modélisation de la cinetique électronique dans un gaz faiblement ionisé*".
Dissertation no. 3043, University of Paris-Sud, Orsay, 1985.

51. Kunhardt E.E. and Y. Tzeng, "*Development of an electron avalanche and its transition into streamers*".
Phys. Rev. A., Vol. 38(1988). P. 1410-1421.

52. Davies A.J. and C.J. Evans, "*Field distorsion in gaseous discharges between parallel-plate electrodes*".
Proc. IEE, Vol 114(1967). P. 1574-50.

53. Davies, A.J. et al., "*Computer simulation of rapidly developing gaseous discharges*".
Proc. Inst. Electr. Eng, Vol. 118(1971). P. 816-819.

54. Kline, L.E., "*Effect of negative ions on current growth and ionizing wave propagation in air*".
J. of Appl. Phys., Vol. 46(1975). P. 1994-2000.

55. Dhali S.K. and P.F. Williams, "*Two-dimensional studies of streamers in gases*".
J. appl. Phys., Vol. 62(1987). P. 4696-4707.

56. Wu C. and E.E. Kunhardt, "*Formation and propagation of streamers in N_2 and N_2-SF_6 mixtures*".
Phys. Rev. A, Vol 37(1988). P. 4396-4406,
M.C. Wang and E.E. Kunhardt, "*Streamer dynamics*".
Phys. Rev. A, Vol. 42(1990). P. 2366-2373.

57. Morrow, R., "*Theory of negative corona in oxygen*".
Phys. Rev. Vol. A32(1985). P. 1799-1805.

58. Gallimberti, I., "*Impulse corona simulation for flue gas treatment*".
Pure & Appl. Chem., Vol. 60(1988). P. 663-674.

59. Morgan, W.L., "*ELENDIF, A Computer Program that Solves the Boltzmann Equation for a Partially Ionized Gas*".
JILA Information Center Report No. 19., Joint Institute for Laboratory Astrophysics, Boulder, CO. Recent versions of this program are available from the CPC Program Library, Department of Applied Mathematics, The Queen's University of Belfast, Belfast BT7 1NN, Northern Ireland.

60. Yousfi, M., Centre de Physique Atomique, Unité de Recherche Associée au CNRS, no. 277, 118 route de Narbonne, 31062, Toulouse Cedex, France (personal communication). Results of the calculations are partly published in Ref. 32.

61. Verhaart, H.F.A., "*Discharge parameters in flue gas*".
Kema Scientific & Technical reports, Vol. 7(1989). P. 377-383.

62a. Bityurin, V.A. et al., "*The Mathematical Model and Computer Code for 1D Time Dependent Streamer Propagation in Air and Flue Gas*".
Final report of subcontract under JOUF-0053-C, Eindhoven University of Technology, Faculty of Electrical Eng., Section of Electrical Energy Systems, 1993. Internal report EG/92/633.

62b. Babaeva, N.Yu. et al., "*The Streamer Propagation Models in N_2-O_2 Mixtures and Flue Gas*".
Final report for NWO contract 07-30-017, Eindhoven University of Technology, Faculty of Electrical Eng., Section of Electrical Energy Systems, 1993. Internal report EG/93/672.

63. Dawson, G.A. and W.P. Winn, "*A model for streamer propagation*".
Z. Phys. Vol. 183(1964). P. 159-171.

64. Bastien, F. and E. Marode, "*The determination of basic quantaties during glow-to-arc transition in a positive point-to-plane discharge*".
J. Phys. D, Vol. 12(1979). P. 249-263.

65. Sato, N., "*Discharge current induced by the motion of charged particles*".
J. Phys. D, Vol. 13(1980). P. L3-6.

66. Gallimberti, I., "*Impulse corona for flue gas treatment*".
Pure Appl. Chem., Vol. 60(1988). P. 663-674.

67. Morrow, R. and L.E. Cram, "*Flux-corrected transport and diffusion on a non-uniform mesh*". J. Comput. Phys. Vol. 57(1985). P. 129-138.

68. Morrow, R., "*Numerical solution of hyperbolic equations for electron drift in strongly non-uniform fields*". J. Comput. Phys., Vol. 43(1981). P. 1-15.

69. Mätzing, H., "*Chemical Kinetics of Flue Gas Cleaning by Electron Beam*",
Kernforschungszentrum Karlsruhe, Germany, 1989. Report KfK 4494.

70. Person, J.C. et al., "*A unified projection of the performance and economics of radiation-initiated NO_x/SO_x emission control technologies*".
U.S. Department of Energy, Pittsburgh Energy Technology Center, Pittsburgh, PA 15236, 1985. Report No. PSI-TR--259/542, DE86 003620.

71. Baulch, D.L. et al., CODATA Task Group on Chemical Kinetics, "*Evaluated kinetic and photochemical data for atmospheric chemistry*".
71a. J. Phys. Chem. Ref. Data, Vol. 9(1980). P. 295-471.
71b. J. Phys. Chem. Ref. Data, Vol. 11(1982). P. 327-497.
71c. J. Phys. Chem. Ref. Data, Vol. 13(1984). P. 1259-1381.

72. Tokunaga, O. et al., "*Radiation Treatment of Exhaust Gases*",
72a Part I: "*Oxidation of NO and reduction of NO2*".
Int. J. Appl. Radiat. and Isotopes, Vol. 29(1978). P. 81-85.
72b Part II: "*Oxidation of Sulfur Dioxide in the Moist Mixture of Oxygen and Nitrogen*".
Int. J. Appl. Radiat. and Isotopes, Vol. 29(1978). P. 87-90.
72c Part IV: "*Oxidation of NO in the Moist Mixture of O_2 and N_2*".
Radiat. Phys. Chem., Vol. 11(1978). P. 117-122.
72d Part V: "*Effect of NH_3 on removal of NO in the moist mixture of O_2 and N_2*".
Radiat. Phys. Chem., Vol. 11(1978). P. 299-303.
72e Part VI: "*Effects of CO and H_2 on the Removal of NO and NO_2 in the Moist Mixture of O_2 and N_2*".
Int. J. Appl. Radiat. and Isotopes, 30(1979). P. 19-23.
72f Part X: "*Formation of N_2O in irradiation of NH3 containing mixture of H_2O, O2 and N_2*". J. Nucl. Sci. Tech., Vol. 16(1979). P. 907-912.

73. Tokunaga, O. and N. Suzuki, "*Radiation Chemical Reactions in NO_x and SO2 Removals from Flue Gas*".
Radiat. Phys. Chem., Vol. 24(1983). P. 145-165.

74. Braun, D., "*Zum Wirkungsgrad von Ozonerzeugern*".
Dissertation, Technical University Aachen, 1991.

75a. Bityurin, V.A. et al., "*Mathematical Model and Computer Code of Chemical and Gasdynamical Decay of Streamer Channel*".
Final report of subcontract under JOUF-0053-C, Eindhoven University of Technology, Faculty of Electrical Eng., 1993. Internal report EG/93/619.

75b. Alekseev, G.Yu. et al., "*The Chemical Kinetics and Heat/Mass Transfer in NO/SO_2 Removal*".
Final report for NWO contract 07-30-017, Eindhoven University of Technology, Faculty of Electrical Eng., 1993. Internal report EG/93/673.

76. "*Chemical Kinetics and Photochemical Data for Use in Stratospheric Modelling. Evaluation Number 9*".
Jet Propulsion Laboratory, California Institute of Technology, NASA, Pasadena, 1990.

77. Stelson, A.W. and J.H. Seinfeld, "*Relative humidity and pH dependence of the vapor pressure of ammonium nitrate-nitric acid solutions at 25 °C*". Atm. Environment, Vol. 16(1982). P. 993-1000.

78. Vance, J., and L. Peters, "*Aerosol formation resulting from the reaction of ammonia and sulfur dioxide*". Ind. Eng. Chem., Fundum., 15(1976). P. 202-206.

79. Creyghton, Y.L.M., "*Pulsed positive corona discharges: fundamental study and application to flue gas treatment*". Dissertation, Eindhoven University of Technology, 1993.

80. Sigmond, R.S., "*The Residual Streamer Channel: Return Strokes and Secondary Streamers*". J. Appl. Phys. Vol. 56(1984). P. 1355-1364.

81. Bayle, P. and A. Cornebois, "*Propagation of Ionizing Shock Waves in electrical Breakdown*". Phys. Rev. Vol. A31(1985). P. 1046-1058.

82. Spyrou, N. and C. Manassis, "*Spectroscopic study of a positive streamer in a point-to-plane discharge in air: evaluation of the electric field distribution*". J. Phys. D: Appl. Phys., Vol. 22(1989). P. 120-128.

83. Allen, N.L. and M. Boutlendj, "*Study of the electric fields required for streamer propagation in humid air*". IEE Procs. A, Vol. 138(1991). P. 37-42.

84. Pirgov, P., "*Electron energy distribution functions and reaction rates for air and flue gas*". Eindhoven: Eindhoven University of Technology, Faculty Electrical Engineering, Section Electrical Energy Systems, 1993. Internal Report EG/93/654.

85. Chuan Wen, "*Time-resolved swarm studies in gases with emphasis on electron detachment and ion conversion*". Dissertation, Eindhoven University of Technology, 1989.

Eindhoven University of Technology Research Reports ISSN 0167-9708
Coden: TEUEDE

Faculty of Electrical Engineering

(254) Velde, M. van de and P.J.M. Cluitmans
EEG ANALYSIS FOR MONITORING OF ANESTHETIC DEPTH.
EUT Report 91-E-254. 1991. ISBN 90-6144-254-0

(255) Smolders, A.B.
AN EFFICIENT METHOD FOR ANALYZING MICROSTRIP ANTENNAS WITH A DIELECTRIC COVER USING A SPECTRAL DOMAIN MOMENT METHOD.
EUT Report 91-E-255. 1991. ISBN 90-6144-255-9

(256) Backx, A.C.P.M. and A.A.H. Damen
IDENTIFICATION FOR THE CONTROL OF MIMO INDUSTRIAL PROCESSES.
EUT Report 91-E-256. 1991. ISBN 90-6144-256-7

(257) Maagt, P.J.I. de and H.G. ter Morsche, J.L.M. van den Broek
A SPATIAL RECONSTRUCTION TECHNIQUE APPLICABLE TO MICROWAVE RADIOMETRY.
EUT Report 92-E-257. 1992. ISBN 90-6144-257-5

(258) Vleeshouwers, J.M.
DERIVATION OF A MODEL OF THE EXCITER OF A BRUSHLESS SYNCHRONOUS MACHINE.
EUT Report 92-E-258. 1992. ISBN 90-6144-258-3

(259) Orlov, V.B.
DEFECT MOTION AS THE ORIGIN OF THE 1/F CONDUCTANCE NOISE IN SOLIDS.
EUT Report 92-E-259. 1992. ISBN 90-6144-259-1

(260) Rooijackers, J.E.
ALGORITHMS FOR SPEECH CODING SYSTEMS BASED ON LINEAR PREDICTION.
EUT Report 92-E-260. 1992. ISBN 90-6144-260-5

(261) Boom, T.J.J. van den and A.A.H. Damen, Martin Klompstra
IDENTIFICATION FOR ROBUST CONTROL USING AN H-infinity NORM.
EUT Report 92-E-261. 1992. ISBN 90-6144-261-3

(262) Groten, M. and W. van Etten
LASER LINEWIDTH MEASUREMENT IN THE PRESENCE OF RIN AND USING THE RECIRCULATING SELF HETERODYNE METHOD.
EUT Report 92-E-262. 1992. ISBN 90-6144-262-1

(263) Smolders, A.B.
RIGOROUS ANALYSIS OF THICK MICROSTRIP ANTENNAS AND WIRE ANTENNAS EMBEDDED IN A SUBSTRATE.
EUT Report 92-E-263. 1992. ISBN 90-6144-263-X

(264) Freriks, L.W. and P.J.M. Cluitmans, M.J. van Gils
THE ADAPTIVE RESONANCE THEORY NETWORK: (Clustering-) behaviour in relation with brainstem auditory evoked potential patterns.
EUT Report 92-E-264. 1992. ISBN 90-6144-264-8

(265) Wellen, J.S. and F. Karouta, M.F.C. Schemmann, E. Smalbrugge, L.M.F. Kaufmann
MANUFACTURING AND CHARACTERIZATION OF GAAS/ALGAAS MULTIPLE QUANTUMWELL RIDGE WAVEGUIDE LASERS.
EUT Report 92-E-265. 1992. ISBN 90-6144-265-6

(266) Cluitmans, L.J.M.
USING GENETIC ALGORITHMS FOR SCHEDULING DATA FLOW GRAPHS.
EUT Report 92-E-266. 1992. ISBN 90-6144-266-4

Eindhoven University of Technology Research Reports ISSN 0467-9708
Coden: TEUEDE

Faculty of Electrical Engineering

(267) Józwiak, L. and A.P.H. van Dijk
A METHOD FOR GENERAL SIMULTANEOUS FULL DECOMPOSITION OF SEQUENTIAL MACHINES: Algorithms and implementation.
EUT Report 92-E-267. 1992. ISBN 90-6144-267-2

(268) Boom, H. van den and W. van Etten, W.H.C. de Krom, P. van Bennekom, F. Huijskens, L. Niessen, F. de Leijer
AN OPTICAL ASK AND FSK PHASE DIVERSITY TRANSMISSION SYSTEM.
EUT Report 92-E-268. 1992. ISBN 90-6144-268-0

(269) Putten, P.H.A. van der
MULTIDISCIPLINAIR SPECIFICEREN EN ONTWERPEN VAN MICROELEKTRONICA IN PRODUKTEN (in Dutch).
EUT Report 93-E-269. 1993. ISBN 90-6144-269-9

(270) Bloks, R.H.J.
PROGRIL: A language for the definition of protocol grammars.
EUT Report 93-E-270. 1993. ISBN 90-6144-270-2

(271) Bloks, R.H.J.
CODE GENERATION FOR THE ATTRIBUTE EVALUATOR OF THE PROTOCOL ENGINE GRAMMAR PROCESSOR UNIT.
EUT Report 93-E-271. 1993. ISBN 90-6144-271-0

(272) Yan, Keping and E.M. van Veldhuizen
FLUE GAS CLEANING BY PULSE CORONA STREAMER.
EUT Report 93-E-272. 1993. ISBN 90-6144-272-9

(273) Smolders, A.B.
FINITE STACKED MICROSTRIP ARRAYS WITH THICK SUBSTRATES.
EUT Report 93-E-273. 1993. ISBN 90-6144-273-7

(274) Bollen, M.H.J. and M.A. van Houten
ON INSULAR POWER SYSTEMS: Drawing up an inventory of phenomena and research possibilities.
EUT Report 93-E-274. 1993. ISBN 90-6144-274-5

(275) Deursen, A.P.J. van
ELECTROMAGNETIC COMPATIBILITY: Part 5, installation and mitigation guidelines, section 3, cabling and wiring.
EUT Report 93-E-275. 1993. ISBN 90-6144-275-3

(276) Bollen, M.H.J.
LITERATURE SEARCH FOR RELIABILITY DATA OF COMPONENTS IN ELECTRIC DISTRIBUTION NETWORKS.
EUT Report 93-E-276. 1993. ISBN 90-6144-276-1

(277) Weiland, Siep
A BEHAVIORAL APPROACH TO BALANCED REPRESENTATIONS OF DYNAMICAL SYSTEMS.
EUT Report 93-E-277. 1993. ISBN 90-6144-277-X

(278) Gorshkov, Yu.A. and V.I. Vladimirov
LINE REVERSAL GAS FLOW TEMPERATURE MEASUREMENTS: Evaluations of the optical arrangements for the instrument.
EUT Report 93-E-278. 1993. ISBN 90-6144-278-8

(279) Creyghton, Y.L.M. and W.R. Rutgers, E.M. van Veldhuizen
IN-SITU INVESTIGATION OF PULSED CORONA DISCHARGE
EUT Report 93-E-279. 1993. ISBN 90-6144-279-6